STRUCTURAL CONTROL OF THE NORRIS HOT SPRINGS AND ASSOCIATED GEOTHERMAL SYSTEM

by

Mia Peyton Wafer

A thesis submitted in partial fulfillment
of the requirements for the degree

of

Master of Science

in

Earth Sciences

MONTANA STATE UNIVERSITY
Bozeman, Montana

May 2023

ACKNOWLEDGEMENTS

I could not have completed this thesis without the support from the MSU Earth Science Department, family, friends, and my funding sources. I want to thank my advisor, Dr. Andrew Laskowski, for his support and encouragement during my time at Montana State. I would also like to thank my committee members, Dr. Devon Orme and Dr. Eric Sproles, both of whom provided invaluable insight. This thesis greatly benefitted from the guidance of my writing group and the Writing Center at MSU. Additionally, This work could not have happened without the financial support of my funding sources: Montana State University, the Tobacco Root Geologic Society, and the NSF-funded PLASMA Institute as well as Petroleum Experts, who provided the Petex Move software.

Thank you to all the graduate students, Earth Science and not, that became my friends and a built-in support system, while also making coming to work a little more fun. Kris Hashberger, Ray Salazar, and Hayden Yates kept me company and helped collect data in the field despite hot days and freezing mornings. I especially want to thank Natali Kragh for all the post-work Bunkhouse conversations. Thank you to Annie Shoemaker, who was almost always present at these conversations, for your support, understanding and everything else. I want to express my deep gratitude to Khalil Droubi, who serves both as an academic inspiration and an incredible friend. Finally, I want to thank my mom, dad, and sister for their unending love and support. Thank you for giving me the gift of loving and appreciating nature and wanting to be outside at all times.

TABLE OF CONTENTS

TABLE OF CONTENTS CONTINUE

LIST OF FIGURES

Figure Page

LIST OF FIGURES CONTINUED

Figure Page

ABSTRACT

Many active and productive geothermal systems are structurally controlled, suggesting that certain structural configurations have higher potentials for geothermal energy. Analyzing potential productive geothermal wells is known as geothermal play fairway analysis (PFA). Identifying these high potential structural configurations is another way to locate geothermal systems without surface expressions, which represent an unquantified natural resource for geothermal energy. By studying geothermal systems with surface expressions, I move closer to being able to locate additional natural resources. The Norris Hot Springs, located in the foothills of the Tobacco Root Mountains, Southwestern Montana, presents a novel study area to test structural control on geothermal system development. I combine geologic mapping, UAV-based photogrammetry, zircon U-Pb geochronology, seismic data, and 3D geologic modeling to date and interpret the multistage development of local structures and their influence on the geothermal system beneath the Norris Hot Springs.

A comprehensive structural model suggests the geothermal system associated with the Norris Hot Springs is hosted by a deep network of faults and fractures in Precambrian gneiss basement. A nearby fault system primarily comprised of high angle NNW-SSE trending normal faults, which often display pervasive alteration and polymetallic vein mineralization, likely connects surficial features with deeper reactivated Laramide-era structures. A primary goal of this study was to investigate the benefits of supplementing traditional field work with novel methods. Results from this study demonstrate the utility of combining geologic mapping, 3D modeling, structural analysis, 3D modeling and UAV surveys for geothermal exploration and constrain the timing and influence of local faulting on geothermal activity at the Norris Hot Springs.

CHAPTER ONE

GENERAL INTRODUCTION

A geothermal system is a natural heat transfer system in which subsurface fluid circulates within bedrock. Geothermal systems can have surface expressions such as mud pots, fumaroles, or hot springs, but often lack one entirely. Humans have taken advantage of geothermal resources as early as 10,000 years ago either as spiritual or recreational sites, and to heat spaces. In 1904, Italian Prince Piero Ginori Conti harnessed geothermal power to extract boric acid from hot springs, and later opened the first geothermal power plant (Nature, 1940). Today, geothermal energy represents a possibility for a sustainable power source (Axelsson et al., 2005). Geothermal exploration focuses on identifying and classifying geologic plays hosting geothermal systems and their associated potentials. This allows scientists to classify geologic settings that have statistically higher probabilities of achieving high geothermal potentials (Faulds et al., 2016, 2018). These settings are called geothermal fairways and identification of productive fairways is called play fairway analysis (PFA) (Faulds et al., 2021a; Moeck, 2014).

PFA helps identify geothermal systems that can be utilized as power sources. A key challenge is locating geothermal systems without surface expressions and understanding subsurface controls to find best case drilling locations. Several structural geometries have been identified as statistically high potential configurations for geothermal activity (Faulds & Hinz, 2015). Typically, these plays involve a high geothermal gradient, normal faulting, and transtensional stresses (Faulds, 2012; Faulds et al., 2004; Siler et al., 2018). These are characteristics that promote geothermal fluid circulation.

In the western US, many workers have taken advantage of the high geothermal gradient resulting from over 100% extension since the Oligocene(Wisian et al., 1999). The Great Basin region has been identified as a geothermal resource because of a combination of the high heat flow and structural geometries that promote geothermal upwelling. Here, it is proposed that geothermal activity in southwestern Montana is analogous to the Great Basin Region and may be an underdeveloped resource for geothermal power.

Southwestern Montana has a complex tectonic history, but most recently has hosted multiple generations of extension (Harms et al., 2004; Mitchell W. Reynolds, 1979; Yonkee & Weil, 2015). The Basin and Range Province, defined by high angle normal faults and alternating peak and valley topography extends to Idaho and southwest Montana. Additionally, reactivated high angle Laramide faults that accommodated orogenic collapse ca. 40 Ma are preferentially oriented for transtensional stress that promote geothermal flow (Decelles, 2004; Siler & Faulds, 2013). Norris, MT, falls between several such regional scale faults, as well as a smaller scale mineralized fault system and a Basin and Range fault structure. Norris was a gold mining hub in the late 1800s due to magmatic ore fluids that were injected into a series of veins just outside the town (Reed & Dilles, 2021). Today, Norris' main attraction is the hot springs, a developed recreational location. I have identified the hot spring itself, which is the primary outflow of a linked geothermal system, just east of the town of Norris. Norris Hot Springs provides a study area for understanding the structural controls geothermal system in southwestern Montana, and a test site for exploring the benefits of combining several traditional and novel methods for characterizing geothermal systems. In the following thesis, I fulfill two research goals:

identifying structural controls of the geothermal system and investigating the benefits of combining traditional and novel methods for geothermal exploration.

References Cited

Andretta, D. B., & Alsup, S. A. (1960). *ELEVENTH ANNUAL FIELD CONFERENCE 185 GEOLOGY AND CENOZOIC HISTORY OF THE NORRIS-ELK CREEK AREA, SOUTHWEST MONTANA*.

Axelsson, G. (2010). Sustainable geothermal utilization – Case histories; definitions; research issues and modelling. *Geothermics*, *39*(4), 283–291. https://doi.org/10.1016/j.geothermics.2010.08.001

Axelsson, G., Stefánsson, V., Björnsson, G., & Liu, J. (2005). Sustainable Management of Geothermal Resources and Utilization for 100-300 Years. In *Proceedings World Geothermal Congress*.

Barton, C. A., & Zoback, M. D. (1995). Fluid flow along potentially active faults in crystalline rock. *Geology*, *23*(8), 683–686. http://pubs.geoscienceworld.org/gsa/geology/article-pdf/23/8/683/3515911/i0091-7613-23-8-683.pdf

Bennet, S. (2011). Geothermal Potential of Transtensional Plate Boundaries. *GRC Transactions*, *35*.

Blackford, N. R., Long, S. P., Stout, A., Rodgers, D. W., Cooper, C. M., Kramer, K., di Fiori, R. v., & Soignard, E. (2022). Late Cretaceous upper-crustal thermal structure of the Sevier hinterland: Implications for the geodynamics of the Nevadaplano. *Geosphere*, *18*(1), 183–210. https://doi.org/10.1130/GES02386.1

Blackwell, D., Wisian, K. W., Benoit, D., & Gollan, B. (1999). Structure of the Dixie Valley geothermal system, a" typical" Basin and Range geothermal system, from thermal and gravity data. *TRANSACTIONS-GEOTHERMAL RESOURCES COUNCIL*, 525–532.

Carl, J. D. (1970). Block Faulting and Development of Drainage, Northern Madison Mountains, Montana. *Geological Society of America Bulletin*, *81*, 2287–2298.

Carrapa, B., DeCelles, P. G., & Romero, M. (2019). Early Inception of the Laramide Orogeny in Southwestern Montana and Northern Wyoming: Implications for Models of Flat-Slab Subduction. *Journal of Geophysical Research: Solid Earth*, *124*(2), 2102–2123. https://doi.org/10.1029/2018JB016888

Chadwick, R., & Kaczmarek, M. (1975). Geothermal Investigations of Selected Montana Hot Springs. *Energy Resources of Montana*, *22*.

Chadwick, R., & Leonard, R. (1979). *Structural Controls of Hot-Spring Systems in Southwest Montana*.

Condit, C. B., Mahan, K. H., Ault, A. K., & Flowers, R. M. (2015). Foreland-directed propagation of high-grade tectonism in the deep roots of a Paleoproterozoic collisional orogen, SW Montana, USA. *Lithosphere*, L460.1. https://doi.org/10.1130/L460.1

Constenius, K. N. (1996). *Late Paleogene extensional collapse of the Cordilleran foreland fold and thrust belt*.

Curewitz, D., & Karson, J. A. (1997). Structural settings of hydrothermal outflow: Fracture permeability maintained by fault propagation and interaction. *Journal of Volcanology and Geothermal Research*, *79*, 149–168.

de la Varga, M., Schaaf, A., & Wellmann, F. (2019). GemPy 1.0: open-source stochastic geological modeling and inversion. *Geoscientific Model Development*, *12*(1), 1–32. https://doi.org/10.5194/gmd-12-1-2019

Decelles, P. G. (2004). *LATE JURASSIC TO EOCENE EVOLUTION OF THE CORDILLERAN THRUST BELT AND FORELAND BASIN SYSTEM, WESTERN U.S.A.*

Dickinson, W. R., & Gehrels, G. E. (2009). Use of U–Pb ages of detrital zircons to infer maximum depositional ages of strata: A test against a Colorado Plateau Mesozoic database. *Earth and Planetary Science Letters*, *288*(1–2), 115–125. https://doi.org/10.1016/j.epsl.2009.09.013

Erslev, E. A., & Koenig, N. v. (2009). Three-dimensional kinematics of Laramide, basement-involved Rocky Mountain deformation, USA: Insights from minor faults and GIS-enhanced structure maps. In *Backbone of the Americas: Shallow Subduction, Plateau Uplift, and Ridge and Terrane Collision*. Geological Society of America. https://doi.org/10.1130/2009.1204(06)

Faulds, J. E. (2012). *Regional Patterns of Geothermal Activity in the Great Basin Region, Western USA: Correlation With Strain Rates*.

Faulds, J. E., Coolbaugh, M., Blewitt, G., & Henry, C. D. (2004). WHY IS NEVADA IN HOT WATER? STRUCTURAL CONTROLS AND TECTONIC MODEL OF GEOTHERMAL SYSTEMS IN THE NORTHWESTERN GREAT BASIN. *Geothermal Resources Council Transactions*, *28*.

Faulds, J. E., Coolbaugh, M. F., Vice, G. S., & Edwards, M. L. (2006). Characterizing structural controls of geothermal fields in the northwestern Great Basin: A progress report. *Geothermal Resources Council Transactions 30* , 69–76.

Faulds, J. E., Craig, J. W., Hinz, N. H., Coolbaugh, M. F., Glen, J. M., Earney, T. E., Schermerhorn, W. D., Peacock, J., Deoreo, S. B., & Siler, D. L. (2018). Discovery of a Blind Geothermal System in Southern Gabbs Valley, Western Nevada, through Application of the Play Fairway Analysis at Multiple Scales. In *GRC Transactions* (Vol. 42).

Faulds, J. E., & Hinz, N. H. (2015). Favorable Tectonic and Structural Settings of Geothermal Systems in the Great Basin Region, Western USA: Proxies for Discovering Blind Geothermal Systems. In *Proceedings World Geothermal Congress*.

Faulds, J. E., Hinz, N. H., Coolbaugh, M. F., Depolo, C. M., Siler, D. L., Shevenell, L. A., Hammond, W. C., Kreemer, C., & Queen, J. H. (2016). Discovering Geothermal Systems in the Great Basin Region: An Integrated Geologic, Geochemical, and Geophysical Approach for Establishing Geothermal Play Fairways. In *PROCEEDINGS*.

Faulds, J. E., Shervais, J. W., Wannamaker, P. E., Forson, C., & Lautze, N. (2021a). Challenges and opportunities for geothermal exploration and hydrothermal research: Recent advances utilizing geothermal play fairway analysis in the western USA. *Proceedings of the Symposium on the Application of Geophyics to Engineering and Environmental Problems, SAGEEP*, *2021-March*. https://doi.org/10.4133/sageep.33-083

Faulds, J. E., Shervais, J. W., Wannamaker, P. E., Forson, C., & Lautze, N. (2021b). Challenges and opportunities for geothermal exploration and hydrothermal research: Recent advances utilizing geothermal play fairway analysis in the western USA. *Proceedings of the Symposium on the Application of Geophyics to Engineering and Environmental Problems, SAGEEP*, *2021-March*. https://doi.org/10.4133/sageep.33-083

Ferrill, D. A., Smart, K. J., & Morris, A. P. (2020). Resolved stress analysis, failure mode, and fault-controlled fluid conduits. *Solid Earth*, *11*(3), 899–908. https://doi.org/10.5194/se-11-899-2020

Foster, D. A., Mueller, P. A., Mogk, D. W., Wooden, J. L., & Vogl, J. J. (2006). Proterozoic evolution of the western margin of the Wyoming craton: implications for the tectonic and magmatic evolution of the northern Rocky Mountains. *Canadian Journal of Earth Sciences*, *43*(10), 1601–1619. https://doi.org/10.1139/e06-052

Furlong, K. P., & Handy, M. R. (n.d.). *Nucleation and growth of fault systems Neoproterozoic stratigraphy View project*. https://www.researchgate.net/publication/237378284

Garihan, J., Schmidt, C., Young, S., & Williams, M. A. (1983). Geology and recurrent movement history of the Bismark- Spanish Peaks- Gardiner Fault System, Southwest Montana. *Rocky Mountain Association of Geologists*.

Garzanti, E. (2019). Petrographic classification of sand and sandstone. *Earth-Science Reviews*, *192*, 545–563. https://doi.org/10.1016/j.earscirev.2018.12.014

Gunderson, J. A. (2012). *Preliminary Geothermal Map of Montana Using Bottom-Hole Temperature Data*.

Gwinn, V. E., & Mutch, T. A. (1965). Intertongued Upper Cretaceous Volcanic and Nonvolcanic Rocks, Central-Western Montana. *GSA Bulletin*.

Haller, K. M., Dart, R. L., Machette, M. N., & Stickney, M. C. (n.d.). *Data for Quaternary faults in western Montana*.

Harms, T. A., Brady, J. B., Robert Burger, H., Cheney, J. T., & Robert, H. (2004). Advances in the Geology of the Tobacco Root Mountains, Montana, and Their Implications for the History of the Northern Wyoming Province. In *Smith ScholarWorks Smith ScholarWorks Geosciences*. Faculty Publications Geosciences. https://scholarworks.smith.edu/geo_facpubs/31

Harvey, M. C., Rowland, J. v., & Luketina, K. M. (2016). Drone with thermal infrared camera provides high resolution georeferenced imagery of the Waikite geothermal area, New Zealand. *Journal of Volcanology and Geothermal Research*, *325*, 61–69. https://doi.org/10.1016/j.jvolgeores.2016.06.014

Haselwimmer, C., Prakash, A., & Holdmann, G. (2013). Quantifying the heat flux and outflow rate of hot springs using airborne thermal imagery: Case study from Pilgrim Hot Springs, Alaska. *Remote Sensing of Environment*, *136*, 37–46. https://doi.org/10.1016/j.rse.2013.04.008

Jacobsen, L. J., Glynn, P. D., Phelps, G. A., Orndorff, R. C., Bawden, G. W., Grauch, V., & Geological Survey, U. (2011). *Chapter 13: U.S. Geological Survey: A Synopsis of Three-dimensional Modeling Mission and Organizational Needs*. http://tapestry.usgs.gov

Janecke, S. U. (2007). Cenozoic extensional processes and tectonics in the northern Rocky Mountains: southwest Montana and eastern Idaho. In *The Journal of the Tobacco Root Geological Society*.

Jolie, E., Scott, S., Faulds, J., Chambefort, I., Axelsson, G., Gutiérrez-Negrín, L. C., Regenspurg, S., Ziegler, M., Ayling, B., Richter, A., & Zemedkun, M. T. (2021). Geological controls on geothermal resources for power generation. In *Nature Reviews Earth and Environment*

(Vol. 2, Issue 5, pp. 324–339). Springer Nature. https://doi.org/10.1038/s43017-021-00154-y

Jones, R. R., McCaffrey, K. J. W., Clegg, P., Wilson, R. W., Holliman, N. S., Holdsworth, R. E., Imber, J., & Waggott, S. (2009). Integration of regional to outcrop digital data: 3D visualisation of multi-scale geological models. *Computers and Geosciences*, *35*(1), 4–18. https://doi.org/10.1016/j.cageo.2007.09.007

Jordan, B. R. (2015). A bird's-eye view of geology: The use of micro drones/UAVs in geologic fieldwork and education. *GSA Today*, 50–52. https://doi.org/10.1130/gsatg232gw.1

Kaempfer, J. M., Guenthner, W. R., & Pearson, D. M. (2021). Proterozoic to Phanerozoic Tectonism in Southwestern Montana Basement Ranges Constrained by Low Temperature Thermochronometric Data. *Tectonics*, *40*(11). https://doi.org/10.1029/2021TC006744

Kellogg, K. S., & Harlan, S. S. (2007). New 40 Ar/ 39 Ar age determinations and paleomagnetic results bear-ing on the tectonic and magmatic history of the northern Madison Range and Madison Valley region, southwestern Montana, U.S.A. In *Rocky Mountain Geology* (Vol. 42, Issue 2). http://pubs.geoscienceworld.org/uwyo/rmg/article-pdf/42/2/157/2956023/157.pdf

Kellogg, K., & Williams, V. (2000). *Geologic map of the Ennis 30' x 60' quadrangle, Madison and Gallatin Counties, Montana, and Park County, Wyoming*. https://doi.org/10.3133/i2690

Kuenzer, C., & Dech, S. (2013). Remote Sensing and Digital Image Processing Thermal Infrared Remote Sensing. In *Editors Sensors*. http://www.springer.com/series/6477

Laskowski, A. K., Decelles, P. G., & Gehrels, G. E. (2013). Detrital zircon geochronology of Cordilleran retroarc foreland basin strata, western North America. *Tectonics*, *32*(5), 1027–1048. https://doi.org/10.1002/tect.20065

Malmivirta, T., Hamberg, J., Lagerspetz, E., Li, X., Peltonen, E., Flores, H., & Nurmi, P. (2019). Hot or Not? Robust and Accurate Continuous Thermal Imaging on FLIR cameras. *International Conference on Pervasive Computing and Communications*.

Marshak, S., Karlstrom, K., & Timmons, J. M. (2000). Inversion of Proterozoic extensional faults: An explanation for the pattern of Laramide and Ancestral Rockies intracratonic deformation, United States. *Geology*, *28*(8), 735. https://doi.org/10.1130/0091-7613(2000)28<735:IOPEFA>2.0.CO;2

Martin, E. L., Barrote, V. R., & Cawood, P. A. (2022). A resource for automated search and collation of geochemical datasets from journal supplements. *Scientific Data*, *9*(1). https://doi.org/10.1038/s41597-022-01730-7

McBride, B., Schmidt, C. J., Guthrie, G., & Sheedlo, M. (1992). Multiple reactivation of a collisional boundary: an example from southwestern Montana. In *Basement Tectonics 8* (pp. 341–357).

Metesh, J. (2000). *Montana Bureau of Mines and Geology Open-file Report No. 415 Geothermal Springs and Wells in Montana*.

Mitchell W. Reynolds. (1979). CHARACTER AND EXTENT OF BASIN-RANGE FAULTING, WESTERN MONTANA AND EAST-CENTRAL IDAHO. *RMAG-UGA-1979 BASIN AND RANGE SYMPOSIUM*.

Moeck, I. S. (2014). Catalog of geothermal play types based on geologic controls. In *Renewable and Sustainable Energy Reviews* (Vol. 37, pp. 867–882). Elsevier Ltd. https://doi.org/10.1016/j.rser.2014.05.032

Morris, A., Ferrill, D. A., & Henderson, D. B. (1996). Slip-tendency analysis and fault reactivation. *Geology*, *24*(3), 275–278. http://pubs.geoscienceworld.org/gsa/geology/article-pdf/24/3/275/3516540/i0091-7613-24-3-275.pdf

Mueller, P. A., & Frost, C. D. (2006). The Wyoming Province: a distinctive Archean craton in Laurentian North America. *Canadian Journal of Earth Sciences*, *43*(10), 1391–1397. https://doi.org/10.1139/e06-075

Mueller, P. A., Shuster, R. D., Wooden, J. L., Erslev, E. A., & Bowes, D. R. (1993). Age and composition of Archean crystalline rocks from the southern Madison Range, Montana: Implications for crustal evolution in the Wyoming craton. *Geological Society of America Bulletin*, *105*(4), 437–446. https://doi.org/10.1130/0016-7606(1993)105<0437:AACOAC>2.3.CO;2

Musy, M., Jacquenot, G., & Dalmasso, G. (2019). Vtkplotter, a python module for scientific visualization and analysis of 3D objects and point clouds based on VTK (visualization toolkit). In *Zenodo*.

Neale, C. M. U., Jaworowski, C., Heasler, H., Sivarajan, S., & Masih, A. (2016). Hydrothermal monitoring in Yellowstone National Park using airborne thermal infrared remote sensing. *Remote Sensing of Environment*, *184*, 628–644. https://doi.org/10.1016/j.rse.2016.04.016

Peterson, J. L. (1984). *INTERPRETATION OF ELECTRICAL SOUNDINGS AND SELF POTENTIAL MEASUREMENTS IN THE NORRIS HOT SPRINGS AREA, MADISON COUNTY, MONTANA*.

Prince Ginori-Conti. Nature 145, 380 (1940). https://doi.org/10.1038/145380a0

Reed, M., & Dilles, J. (2021). *ORE DEPOSITS OF BUTTE, MONTANA*.

Ronemus, C. B., Orme, D. A., Guenthner, W. R., Cox, S. E., & Kussmaul, C. A. L. (2023). Orogens of Big Sky Country: Reconstructing the Deep-Time Tectonothermal History of the Beartooth Mountains, Montana and Wyoming, USA. *Tectonics*, *42*(1). https://doi.org/10.1029/2022TC007541

Rounce, D. R., Hock, R., & Shean, D. E. (2020). Glacier Mass Change in High Mountain Asia Through 2100 Using the Open-Source Python Glacier Evolution Model (PyGEM). *Frontiers in Earth Science*, *7*. https://doi.org/10.3389/feart.2019.00331

Scarberry, K. C., Yakovlev, P. v, & Schwartz, T. M. (2021). *MESOZOIC MAGMATISM IN MONTANA*.

Sibson, R. H. (1994). Crustal stress, faulting and fluid flow. *Geological Society Special Publication*. http://sp.lyellcollection.org/

Siler, D. L., & Faulds, J. E. (2013). *Three-Dimensional Geothermal Fairway Mapping: Examples from Great Basin, USA*.

Siler, D. L., Faulds, J. E., Hinz, N. H., Dering, G. M., Edwards, J. H., & Mayhew, B. (2019). Three-dimensional geologic mapping to assess geothermal potential: examples from Nevada and Oregon. *Geothermal Energy*, *7*(1). https://doi.org/10.1186/s40517-018-0117-0

Siler, D. L., Hinz, N. H., & Faulds, J. E. (2018). *Stress concentrations at structural discontinuities in active fault zones in the western United States: Implications for permeability and fluid flow in geothermal fields*. http://pubs.geoscienceworld.org/gsa/gsabulletin/article-pdf/130/7-8/1273/4224719/1273.pdf

Siler, D. L., & Pepin, J. D. (2021a). 3-D Geologic Controls of Hydrothermal Fluid Flow at Brady geothermal field, Nevada, USA. *Geothermics*, *94*. https://doi.org/10.1016/j.geothermics.2021.102112

Siler, D. L., & Pepin, J. D. (2021b). 3-D Geologic Controls of Hydrothermal Fluid Flow at Brady geothermal field, Nevada, USA. *Geothermics*, *94*. https://doi.org/10.1016/j.geothermics.2021.102112

Siler, D. L., Pepin, J. D., Vesselinov, V. v., Mudunuru, M. K., & Ahmmed, B. (2021). Machine learning to identify geologic factors associated with production in geothermal fields: a case-study using 3D geologic data, Brady geothermal field, Nevada. *Geothermal Energy*, *9*(1). https://doi.org/10.1186/s40517-021-00199-8

Snee, J.-E. L., & Miller, E. L. (2022). Magmatism, migrating topography, and the transition from Sevier shortening to Basin and Range extension, western United States. In *Tectonic Evolution of the Sevier-Laramide Hinterland, Thrust Belt, and Foreland, and Postorogenic*

Slab Rollback (180–20 Ma) (pp. 335–357). Geological Society of America. https://doi.org/10.1130/2021.2555(13)

Snoke, A. W., & Chapman, J. B. (2021). Central Cordillera. *Encyclopedia of Geology*, 157–172. https://doi.org/10.1016/B978-0-12-409548-9.12124-4

Spencer, E. W., & Kozak, S. J. (1975). Precambrian Evolution of the Spanish Peaks Area, Montana. *Geological Society of America Bulletin*, *86*, 785–792. http://pubs.geoscienceworld.org/gsa/gsabulletin/article-pdf/86/6/785/3429179/i0016-7606-86-6-785.pdf

Stickney, M. C., & Bartholomew, M. J. (1987). SEISMICITY AND LATE QUATERNARY FAULTING OF THE NORTHERN BASIN AND RANGE PROVINCE, MONTANA AND IDAHO. In *Bulletin of the Seismological Society of America* (Vol. 77, Issue 5). http://pubs.geoscienceworld.org/ssa/bssa/article-pdf/77/5/1602/5333837/bssa0770051602.pdf

Taillefer, A., Guillou-Frottier, L., Soliva, R., Magri, F., Lopez, S., Courrioux, G., Millot, R., Ladouche, B., & le Goff, E. (2018). Topographic and Faults Control of Hydrothermal Circulation Along Dormant Faults in an Orogen. *Geochemistry, Geophysics, Geosystems*, *19*(12), 4972–4995. https://doi.org/10.1029/2018GC007965

Thornton, J. M., Mariethoz, G., & Brunner, P. (2018). A 3D geological model of a structurally complex alpine region as a basis for interdisciplinary research. *Scientific Data*, *5*. https://doi.org/10.1038/sdata.2018.238

Thurlow, E. E. (1941). *Geology and ore deposits of the Lower Hot Springs Mining District Madison County, Montana*.

Turner, A. K. (2006). Challenges and trends for geological modelling and visualisation. *Bulletin of Engineering Geology and the Environment*, *65*(2), 109–127. https://doi.org/10.1007/s10064-005-0015-0

Vermeesch, P. (2018). IsoplotR: A free and open toolbox for geochronology. *Geoscience Frontiers*, *9*(5), 1479–1493. https://doi.org/10.1016/j.gsf.2018.04.001

Vermeesch, P. (2021). Maximum depositional age estimation revisited. *Geoscience Frontiers*, *12*(2), 843–850. https://doi.org/10.1016/j.gsf.2020.08.008

Villarreal, C. A., Garzón, C. G., Mora, J. P., Rojas, J. D., & Ríos, C. A. (2022). Workflow for capturing information and characterizing difficult-to-access geological outcrops using unmanned aerial vehicle-based digital photogrammetric data. *Journal of Industrial Information Integration*, *26*. https://doi.org/10.1016/j.jii.2021.100292

Vuke, S., Lonn, J., Berg, R., & Karl, K. (2002). *Preliminary geologic map of the Bozeman 30' x 60' Quadrangle*.

Vuke, S. M. (2020). Synorogenic basin deposits and associated Laramide uplifts in the Montana part of the Cordilleran foreland basin system. *Geology of Montana*, *1*.

Walter, T. R., Jousset, P., Allahbakhshi, M., Witt, T., Gudmundsson, M. T., & Hersir, G. P. (2020). Underwater and drone based photogrammetry reveals structural control at Geysir geothermal field in Iceland. *Journal of Volcanology and Geothermal Research*, *391*. https://doi.org/10.1016/j.jvolgeores.2018.01.010

Westoby, M. J., Brasington, J., Glasser, N. F., Hambrey, M. J., & Reynolds, J. M. (2012). 'Structure-from-Motion' photogrammetry: A low-cost, effective tool for geoscience applications. *Geomorphology*, *179*, 300–314. https://doi.org/10.1016/j.geomorph.2012.08.021

Whitmeyer, S., & Karl E. Karlstrom. (2007). Tectonic model for Proterozoic growth of North America. *Geosphere*, *3*(4), 220. https://doi.org/10.1130/GES00055.1

Willams, C. F., Reed, M. J., DeAngelo, J., & Galanis, S. P. (2009). Quantifying the undiscovered geothermal resources of the United States. *GRC Transactions*, *33*.

Wisian, K. W., Blackwell, D. D., & Richards, M. (1999). *HEAT FLOW IN THE WESTERN UNITED STATES AND EXTENSIONAL GEOTHERMAL SYSTEMS*. www.smu.edu/~geothermal

Wu, Q., & Xu, H. (2004). On three-dimensional geological modeling and visualization. *Science in China, Series D: Earth Sciences*, *47*(8), 739–748. https://doi.org/10.1360/02yd0475

Yonkee, W. A., & Weil, A. B. (2015). Tectonic evolution of the Sevier and Laramide belts within the North American Cordillera orogenic system. *Earth-Science Reviews*, *150*, 531–593. https://doi.org/10.1016/j.earscirev.2015.08.001

CHAPTER TWO

ASSESSING STRUCTURAL CONTROLS ON THE GEOTHERMAL ACTIVITY AT NORRIS HOT SPRINGS, SW MONTANA

Introduction

Geothermal systems with no surface expression, or blind geothermal systems, are an unquantified natural resource waiting to be tapped for heating or energy production (Faulds & Hinz, 2015; Willams et al., 2009). Because they have no surface expression, these geothermal systems are often challenging to locate (Faulds et al., 2021b). Geothermal systems where fluid circulation is accommodated by faults and fractures are termed structurally controlled (Fig. 1) (Faulds et al., 2004). By studying structurally controlled geothermal systems with surface expressions, researchers can identify structural configurations with high geothermal potential and search for a specific configuration instead of relying on a surface expression (Faulds et al., 2006, 2021; Jolie et al., 2021; Siler et al., 2019; Williams et al., 2009).

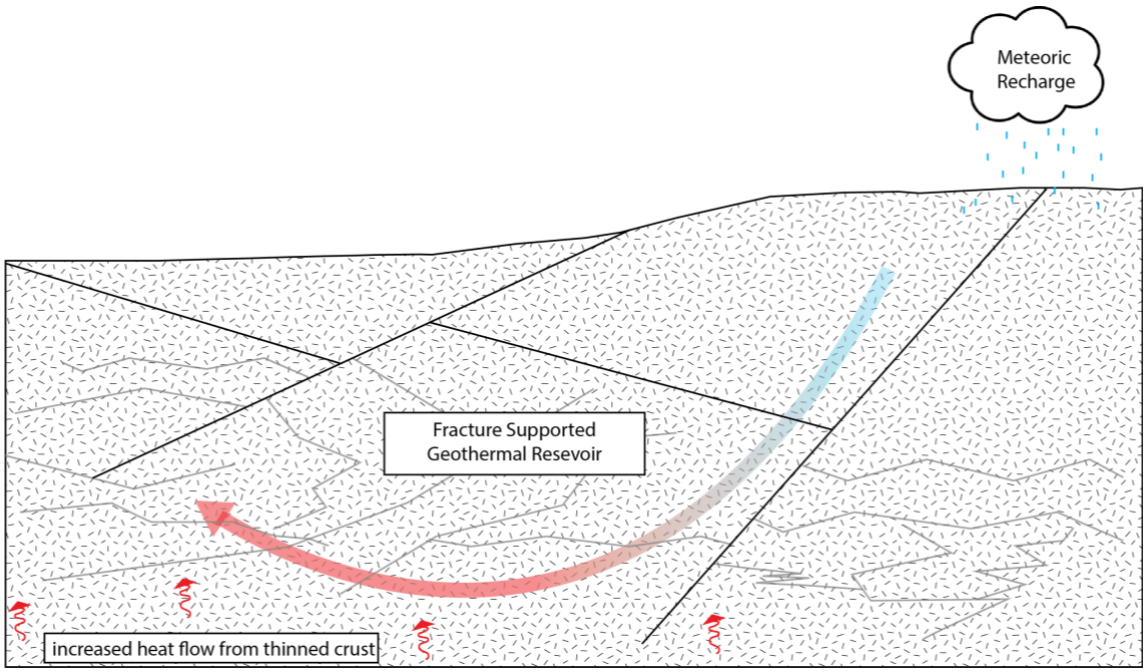

Figure 1. Generalized schematic of a structurally controlled geothermal system in a crystalline basement. Arrows represent fluid flow. Geothermal fluid originates as meteoric water and circulates through faults and fractures while being heated by increased heat flow from thin crust.

Faults accommodate meteoric recharge and carry fluid to depth while additional fractures can serve as geothermal reservoirs and fluid conduits (Ferrill et al., 2020; Taillefer et al., 2018). Ultimately, geothermal resource potential is a quantifiable characteristic of any geologic system. Geologic factors that influence geothermal potential include lithology, structures, and temperature distribution (Jolie et al., 2021; Moeck, 2014; Siler et al., 2021; Siler & Pepin, 2021a).

Most hot springs in southwestern Montana are surface expressions of amagmatic geothermal systems (Chadwick & Kaczmarek, 1975). In amagmatic geothermal systems, high heat flow is generated due to crustal extension, and the geothermal gradient is increased regionally (Wisian et al., 1999). Crustal extension is accommodated by the same structures that can be controlling fluid circulation in the geothermal systems (Chadwick & Leonard, 1979).

Structurally controlled geothermal systems provide an opportunity to identify geothermal resources based on their structural geometry and orientations as opposed to surficial outflows (Jolie et al., 2021). This concept is the foundation for discovering structurally controlled blind geothermal systems. Therefore, understanding the structural history of a region provides necessary context for geothermal exploration. Here, I conduct a case study of a known geothermal system, identified by its surficial outflow, Norris Hot Springs.

Structurally Controlled Geothermal Systems

Tectonic and structural features such as faults and fractures often control fluid mobility and up flow of geothermal systems, especially in nonporous bedrock (Blackwell et al., 1999; Faulds et al., 2004; Siler & Pepin, 2021a).These systems are referred to as structurally controlled. In low permeability lithologies, faults and fractures often serve as secondary fluid conduits for geothermal systems. However, the failure mode of these structures can result either in fluid conduits or seals (Fig. 2) (Ferrill et al., 2020).

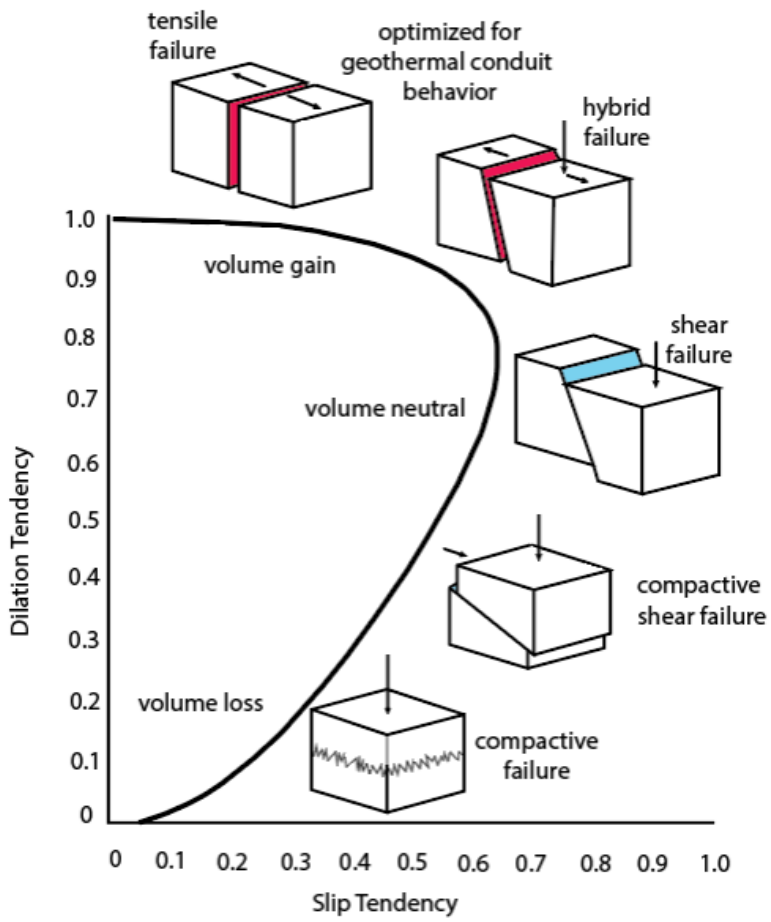

Figure 2. Failure behaviors in rock plotted as a function of dilation tendency and slip tendency. Tensile failure and hybrid failure are optimized for geothermal conduit behavior. Adapted from Ferrill et al. (2020).

Failure mode is determined by the orientation of the structure, or slip surface, and the stresses acting on that surface. The stress state of a fault is the result of the normal and shear stresses acting on a fault plane or zone. Several parameters can be calculated from the stress state and orientation of the plane to predict failure: slip and dilation tendencies. Slip tendency is the ratio of shear stress to effective normal stress. Essentially, it refers to the point at which the fault will slip or deform. Dilation tendency is defined as the stress acting normal to a given surface and is related to whether the fault will dilate during deformation. Together, slip tendency versus

dilation tendency provides a likely failure mode and associated volume change that influences permeability behavior of the rock (Ferrill et al., 2020; Morris et al., 1996). High dilation tendency and low to intermediate slip tendency values are optimized for geothermal fluid flow (Fig. 3). Both characteristics, but primarily dilation tendency, are dependent on orientation of the structure relative to the stress field at the time of deformation. Faults that fall in this category are termed critically stressed, because they are essentially failing slowly, although rock experiencing any mode of failure is considered critically stressed (Morris et al., 1996).

Recently, machine learning, a subset of artificial intelligence focused on training computers to recognize patterns, has been employed to identify the factors that have the most bearing on the productivity of a geothermal well (e.g., Siler & Pepin, 2021b; Faulds et al., 2020). These include characteristics like fault density, fault intersection and dilation and slip tendency and emphasize the importance of understanding the stress state and fault geometries of potential areas for geothermal exploration (Siler et al., 2018, 2019; Siler & Pepin, 2021a). They find that fault and fault network factors are identified as having the most influence on geothermal productivity. Slip and dilation tendencies are values derived from these stresses. Critically stressed faults that are preferentially oriented to increase both slip and dilation tendencies often result in fluid conduits and promote geothermal fluid flow (Ferrill et al., 2020). The geometry and kinematics of faults are essential to understanding their potential for circulating geothermal fluids.

Several structural configurations have been identified as favorable tectonic settings for high potential geothermal systems. Most relevant to this study are major normal faults, fault intersections and step-over faults. (Fig. 4) (Curewitz & Karson, 1997; Faulds & Hinz, 2015).

These extensional structures paired with an appropriately oriented stress field provide the mechanisms necessary for geothermal flow.

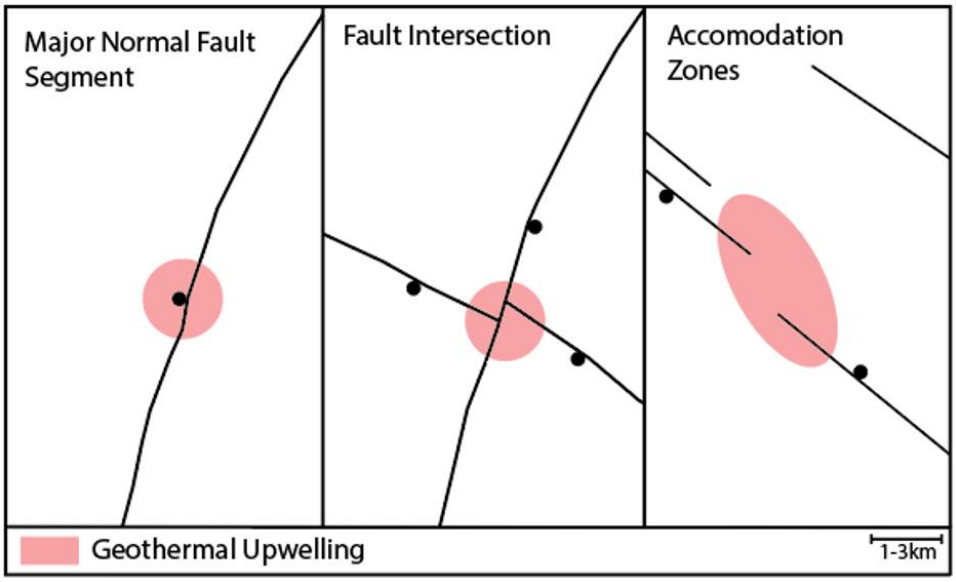

Figure 3. Tectonically favorable settings for structurally controlled geothermal systems observed near Norris, MT. Ball indicates down dropped hanging wall block of a normal fault. Adapted from Faulds and Hinz (2015).

Additionally, increased permeability from dense fracture zones and fault intersections allows for the fluid mobility and heat convection necessary to develop high potential geothermal systems (Barton & Zoback, 1995; Faulds et al., 2006; Siler & Faulds, 2013).

Regions that are undergoing extensional deformation are often targeted for geothermal exploration because they pair elevated heat flow and preferentially oriented structures (Axelsson, 2010). Additionally, normal faulting results in components of transtensional stress that promotes geothermal circulation (Bennet, 2011; Sibson, 1994). Components of compressional stress reduce volume change across the slip plane and inhibit fluid flow (Fig. 3). Oblique normal slip on appropriately oriented structures results in increased fluid and heat circulation through the

fault network. In the western United States, northwesterly striking faults are the most preferentially oriented faults because of the northwest directed extensional strain field increases slip and dilation tendencies (Faulds et al., 2006; Siler & Faulds, 2013; Siler & Pepin, 2021b).

Most previous work on structurally controlled geothermal systems has focused on the Great Basin region in Nevada. Although separated by the Snake River Plain, Idaho and southwest Montana also have the defining characteristics of Basin and Range style extension (Reynolds, 1979). The geology of southwestern Montana is dominated by NW-SE trending normal faults marked by successive ranges and sedimentary basins. Many of the basins in southwest Montana have been identified as areas with higher potential for geothermal systems, with several of the basins actively being explored for development of direct heat applications (Metesh, 2000). Bottom-hole temperatures of various wells throughout Montana range from 4-200℃ (Gunderson, 2012). I hypothesize that the high geothermal potential generated by Basin and Range style faults identified in Nevada extends into Montana and may be a region for new discovery of structurally controlled geothermal resources.

Norris Hot Springs

Norris Hot Springs, located in Norris, MT (45.570433, -111.690251), is the surface expression of a high temperature geothermal system. The spring's surface temperature was measured at 53℃, with a producing rate of 400 liters/minute (Sondregger and Bergantino,1981). The producing depth of the well is at least 3.6km, according to base temperatures calculated from (Peterson, 1984). Norris Hot Springs is in the Madison Valley, which ranges from Ennis Lake to the south, the Madison Range to the east, and the Tobacco Root Batholith to the west. It lies on an uplifted basement block defined by several regional scale normal faults: the

Carmichael Fault, the Elk Creek Fault, the Cherry Creek Fault, and the Spanish Peaks (Carl, 1970). Extension in this region over prints compressional thick- and thin-skinned deformation (McBride et al., 1992; S. M. Vuke, 2020). This study seeks to understand the geometry of the faults around the hot springs and identify those preferentially oriented for geothermal flow.

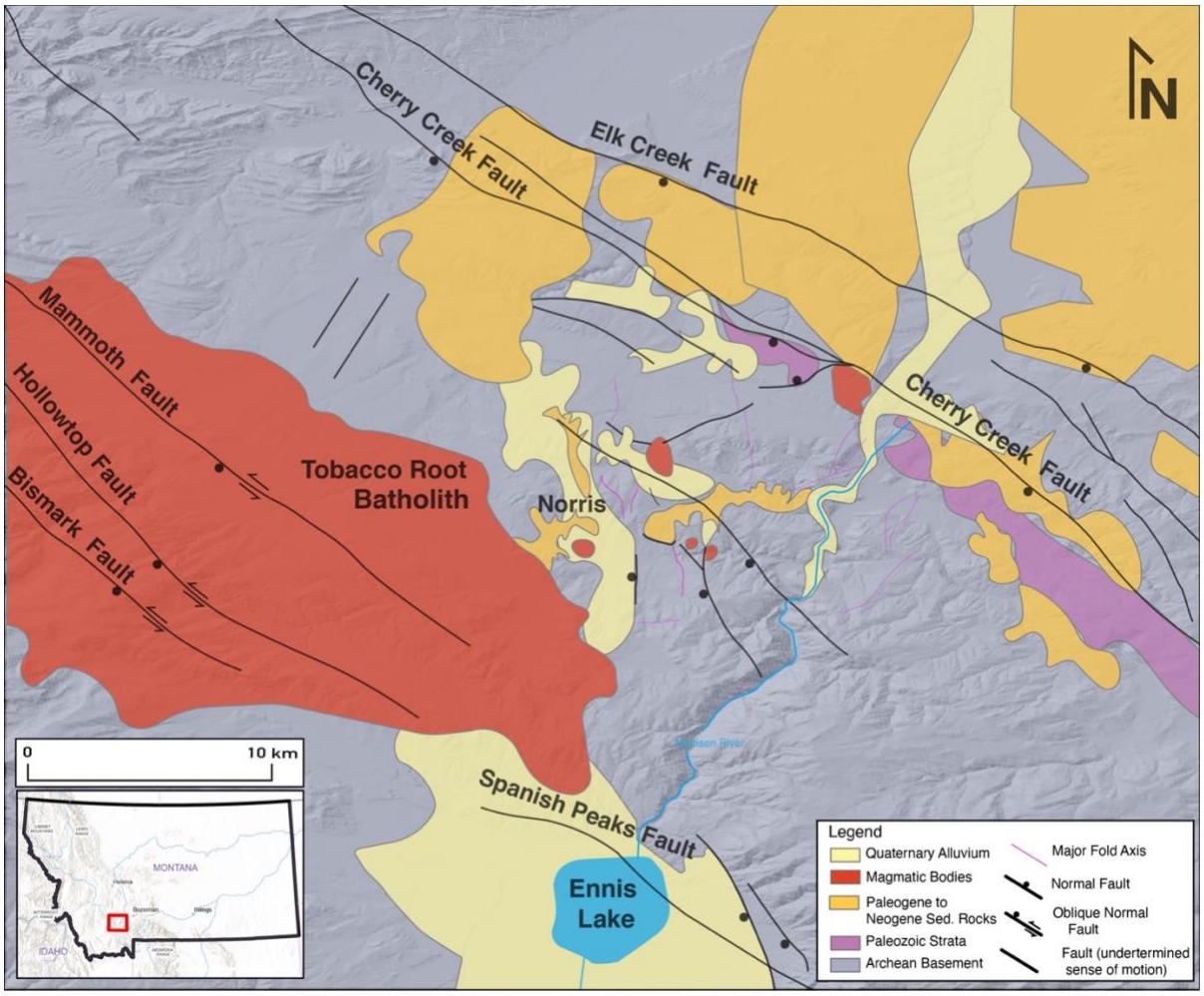

Figure 4. Regional geologic setting of the Norris Hot Springs. Norris, MT lies on an uplifted basement block with minor surficial cover. NW structural grain defined by reactivated Laramide faults and oblique normal faults.

It has been hypothesized that the geothermal system feeding Norris Hot Springs is structurally controlled and that critically stressed faults are providing fluid mobility (Chadwick

& Kaczmarek, 1975). High resolution (1:12,000) geologic mapping and 3D modeling of the structural geometries will provide insight into which structures are controlling the geothermal systems. This hypothesis will be tested by documenting the geometry and occurrence of thermal features in the shallow subsurface and relating these to the interpreted structural geometry in detailed geologic map and 3D block models. I opt to use modeling to test our hypotheses because many data types can be incorporated into the final product. Structures can be projected into the subsurface based on field observations, earthquake data and common structural assumptions. Stress analysis can then be completed to understand which faults are critically stressed. Here, I supplement field and modeling results with optical and thermal UAV imagery of the surface surrounding the hot springs and key faults. Characterizing the surface expression of the system allows for examination of possible spatial correlation between fault traces and outflow. Norris Hot Springs provides a location for a case study of structural control on a geothermal system and to provide insight into the application of our methods to other locations.

Modeling

In the past ten years, the United States Geological Survey (USGS) has recognized the necessity of resources for geological, hydrogeological, and biological modeling and visualization in three dimensions (3D) (Jacobsen et al., 2011). Representing various types of data from all fields in multiple dimensions is often more intuitive for untrained users and makes accessing and understanding information more accessible. These types of models can incorporate vast amounts of data in different formats (Jones et al., 2009; Thornton et al., 2018; Wu & Xu, 2004). Visualizing physical science data in 3D dimensions is intuitive and allows for easy overlay of

various data types. It also eliminates the need for a trained user, and often simplifies understanding structural or stratigraphic complexities in geologic cases (Turner, 2006).

Understanding features in three dimensions is essential for interpreting the subsurface geology and provides more information than traditional methods like geologic maps and cross sections. Specifically for studying geothermal resources, combining field observations with remote sensing, well/borehole, and seismic data provides the most holistic characterization and is the natural advancement for PFA (Faulds et al., 2016, 2017; Siler et al., 2019; Siler & Faulds, 2013; Siler & Pepin, 2021b). Modeling can be conducted in prepackaged modeling products or constructed in a programming language. There are pros and cons to both. For example, many modeling software packages offer integrated data analysis, but licenses for these products can be cost prohibitive. Alternatively, writing a model from scratch in a coding environment can be more work intensive at first but offers enhanced versatility and adaptability.

Geologic block models are common in mining and oil and gas industries because they combine and visualize several important data types. They work well for geothermal exploration as well. Identifying and describing fault and fracture networks are important factors in locating productive geothermal systems. Block models can visualize fault systems to observe stratigraphic offset and interactions at depth, information that is important for locating potential geothermal resources. Data from boreholes or seismic imaging can provide additional constraints for these models. Determining the stress states of these faults is equally important. Stress analyses can be conducted in these block models because the faults are oriented, and a stress state can be projected onto the entire block. Using a block model is the most comprehensive technique for visualizing and analyzing all aspects of a geothermal system.

Geologic Applications of UAVs

Development and accessibility of uncrewed aerial vehicles (UAVs), henceforth drones, have advanced significantly in the past 20 years. Micro-UAVs, popularly known as drones, are vehicles that often have more than two propellers and are outfitted with a GPS system and the ability to attach a variety of sensors. They are most used for aerial photography and videography but are frequently assets to earth science research (Kuenzer & Dech, 2013; Mullen et al., 2022; Neale et al., 2016; Villarreal et al., 2022; Westoby et al., 2012) . Recent developments in drone and sensor technology have increased accessibility and affordability. These systems collect premier imagery due to enhanced maneuverability, stability, and control compared to satellite or planes (Jordan, 2015). Drones can also survey areas inaccessible by foot such as natural disaster sites or hazardous geothermal terrain. Data collected by drones can be transferred with telemetry during flight or by uploading data after the flight is completed. Several products and services are available for post-processing imagery and Structure from Motion (SfM) photogrammetry. SfM is the process of estimating the 3D structure of a scene from a set of 2D images. In combination with SfM techniques, imagery obtained with UAVs through a variety of sensors let geologists create accessible products like digital surface models (DSMs) or virtual rock outcrops (Westoby et al., 2012). A wide range of available sensors allow for UAVs to be used for multiple applications in earth science.

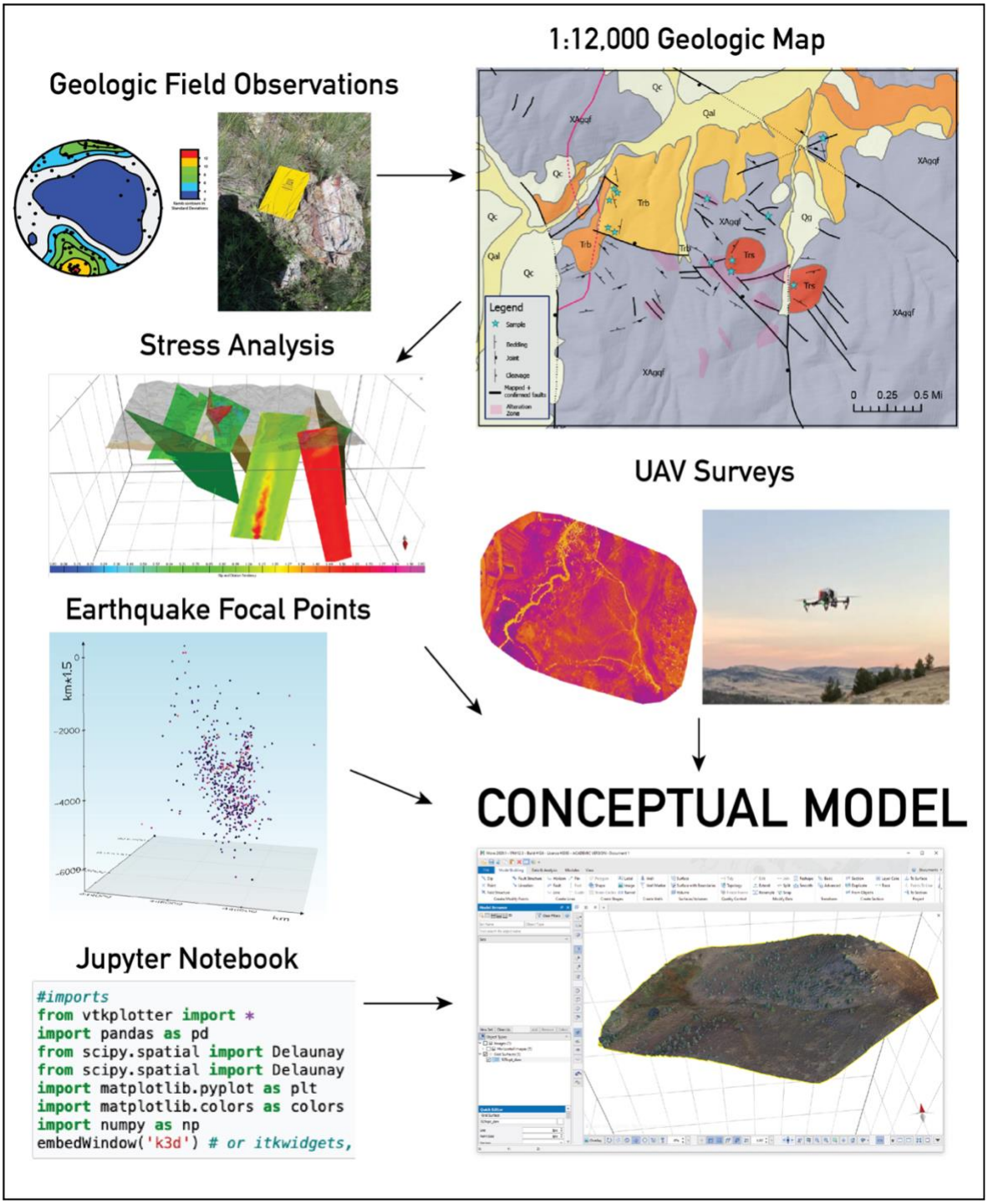

Figure 5. Conceptual workflow for a comprehensive structural model for the Norris Hot Springs and linked geothermal system. Combining traditional and novel techniques provide new insight into the controls of the geothermal system.

UAVs survey geothermal hotspots to monitor activity, identify areas for exploration and investigate structural control on geothermal systems (Haselwimmer et al., 2013; Jordan, 2015; Neale et al., 2016). Drones are particularly effective because of two reasons: LiDAR sensors can detect miniscule fault movement and UAVs can be outfitted with thermal cameras. With SfM, these two types of imagery can be rendered in two or three dimensions to be used as base maps or digital surface models, respectively. Drones are excellent for reconnaissance field mapping and aerial surveys which serve as the foundation for linking structural features with thermal features (Harvey et al., 2016; Walter et al., 2020). Our results suggest that the Norris geothermal system is structurally controlled, and I can gain insight into the subsurface using structural mapping, ground observations, and UAV remote sensing.

Geologic Setting

The study area is a portion of the USGS 7.5' Norris quadrangle located in southwestern Montana. It lies in an area formerly known as Norris Hills, immediately to the east of the town of Norris, MT. This region has undergone a complex deformational history dating back to the Archean (Condit et al., 2015; Foster et al., 2006; Harms et al., 2004; Kaempfer et al., 2021; Ronemus et al., 2023). North America is comprised of several ancient crustal blocks and several accreted terranes and juvenile magmatic rocks (Decelles, 2004) . Laurentia, the ancient core of North America, began to amalgamate during the Paleoproterozoic (Whitmeyer & Karl E. Karlstrom, 2007). The collision of the Wyoming (>2.5 Ga), Superior (>2.5 Ga), and Hearne-Rae (2.7-1.8 Ga) cratons was termed the Trans-Hudson Orogeny (2.0-1.8 Ga) (Mueller & Frost, 2006). Crystalline basement rock exposed at Norris is a part of the original Wyoming Craton (Harms et al., 2004). Laurentia experienced several additional orogenies to form today's stable

North American Craton (Mueller et al., 1993). Notably, the Big Sky Orogeny (1.7Ga) deformed rocks in present-day Wyoming and Montana (Harms et al., 2004).

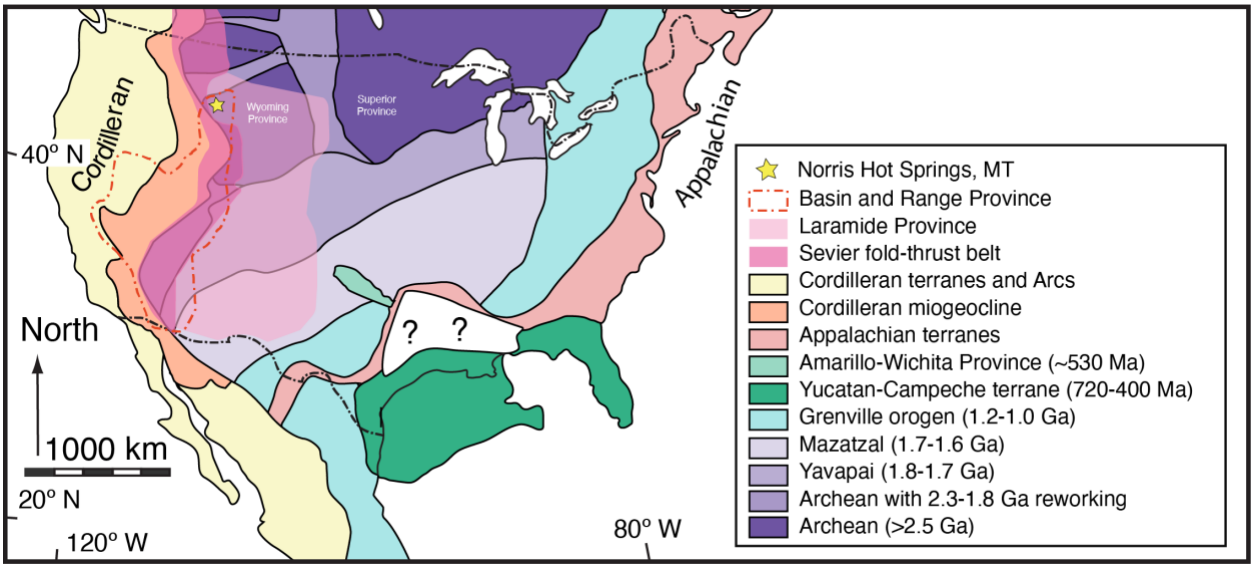

Figure 6. Major tectonic provinces of North America adapted from Laskowski et al., 2013. Norris, MT is located on a portion of the Wyoming craton that has been deformed by both Laramide structures and Basin and Range style structures.

By the late Jurassic, the western boundary of the North American plate reorganized into a cohesive east dipping subduction zone and the formation of a Cordilleran style orogenic system was underway (Decelles, 2004; Snoke & Chapman, 2021)**.** Crustal thickening associated with the Cordilleran retroarc fold-thrust belt was accommodated during Sevier and Laramide orogenesis (Blackford et al., 2022; Yonkee & Weil, 2015). Laramide orogenesis is associated with steeply dipping basement involved reverse faults, henceforth Laramide faults (Carrapa et al., 2019; Erslev & Koenig, 2009). A late Cretaceous inboard sweep of Cordilleran associated magmatism emplaced plutons far to the east, including the Boulder Batholith outside Butte, Montana, and the Tobacco Root Batholith just west of Norris, MT (Scarberry et al., 2021). Magmatic ore bodies and coeval lode deposits are present at each of these batholiths (Reed & Dilles, 2021). Orogenic

collapse of the thickened crust began at about 49 Ma likely because of a rapid decrease of plate convergence rate at the continental margin (Constenius, 1996; Decelles, 2004). A phenomenon observed frequently in southwestern Montana are reactivated Laramide compressional structures accommodating extensional collapse. Post-Laramide Eocene-Oligocene Continental collapse was accompanied by a flare up of bimodal volcanism in the Mesozoic (Scarberry et al., 2021). Continental equilibrium was restored ca. 20 Ma and was relatively stable until the onset of Basin and Range style extension (Constenius, 1996; Snee & Miller, 2022). Basin and Range style extension is exemplified best in the Great Basin of Nevada**,** but evidence suggests the same structural style extends into southern Idaho and southwestern Montana (Reynolds, 1979)**.**

Previously catalogued structural history in Norris includes the events discussed in the prior paragraph. Kellogg documents several distinct phases of folding in the crystalline basement rock. First,

> "a stretching parallel to the axial direction (F1), a folding transverse to the direction of tectonic transport, producing large-scale, isoclinal to tight folds (F2) and late km-scale gently warping fold (F3)."

Periods of rapid strain are indicated by small zones of high temperature ductile shear. These outcrops are highly mylonitized L-S tectonites and are locally exposed in the Norris quadrangle. In some areas, basement rock is cut by quartz veins and silicified. This alteration is associated with phases of mineralization from the emplacement of the Tobacco Root Batholith. Two rhyolite vitrophyres are notably not altered or foliated, although both exhibit flow banding and evidence of faulting.

A complete report of hot springs and thermal features was completed in 2000 by the Montana Bureau of Mines and Geology (MBMG) (Metesh, 2000). This report catalogs many potential geothermal resources, especially in west Montana. Temperatures of thermal wells vary

widely, but hot springs temperatures > 50℃ cluster in the southwestern portion of the state and extend northwest through the Northern Rocky Mountains. Most geothermal systems in Montana are amagmatic and likely structurally controlled (Chadwick & Leonard, 1979).

The study area is centered on the southern block of a three-block horst and graben fault system (Carl, 1970). The two primary faults associated with this system are the Elk and Cherry Creek faults; both are oriented NWSE and regional scale. The Spanish Peaks fault to the southeast of the study area is suspected to be the southern bound of the third block but does not extend down dip of the Elk and Cherry Creek faults. The Elk and Cherry Creek faults are reactivated Laramide structures with down to the southwest normal movement in the Cenozoic (Andretta & Alsup, 1960; Haller et al., 1994). Basement rock exposed in the study area was previously uplifted by these Laramide structures and remains exposed today. The Spanish Peaks fault system is also a reactivated Laramide structure, but its Cenozoic displacement is down to the northeast (Garihan et al., 1983). Minor faults formed and accommodated stress throughout the late Cenozoic (Stickney & Bartholomew, 1987).

The Norris area was formerly known as the Lower Hot Springs Creek mining district, and much of the previous geologic work is exploration oriented (e.g., Thurlow, 1941). Previous work is comprised of guides and papers focused on mineralization and alteration of the Lower Hot Springs mining district highlighting productive veins in the area. Mining in the area was focused on lode type gold mining, with accessory phases of silver, galena, and assorted sulfides (Thurlow, 1941). Mines produced within the last two centuries. There were six separate claims, but the most profitable was the Boaz Mine, which raked in over two million dollars' worth of

gold (Thurlow, 1941). There are still active claims, and residual evidence of mining activity is present and exposes fault planes across the area.

Additional previous work includes several master's theses (Peterson, 1984; Thurlow, 1941) focused on the geothermal area from geophysical and economic perspectives, respectively. The USGS and MBMG have both conducted statewide investigations of hot springs geothermal areas of interest (Chadwick & Kaczmarek, 1975; Chadwick & Leonard, 1979; Gunderson, 2012). The Bozeman 1:100,000 scale geologic map, which encompasses the larger-scale Norris quadrangle, has most recently been updated by Vuke and others in 2014. The 1:24,000 scale Norris quadrangle geologic map was updated in 1994 by Kellogg. Andretta and Alsup (1960) have also produced a detailed road log of the area.

The geologic history of southwestern Montana exposed at Norris is complex. Many structural trends developed as early as the Paleoproterozic with the consolidation for Laurentia (Janecke, 2007). Formation of the North American Cordillera resulted in crustal thickening and the emplacement of magmatic bodies in Montana, before the subsequent collapse of the so called Nevadaplano (Constenius, 1996). Extension accommodated by Basin and Range structures continues to the present. Previous work investigates geothermal resources throughout the state, but here I complete a comprehensive study and geologic model of the Norris Hot Springs and associated geothermal system.

Methodology

Field Mapping

A detailed map of a portion of the Norris 7.5' quadrangle was constructed over 30 days of fieldwork throughout the 2022 summer season. Approximately 300 structural data points were

collected including bedding, foliation, jointing, and fault measurements. Measurements and photographs of key features were collected and recorded using the iOS application Field Clino on an iPhone 12 Mini. Plane and lineation orientations collected using the iPhone were compared to measurements recorded with a Brunton compass for the first 50 measurements to ensure accuracy. Stratigraphic contacts, faults, veins, and prospecting pits were mapped directly onto aerial imagery derived from the UAV flights. Field data was exported from the application into Excel for categorization and imported into Esri ArcGIS Pro for visualization and analysis. Structural data was used to derive stress states and produce cross sections that were later incorporated into geologic block models. Several samples were also collected for zircon U-Pb geochronology and petrographic analysis.

U-Pb Geochronology

Several samples were collected from the Red Bluff Unit ($P_E$rb) to provide an upper limit on faulting around the hot springs. Sample locations were recorded in the same manner as orientation data to maintain uniformity. Zircons were separated from ~3.0L of bulk samples using jaw crusher, sieving, Frantz magnetic separation, and density separation and hand picking. Zircons, n=81, were mounted in epoxy and sent to California State University, Northridge (CSUN) to be analyzed as a part of the National Science Foundation-funded PLASMA Institute.

The sample was imaged on a Gatan miniCL detector attached to a FEI Quanta 600 SEM. CSUN's PLASMA lab uses a Teledyne Cetec Analyte G2 Excimer Laser and a ThermoScientific Element2 SF-ICPMS to measure uranium-lead isotopes. Spots were selected by consulting the CL images to avoid metamorphic rims. Laser beam diameter was ~25 microns, and each analysis consisted of a 20 second integration and an additional 20 second delay to stop and move the

beam. Ablation pits measure ~20-30 microns depth. ^{202}Hg, ^{204}(Pb+Hg), ^{206}Pb, ^{207}Pb, ^{208}Pb, were measured in counting mode, while ^{232}Th, and ^{238}U were measured in analogue mode.

Analytical results were processed by the PLASMA Lab in Iolite. Dates were calculated using IsoplotR (Vermeesch, 2018). Maximum depositional ages (MDA) were determined using two methods: youngest grain cluster within two sigma (YC2σ) and youngest statistical population (YSP) (Dickinson & Gehrels, 2009). I also calculated maximum likelihood age (MLA) to avoid the younging bias described by Vermeesh (2021).

UAV Remote Sensing

UAV imagery was used to supplement fieldwork and geologic models. This method was selected over plane or satellite imagery because UAVs are high precision and can execute predetermined flight plans to obtain optical and thermal imagery at much lower price. DJI Inspire 1 v.2.0 drone was used for all flights that produced usable thermal imagery and most optical imagery. A Mavic 2 Pro was used for several additional flights. Either drone was equipped with a DJI Zenmuse X3 and a Zenmuse XT for optical and thermal imagery, respectively.

There were two phases of drone flights: reconnaissance and thermal mapping. For both, flight plans were created in Pix4Dcapture to ensure 80% image capture overlap at 250 ft elevation necessary to do Structure from Motion (SfM). Additionally, the camera was pointed 90 degrees down, and the drone was set to move “slow +” and took images on safe mode, meaning the drone would come to a complete stop before capturing an image to reduce image distortion. At least 15 satellites were being used for GPS location during each flight. Reconnaissance flights occurred from August to October between 10am and 1pm and focused on collecting optical

imagery to generate digital surface models of key outcrops and the area of the hot spring outflow. Agisoft Metashape and Pix4D processed the imagery and produced orthomosaics and models with SfM. The optical orthomosaics also served as a base map for field mapping and comparing topographic features with previously mapped geologic features.

After key areas of interest were identified, the drone was outfitted with a thermal camera to survey surficial temperature anomalies. All thermal flights were flown in September 2022, before dawn to minimize environmental and solar impacts. Thermal cameras can either record exact ground temperature or record qualitative differences. This study opted for qualitative temperature changes for several reasons. Primarily, researchers hoped to identify a thermal anomaly, although the absolute temperature of such an anomaly is outside the scope of this project. Additionally, quantitative thermography is more expensive and requires black body reference points. Therefore, qualitative thermal differences served the purposes of this study adequately.

Initially, thermal imagery was processed using Pix4Dmapper thermal processing presets and camera specific specifications, but photogrammetry often resulted in distorted imagery. DroneDeploy is a web-based photogrammetry service that produced satisfactory results. Another benefit of DroneDeploy is that it produced digital surface models and thermal models simultaneously, though the digital surface models from thermal imagery are often more distorted than those produced by optical imagery analysis. These images and models were used to identify thermal anomalies and investigate correlation to structural features.

Modeling

Two different modeling approaches were utilized: a prepackaged product called Petex Move and an open-source Jupyter Notebook. Modeling efforts focused on describing fault orientations and relationships because of the primarily homogenous lithology around Norris, MT. Local lithology is limited to Archean basement rock, small volcanic plugs, and surficial deposits of varying depositional style and age. Fault offset cannot be determined from stratigraphy and field observations suggest the geothermal system is entirely hosted by basement rock, so lithology is irrelevant. Instead, the models focus strictly on fault networks, topographic expressions, and stress analysis. After reviewing the available software packages, Move by Petroleum Experts was selected to create 3D structural models of the area because of its inherent analysis capabilities and academic licensing. Field data was incorporated into twenty-three cross sections to constrain fault planes to depth. In a Petex Move cross section, a fault is represented by a line. When a grid of cross sections is imported into the Move software, Move uses a spline interpolation to create a mesh by connecting all the "lines" into a 3D fault surface.

Two Petex Move models were created, one where fault dip did not change and one where dip shallowed at depth to anticipate any results of any listric faulting. Move includes built in analysis modules for 2D and 3D modeling. A stress analysis based on a user determined state of stress was completed. The stress analysis module computed current day slip and dilation tendencies along faults and was used to explore potential paleo stress scenarios. Regional stress data was derived from local joint sets and gravitational studies (Faulds, 2012; Wisian et al., 1999). The Move models were successful, but several shortcomings in the 3D mesh interpolation and desired output inspired additional model building with alternative methods.

As resources for programming become more widely accessible, many earth scientists advocate for the integration of this near endless repository of knowledge into the earth sciences (e.g., de la Varga et al., 2019; Martin et al., 2022; Rounce et al., 2020). Utilizing open-source resources and promoting open-source science also fosters diversity and inclusivity in science. NASA states, “Open-source science requires a culture shift to a more inclusive, transparent, and collaborative scientific process, which will increase the pace and quality of scientific progress”. With this in mind, I also attempted to reproduce the geologic models in Python, using a Jupyter Notebook. Python is a free, accessible coding language and can be used in Jupyter Notebooks. Jupyter Notebooks are accessible formats for producing and publishing clear, readable, highly commented code.

This method heavily depended on two Python packages: VTKPlotter and vedo. Vtkplotter is a module designed for easy analysis and visualization of 3D objects and point clouds based on Visual Toolkit (VTK) and Numerical Python (NumPy) (Musy et al., 2019). These methods are adapted from Ahinoam Pollack’s GitHub repository (https://github.com/ahinoamp) for creating a geothermal model of a FORGE location, which is also featured in VTKPlotter documentation.

To extract data for this model, the new 1:12,000 map (Fig. 10) was digitized into an Esri ArcPro.aprx file. X, Y, and Z coordinate points of each fault trace were scraped from the fault shapefile and underlying DEM using a geoprocessing toolbox. Average dip from each fault was used to extrapolate the coordinate points into the sub surface.

$$\begin{bmatrix} X_{surface} \\ Y_{surface} \\ Z_{surface} \end{bmatrix} + \begin{bmatrix} X_{surface} + fdepth(\tan(90 - dip)) \\ Y_{surface} + fdepth(\tan(90 - dip)) \\ -fdepth \end{bmatrix} = \begin{bmatrix} X_{subsurface} \\ Y_{subsurface} \\ Z_{subsurface} \end{bmatrix}$$

This calculation can be iterated as many times as necessary to increase density of control points for interpolation of fault surface from a point cloud. The finalized set of values for each faults surface coordinates and subsurface terminating coordinates were saved as individual comma separated values (CSV) files and uploaded to a GitHub repository. Additional data was also saved in the repository, including topographic and isotherm elevation data and earthquake focal point.

A Jupyter Notebook was created and required packages were imported. CSVs containing values for the Norris digital elevation model, faults, and isotherms were read into the Jupyter environment using the Pandas (pd) package.

```
#import data

url = "https://raw.githubusercontent.com/mwafe/norris/master/"

NorrisDEMPD = pd.read_csv(url+"norris_dem.csv")
isothermPD = pd.read_csv(url+"75isotherm.csv")


normyPD = pd.read_csv(url+"normy.csv")
hotspringPD = pd.read_csv(url+"hotspring.csv")
rangebounderPD = pd.read_csv(url+"rangebounder.csv")
carmichaelPD = pd.read_csv(url+"carmichael.csv")
cherryPD = pd.read_csv(url+"cherry.csv")
creekPD = pd.read_csv(url+"creek.csv")
forkPD = pd.read_csv(url+"fork.csv")
sblockPD = pd.read_csv(url+"sblock.csv")
trbPD = pd.read_csv(url+"trb.csv")

quakesPD = pd.read_csv(url+"quakes.csv")
```

Figure 7. Code snippet from the Norris.ipynb Jupyter Notebook showing the functions used for extracting data from the GitHub repository.

After the CSVs are loaded into the workspace, each feature can be expressed as a point in a point cloud in 3D space, allowing for the interpolation of surfaces through these point clouds. The Vtkplotter package includes a tool for extracting meshes from point clouds using a Delaunay triangulation, “delaunay2d”. The Delaunay triangulation is a type of interpolation based on

nearest neighbors of a given point cloud. This permitted more control over the dip and expression of the fault surfaces than the Move function because they were interpolated over a grid of points instead of several lines, i.e., with more control points. However, the projection into the subsurface is determined from field data and typical structural geometries. There are no subsurface constraints. Move was also constricted by the need to express faults as graphical lines, whereas the point clouds, and therefore fault surfaces, can be described mathematically.

```
In [4]: #Set up land surface

        NorrisDEM = delaunay2d(NorrisDEMPD.values)


        # in order to color it by the elevation, we use the z values of the mesh
        zvals = NorrisDEM.points()[:, 2] #select all rows in column with index o
        NorrisDEM.cmap("terrain", zvals, vmin=1100)
        NorrisDEM.name = "Norris DEM" # give the object a name

In [5]: #Isotherm mesh
        isotherm = delaunay2d(isothermPD.values)
        isotherm.name = "75C temperature isosurface"
```

Figure 8. Code snippets showing conversion of CSVs to mesh surfaces using Delaunay 2D.

This function was also used to render surface topography and subsurface isotherms. Earthquake focal points plotted in this model to examine geometric distribution between mapped faults and any trends in earthquake space. The user can examine the interaction between mapped faults and earthquake focal points. The final model is a Jupyter Notebook script that produces an interactive python window.

Results

Field Observations

As part of my field observations, I updated a portion of the existing geologic map (Kellogg, 1994) and increased the resolution from 1:24,000 scale to 1:12,000 scale. Crystalline basement rock is the predominantly exposed rock type in Norris, MT. It is primarily comprised of a moderately foliated quartzofeldspathic gneiss with several metabasaltic intrusions and mylonitized zones, indicating rapid strain. Approximately one km southeast of Norris Hot Springs, the basement has been intruded by two dark gray flow banded rhyolite vitrophyres. Notably, these outcrops are not altered, suggesting they postdate mineralization.

The Red Bluff Formation ($P_E$rb) is a Tertiary surficial deposit that caps a cliff overlooking a paleo valley of the Madison River and is separated into two members, distinguished by outcrop style and clast size. The basal unit is described as a boulder conglomerate with an original thickness of under 30m. The matrix has weathered away, leaving behind a boulder field of primarily basement rock and Tobacco Root Batholith. The upper $P_E$rb unit is a dark red, strongly indurated litharenite breccia. Although the upper $P_E$rb is well-bedded, beds are laterally inconsistent or lenticular.

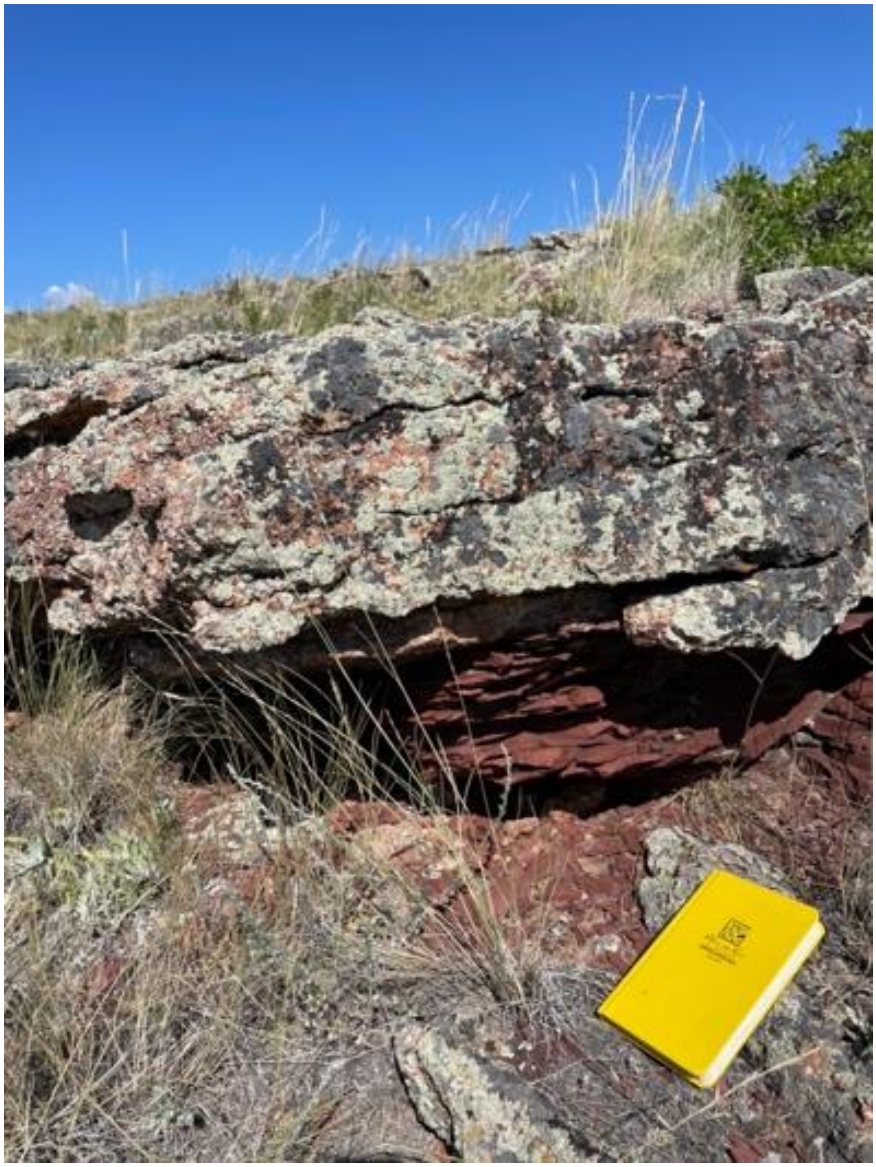

Figure 9. Irregular bedding of the Red Bluff Formation. Grain size of the upper bed ranges from coarse sand to gravel and is matrix supported, while the lower bed has a siltstone texture.

Grain size varies significantly between beds from gravel to silt (Fig. 9). PErb displays no primary porosity or permeability at the outcrop scale and is strongly indurated closer to hot springs activity, suggesting silicification from geothermal waters. This unit is typically exemplified by a change in soil color, from the light beige of the basement rock to a brick red.

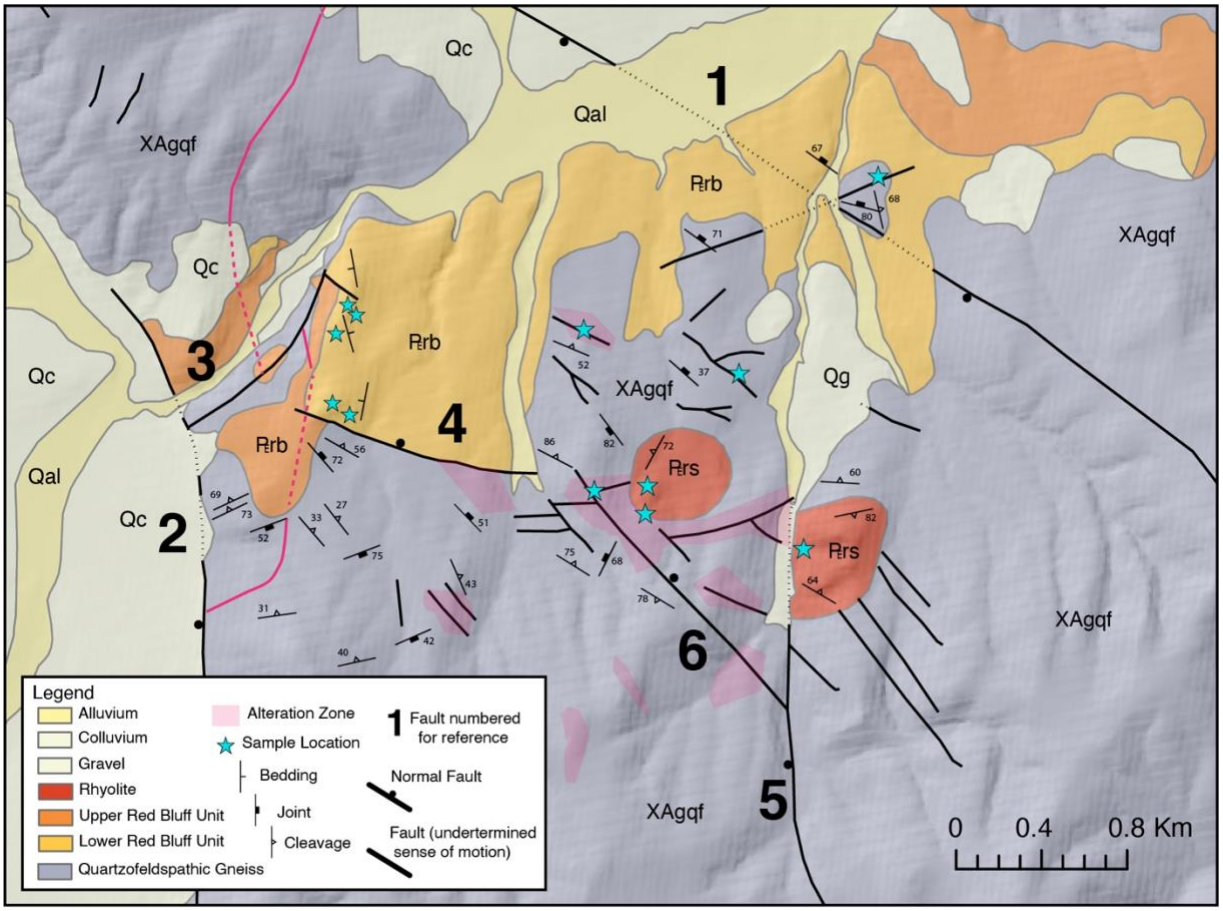

Figure 10. New 1:12,000 scale geologic map of the study area outside of Norris, Montana. Faults are numbered for reference.

Normal faulting is the dominant modern structural regime, but many subsidiary faults with indeterminate senses of motion are exposed in the study area. Fault 1 (Fig. 10) is the most laterally extensive fault in this study area. It's measured average orientation is 305, 60 and roughly aligns with the regional structural grain defined by Laramide deformation. Fault 2, located near the western extent of the study area, is a steeply dipping NS normal fault that down drops Quaternary sediment to the west. Fault 3 forks NE off Fault 2, and has limited outcrop, but is evidenced by a break in slope and offset fault hinge. Fault 4 has an average orientation of 288, 25 and likely interacts with Fault 3 at depth. Another steeply dipping NS trending fault, Fault 5,

bisects the southern map area and likely served as the fluid pathway for mineralization. It veers southeast at the southern extent of the map area. Fault 5 forks sharply to the northwest, a segment referred to as Fault 6, that dips east intersecting Fault 5 at depth. Several smaller scale W and NW trending intersecting mineralized faults break off Fault 6. Faults 7-12 trace < 0.5km and are intruded by the eastern rhyolite dome.

Faults offset polyphase basement deformation. I observe a stretching lineation described by Kellogg (1994) (as well as isoclinal fold across the field area. Larger scale folds are locally refolded in key outcrops. Specifically, in the western half of the study area a distinctive anticline extends from just south of the extent of the $P_E$rb to directly north of the town of Norris (S. Vuke et al., 2002).

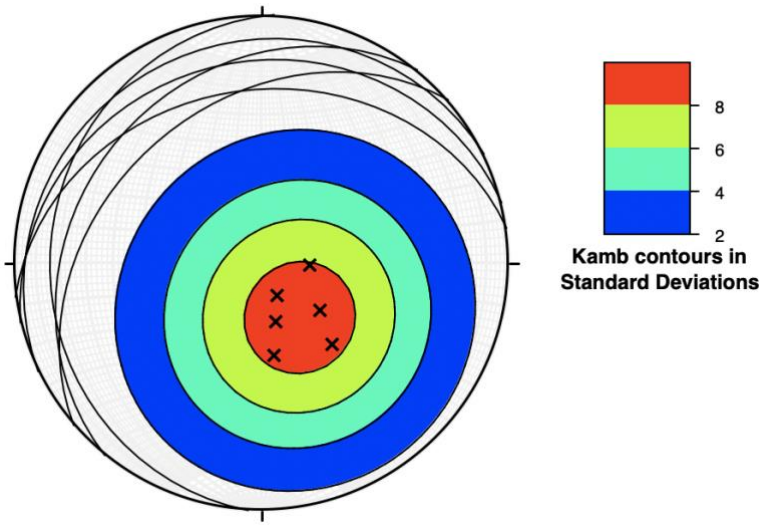

Figure 11. Cleavage planes associated with anticline offset by the Hot Springs. Kamb contours represent the poles to cleavage planes deviation from a normal distribution.

The hinge of a large scale basement fold is briefly covered in a grassy and sediment covered hillslope, and reappears offset, suggesting a blind fault adjacent to the hot spring's

outlet. A break in slope supports the presence of a blind structure. The anticline bisects the fault area at almost precisely the location of the outlet.

Mineralization and alteration are present in or around many relevant structures. There is also evidence of leaching, but it is unclear if the process is naturally occurring or a result of mining activity. Altered quartz veins cut the basement rock throughout the study area. Many of the quartz veins are heavily altered and contain sulfides. These veins often alter and silicify the host rock resulting in several resistant ridges. Rock walls bounding these veins are often striated, suggesting a component of slip on these structures, but the basement homogeneity makes it difficult to quantify offset.

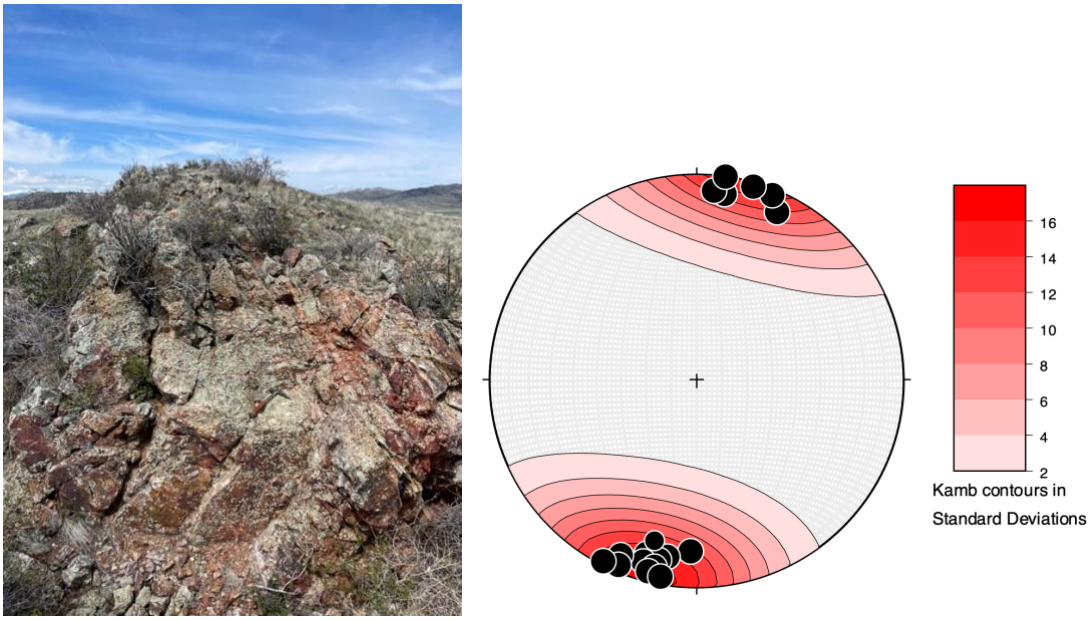

Figure 12. Typical outcrop of fractured, altered basement rock. Accompanying stereonet shows primary joint set in the area.

Joint and fracture data was collected to discern any patterns and to conduct a stress inversion. Age relationships between joint sets are convoluted due to the extremely fractured

nature of most outcrops. The dominant trend strikes NW SE and is nearly vertical (Fig. 12), suggesting a stress state consistent with an NW extensional field.

Although characterizing ductile deformation is outside the scope of this project, F2 fold hinges proved useful for identifying offset in a basement dominated environment. Slickensides suggest slip on abundant quartz veins. Mining activity both destroyed and revealed outcrops throughout the area. NWSE structures are common, but relationships can be convoluted, due to the fractured and low exposure nature of many outcrops. Normal faulting is ubiquitous and likely accommodated past mineralization and geothermal activity.

Petrography of the Red Bluff and U-Pb Geochronology

The Red Bluff formation ($P_E$rb) has not previously been dated or described in depth. Petrographic analysis eliminates $P_E$rb as a potential stratigraphic geothermal fluid conduit. Several thin sections were produced from beds with varying textures of the Red Bluff Unit for petrographic analysis. There is no metamorphic or depositional fabric, but there is abundant brittle fracturing in individual clasts. Clasts are primarily large potassium feldspar grains, sutured quartz grains, or lithics. These are interpreted to be relict grains from the Tobacco Root Batholith and Archean basement, respectively. The matrix is the same material as identifiable clasts and cemented with Fe-oxides.

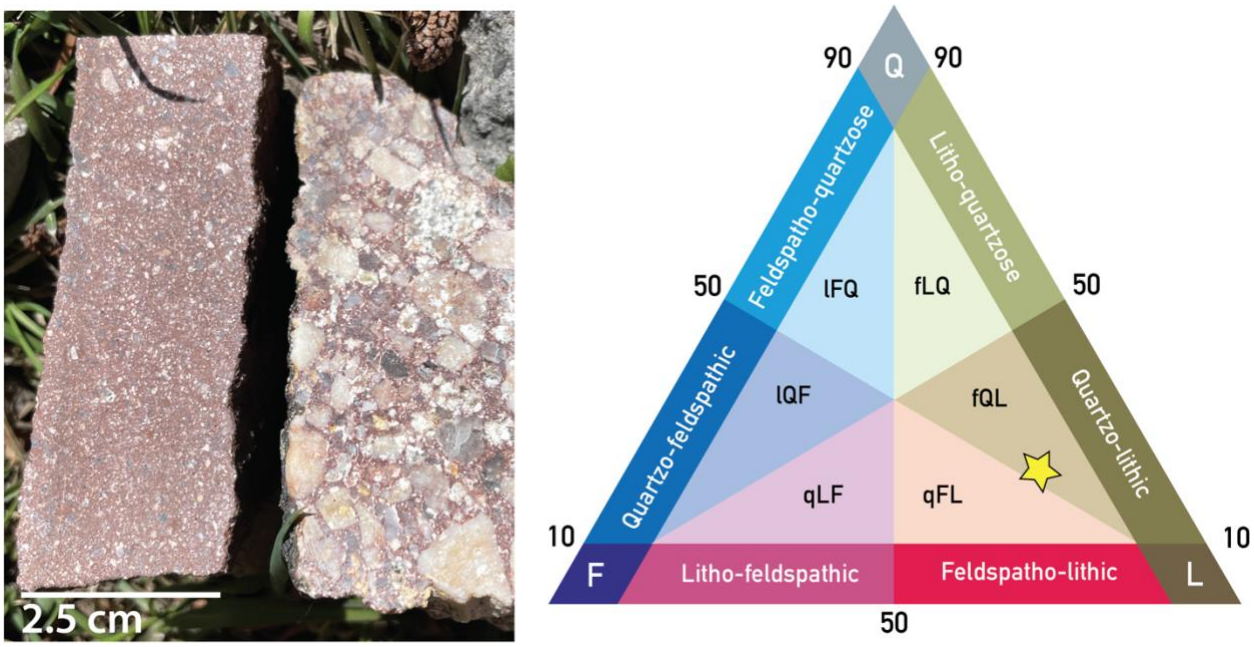

Figure 13. The Red Bluff samples in hand sample from adjacent beds. Dramatic change in range of grain sizes. Point counted sample displayed on ternary diagram (Garzanti, 2019).

All samples, regardless of grain size, display extremely low porosity and negligible permeability. Therefore, permeability at the outcrop scale must be controlled by fracturing and faulting. PErb is cut by several faults, permitting age constraints to be determined with zircon geochronology. The sample was analyzed and interpreted as a detrital sample, n= 78.

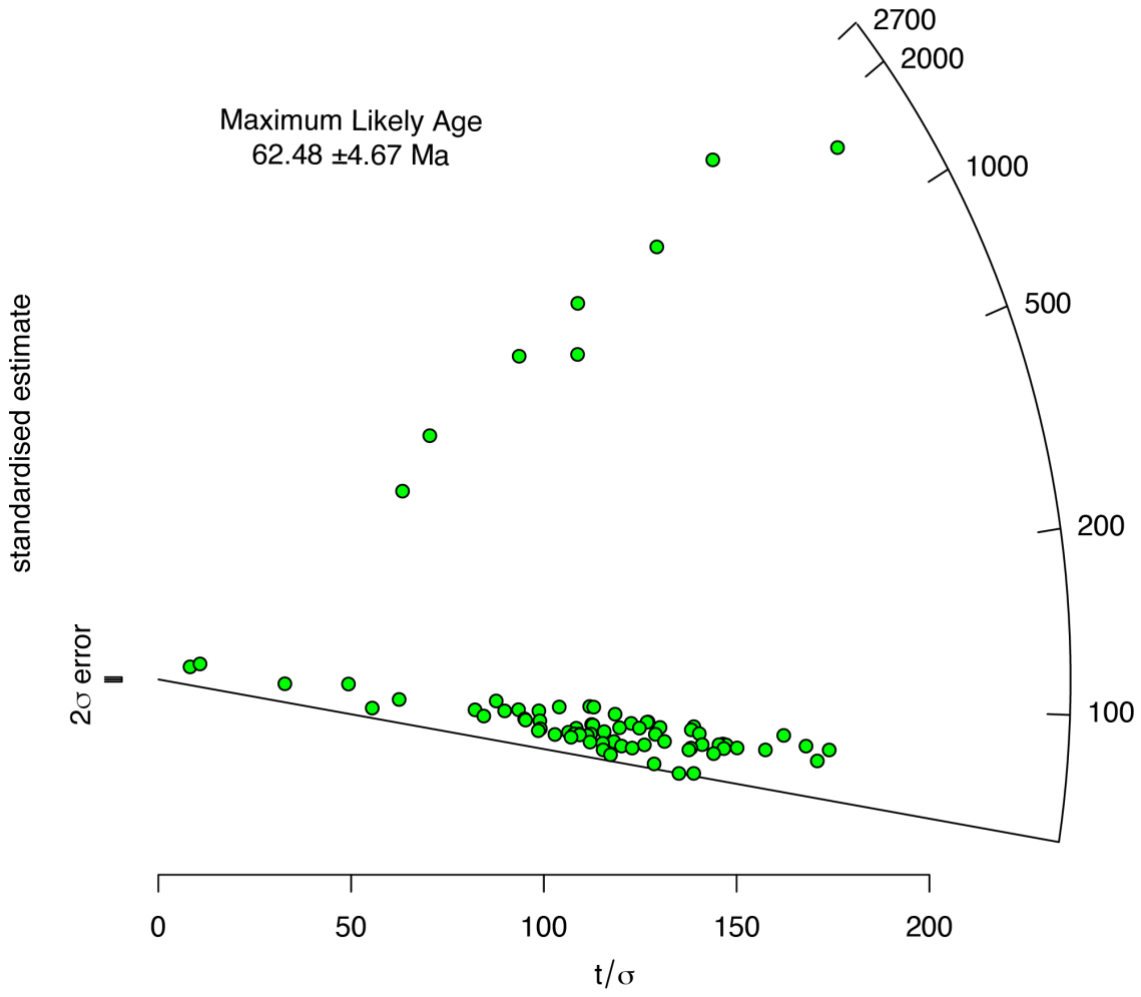

Figure 14. Radial plot from IsoplotR showing MLA of Trb sample. MLA is calculated as 62.48 ±4.67 Ma, which coincides with MDAs of 63.52±0.96 Ma and 62.67±0.63 Ma using YC2σ and YSQ, respectively.

There is significant spread on the dates returned from this sample. Dates clustered between 65-95 Ma, with an outlier population around 2.2 Ga. These ages correlate to periods of magmatism and volcanism in southwestern Montana. The maximum depositional age (MDA) was calculated using the YC2σ and YSP, which yielded MDAs of 63.52 ± 0.96 Ma and 62.67±0.63 Ma

respectively. I calculated maximum likelihood age (MLA) for this sample to be 62.48 ±4.67 Ma (Fig. 14) (Vermeesch, 2021). Systematic error is 1%, or 0.62 Myr.

UAV Remote Sensing

Five reconnaissance optical flights processed in Pix4D produced an RBG orthomosaic and digital surface model (DSM). One flight surveyed an area containing several smaller scale (<50m) features were mapped as faults (Kellogg, 1994). The resulting DSM has an accuracy of under one meter.

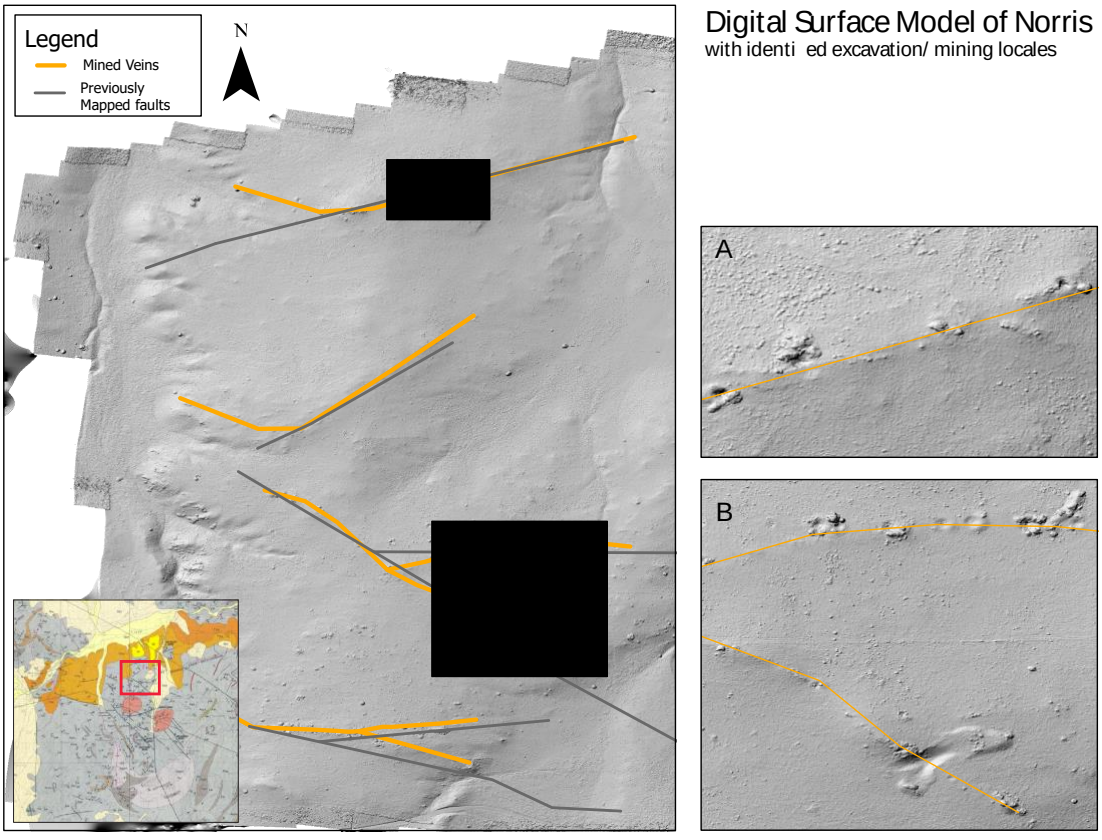

Figure 15. Digital surface models of excavated quartz veins and faults derived from optical UAV flights. Detailed base maps allow for comparison between previously mapped structures and topographic features.

RBG orthomosaics show minimal grassy vegetative cover over a thin soil horizon and bedrock. Digital surface models (DSMs) derived from optical imagery provide more information. Quartz veins have intruded the surface and silicified the bedrock and made it more resistant, resulting in the small topographic ridges visible in the DSM. The DSM also exposes exploration pits along the quartz veins that are more difficult to identify in RGB imagery. Fieldwork determined that slip is difficult to identify or quantify within or next to the quartz veins, but slickensides indicate that slip has occurred along the veins. Mine workers likely identified these quartz veins and exploited the well exposed outcrops, and subsequently destroyed most evidence of faulting. However, occasionally these pits expose distinct fault planes in zones of deformation.

Faults were directly mapped onto the DSM, which served as a base map. Previously mapped faults were overlain to identify discrepancies between field mapping and topographic expression. High-resolution UAV imagery permits more accurate and precise mapping of surficial features. The scale of the published Norris quadrangle geologic map allows associated error, but drone surveys result in more accurate and precise mapping.

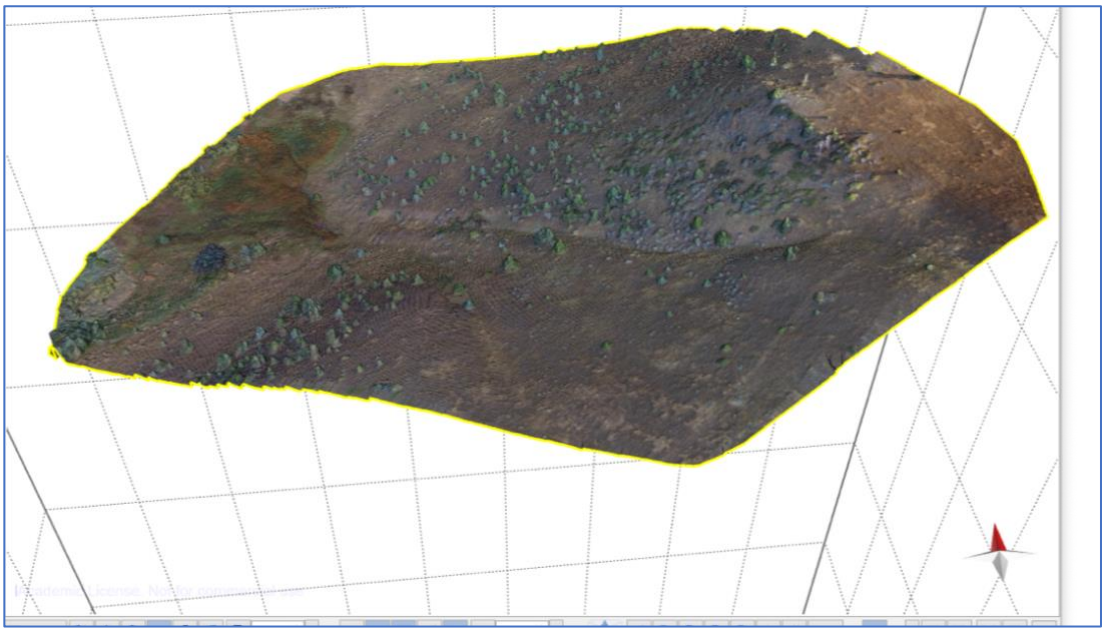

Figure 16. 3D rendering of optical UAV orthoimagery in Move software. The surficial expression of the geothermal system is indicated by the fan like increase in vegetation in the SW portion of the imagery.

Geomorphic features suggest a channel for primary drainage of snowpack just offset from the surficial outflow of the geothermal system (Fig. 16). The extent of the outflow is indicated by vegetation growth on an early-stage alluvial fan. The outlet itself is a singular spring that lies just topographically below a mapped fault zone, to the north of a steep hillslope.

Ten flights were completed focused on collecting thermal imagery of key areas of interest. They provided details about hot spring outflow and attempted to record any additional thermal anomalies. After PiX4D struggled with interconnectivity, additional attempts at thermal image processing proved difficult and outside the scope of this project. Instead, DroneDeploy, a cloud-based photogrammetry service was used to process the thermal imagery.

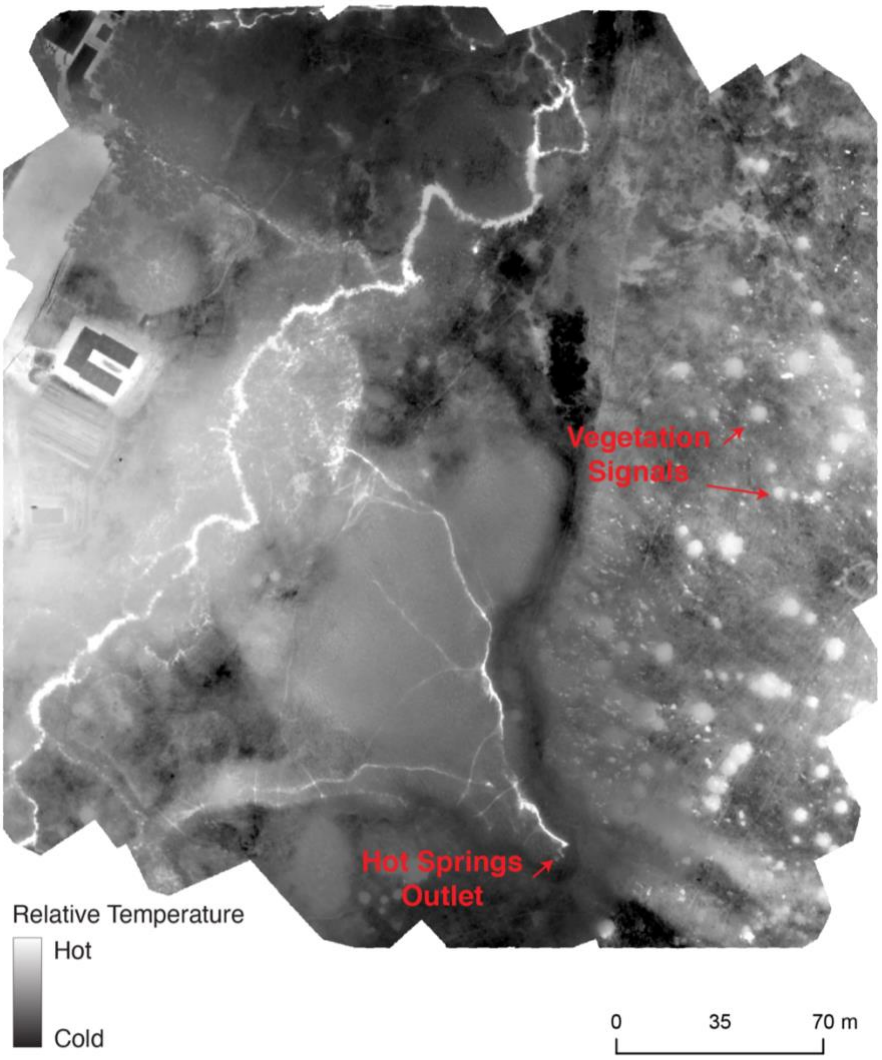

Figure 17. Thermal orthoimage of Norris Hot Springs and the geothermal outflow 10/24/2022.

As seen above, the hot springs outlet and it's drainage pattern into the downslope creek to the North can be seen clearly on thermal imagery. The outlet is the most distinct thermal feature across all flights. Vegetation obscured ground surface thermal anomalies, which require additional analysis. A map was created to classify the imagery from the most complete image.

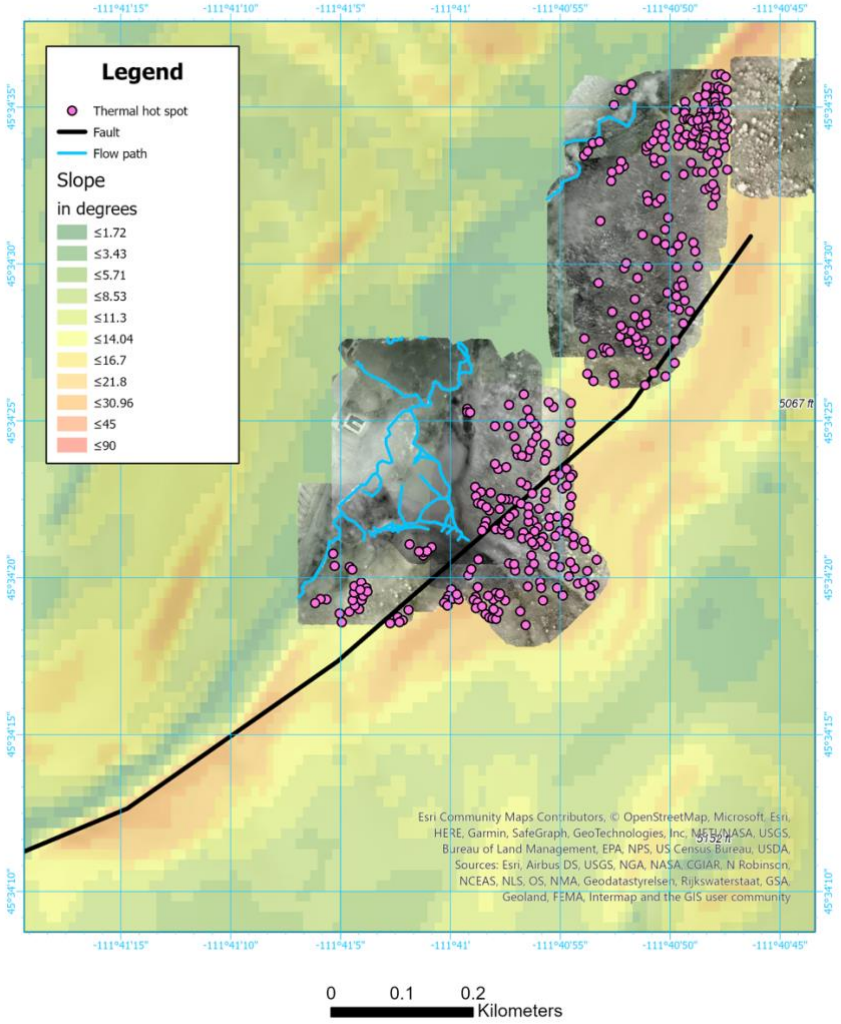

Figure 18. Map of thermal hot spots overlain on a slope map. The break in slope is likely a result of faulting activity. Thermal hot spots are isolated in pink, geothermal outflow is outlined with blue. Almost all point features are likely reflecting vegetation, as opposed to thermal signatures related to the geothermal system.

Using remote sensing to supplement this fieldwork provided invaluable insights. Initial drone surveys revealed key outcrops that may have been otherwise overlooked. High resolution DSMs also allow for remote interpretations of topographic and structural features. Thermal

imagery provides one of the most useful interpretations for geothermal exploration. The hot springs outlet is obscure in the field but can viewed and mapped clearly in thermal images. The outflow imaging shows that there is one primary surficial expression with minor visible ground surface anomalies.

Modeling

Petex Move. The first two geologic block models were produced in Petex Move. Each was constructed from a grid of cross sections with varying fault dip interpretations. Cross section construction utilized strike and dip field measurements. Five-ten orientations were collected for each exposed fault zone to eliminate outlier undulation measurements. Average dip was used in each cross section. The model focused on the area corresponds to the geologic map produced in Fig. 10.

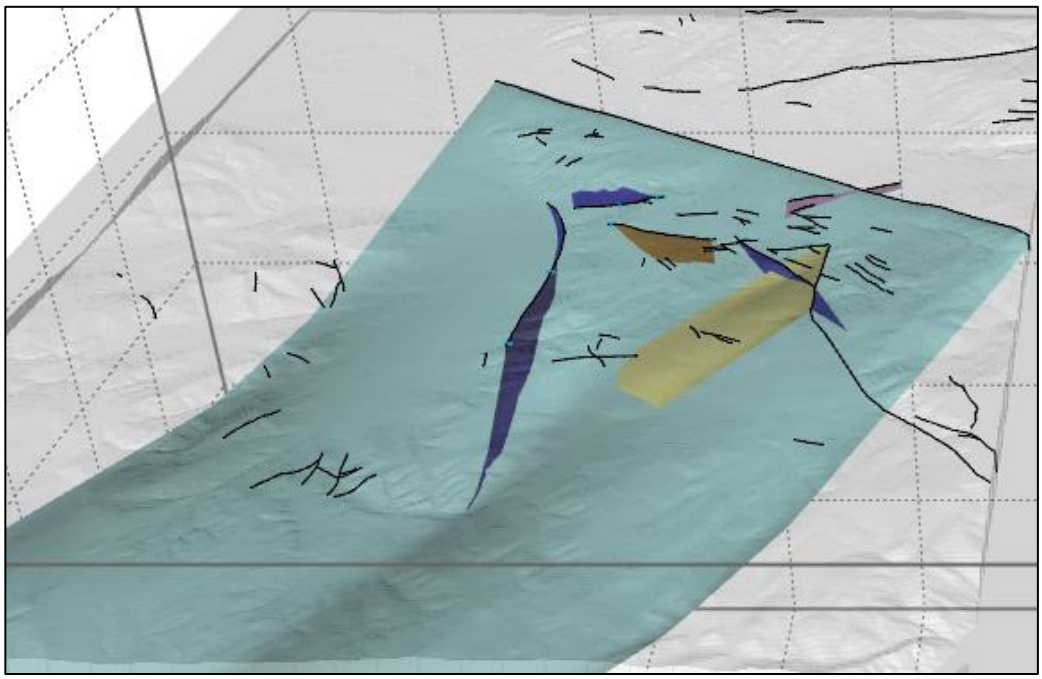

Figure 19. Fault planes visualized in Petex Move prior to stress analysis.

The digital elevation model (DEM) was imported from USGS' Three-Dimensional Elevation Program and served as a base map. Fault traces exported as shapefiles from ArcGIS are visualized on top the DEM in black, and the fault planes are displayed in various colors. Only faults deemed relevant to geothermal activity (either directly adjacent to the outlet, deep enough for appropriate temperatures, or preferentially oriented for geothermal flow) are included as 3D meshes. Move utilizes a grid of cross sections to interpolate the fault surface, meaning the model was constrained by 2-5 lines and used a kriging method to interpolate through the blank space. Less constraints laterally across the meshes resulted in less uniform and inaccurately curved or over shortened or narrowed fault planes. However, the major benefits of using Move are built in analysis functions. The stress analysis function was executed and displayed on all fault places.

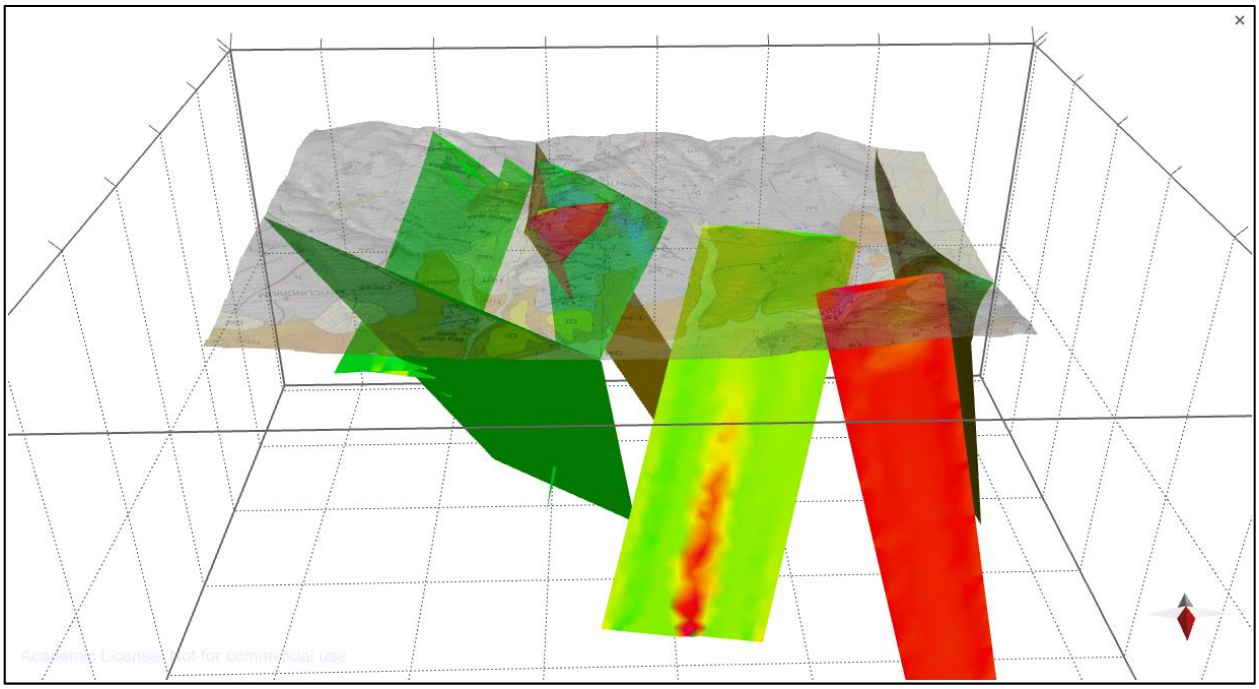

Figure 20. Stress analysis overlain on a preliminary Move model.

I used a regional N45W directed extensional stress state to determine the stress states of each fault. As expected, the “Hot Springs” fault zone, Fault 3, is critically stressed at today’s stress state and displays a high ratio of slip vs. dilation tendencies, suggesting a failure behavior that promotes conduit behavior. I also experimented with paleo stress states, revealing that the older faults could have been critically stressed during mineralization during the Laramide orogeny, when transport was primarily East directed. This visualization makes it simpler to understand subsurface fault interaction and how changing regional stresses may affect stress states of individual faults.

Python script with VTKPlotter + . I decided to explore additional modeling avenues to compare the two methods. I wrote a Python script hosted in a Jupyter Notebook that outputs a 3D model of a portion of the Norris Quadrangle. The notebook is stored in a public GitHub repository (https://github.com/mwafe/norris/) along with all necessary CSV files for reproducibility.

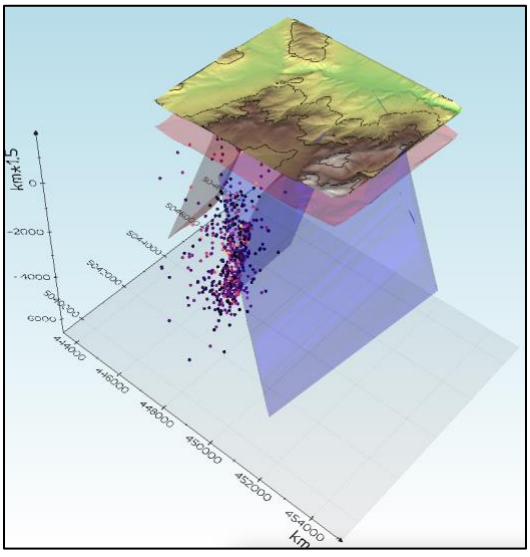

Figure 21. Original iteration of output of the Norris.pynb Jupyter Notebook focusing on faults.

There are two outputs: Model 1 focused on the 1:12,000 geologic map of the study area and Model 2 included regional features that holds greater implications for the stress state of southwestern Montana. Faults were projected at either the average dip measured in the field or 30 or 60 degrees depending on interpreted structural relationships. Fault depths were constrained by seismic data or estimated using likely fault length to depth relationships (Furlong & Handy, 2016).

```
plt += rangebounder.c("blue").opacity(1).flag()
#plt += carmichael.c("blue").opacity(0.3).flag() # problem plot
#plt += cherry.c("blue").opacity(0.3).flag() #problem plot
plt += creek.c("blue").opacity(1).flag()
plt += fork.c("blue").opacity(1).flag()
#plt += sblock.c("blue").opacity(0.3).flag() # problem
plt += trb.c("blue").opacity(1).flag()
plt += quakesPts.flag()
plt.show(viewup="z", zoom=1)
```

Figure 22. Code snippet illustrating plotting faults.

Earthquake focal points are colorized according to their degree of magnitude, with purple representing strongest (M~4). Focal points suggest the minimum depth of major structures. Active seismicity also confirms that there are critically stressed faults close to Norris Hot Springs that are at the necessary depth for the reservoir base temperature.

The second output model which incorporates regional structures reveals that reactivated Laramide structures are preferentially oriented for stimulating geothermal fluid circulation and penetrate to the depths necessary to heat the fluid to the temperatures expressed at the Norris geothermal system. This visualization shows potential scenarios for interactions between deeper structures that control the regional geology of Norris and the smaller scale structures mapped in

this study. Seismicity around Norris confirms large scale active structures, fulfilling expectations for critically stressed faults controlling geothermal upwelling.

I find that creating a model with Python gives the user enhanced control and adaptability of the model. For example, after a smaller scale model focused primarily on the mapped area omitted faults that seemed relevant to the fault network, the necessary input to include that fault can quickly be generated and altered. I can assign slip vs. dilation tendencies from the Move model to combine all data in the Jupyter Notebook. 3D geologic block modeling effectively displays relationships that are convoluted in map view. The final output reveals the spatial relationships between regional and small-scale structures and how they may be controlling the geothermal system.

Discussion

Chronology

Understanding the development and geometry of structures surrounding the Norris Hot Springs is necessary for determining controls on the associated geothermal system. Early basement deformation observed at Norris was likely associated with Paleozoic and Precambrian tectonic events (Condit et al., 2015; Marshak et al., 2000; Spencer & Kozak, 1975). The Norris Hot Springs are located on an uplifted basement block in southwestern Montana. The block was uplifted ca. 80-50 Ma during thick skinned deformation associated with the Laramide orogeny, along structures herein referred to as Laramide faults. During this uplift event, the basement was folded via fault propagation folds (Carrapa et al., 2019). The Elk Creek fault, the Cherry Creek fault and the Spanish Peaks fault system are major NW trending high angle Laramide faults

partially responsible for uplifting the block (Carl, 1970; K. Kellogg & Williams, 2000; S. Vuke et al., 2002).

Based on field observations and structural measurements, I interpret Fault 1 to be the oldest fault in the study area, originating as a compressional Laramide structure due to it's alignment with the structural grain defined by Laramide structures. Fault 1 does not offset any quartz veins in the area, indicating the upper limit of vein formation postdates activity on Fault 1. Gold, silver, and sulfide accessory minerals associated with quartz veins in this area suggest vein injection was at least partially coeval with emplacement of the Tobacco Root Batholith to the west ca. 71 Ma. Additionally, many of these quartz veins and mineralized faults (Fault 6, 7-12) share the same NW orientation as Laramide thrust structures that were active ca. 70 Ma and are assumed to have accommodated injection and mineralization. Faults 7-12 which abut the eastern rhyolite vitrophyre do not offset or alter the outcrop, suggesting the rhyolite intrusion postdates mineralization of faults and quartz veins. These field observations are consistent with previous dating of this rhyolite intrusion providing an age of ~51 Ma (Kellogg & Harlan, 2007). The eastern rhyolite outcrop tapers into an alluvial valley and is interpreted to have been bisected by Fault 5, constraining slip to post 51 Ma. I interpret Faults 1, 5, and 6 originated as Laramide contractional structures and were reactivated as normal faults at the onset of orogenic collapse ca. 40 Ma (Constenius, 1996; Snee & Miller, 2022)**.** Finally, Fault 2 is a classic Basin and Range style high-angle normal fault, exhuming basement rock in its footwall and down dropping Quaternary sediments to the west in its hanging wall. Evidence of recent seismic activity suggests Fault 2 is still active today (Stickney personal comms., Stickney & Bartholomew, 1987).

The Red Bluff unit ($P_E$rb) is intersected by Fault 1, yet no offset was observed in the field. It is possible limited fault evidence is a consequence of the extremely limited outcrop exposure in this portion of the field area. $P_E$rb lies unconformably on the crystalline basement rock and has been interpreted either as a lahar or catastrophic debris flows. I interpret the Red Bluff unit as a series of debris flow deposits for the following reasons: lack of sedimentary structures, discontinuous beds, and extreme heterogeneity in both the composition and age of clasts. Results from detrital zircon U-Pb geochronology suggest zircon grains from $P_E$rb were sourced from more than one region. I determined an MLA age of 62.48 +/- 4.7 Ma, suggesting that it's Mesozoic volcanic source could have been the Elkhorn volcanic suite, which has an age range of 75-70 Ma (Gwinn & Mutch, 1965). Other possible detrital sources are the Tobacco Root Batholith (Scarberry et al., 2021), small ca. 50 Ma volcanic plugs in the region (K. S. Kellogg & Harlan, 2007), and the Archean Wyoming craton (Mueller et al., 1996, Laskowski 2013). $P_E$rb crops out adjacent to a paleo valley of the Madison River, which now contains Hot Springs Creek. Faults 3 and 4 down drop the upper $P_E$rb unit to the north, constraining timing of faulting as post depositional, yet there are no other age constraints.

Although it is beyond the scope of this study to assume a start time for all geothermal activity in Montana, I suggest modern geothermal activity in the Norris Hot Springs area is directly related to Basin and Range extension. Thinning of the crust due to orogenic collapse and Basin and Range extension led to an increased heat gradient throughout southwestern Montana, like documented increases in the thermal gradient of the Great Basin region of Nevada (Faulds, 2012; Wisian et al., 1999). Deep structures such as reactivated Laramide faults may facilitate meteoric recharge of geothermal reservoirs (Barton & Zoback, 1995; Chadwick & Leonard,

1979; Ferrill et al., 2020). Basin and Range style faults and in particular, regions where normal faults intersect, may favor and result in the surface expression of geothermal activity. Modern earthquake epicenters, as well as focal point data from Stickney (personal comms) documenting a swarm of earthquakes in the Norris valley in 1987 provide additional insights into fault activity in this region. Earthquake activity within the Norris Valley in the last 200 years reveals slip along NW trending structures, suggesting similarly oriented faults could be critically stressed. Focal points from the 1987 swarm suggest an active system of two intersecting fault planes consistent with the orientations of Faults 2 and 5, or alternatively, similarly oriented blind faults. This information is relevant when I consider the established idea that properly oriented and critically stressed faults promote geothermal circulation.

Structural Relationships

Key fault interactions in Norris provide the necessary permeability for geothermal fluid circulation and permit the surface expression of the geothermal system. Important fault trace interactions include 5-6, 5-1, and 2-3. Each represents a normal fault intersection, one of the tectonically favorable geometries (Fig.3) (Faulds & Hinz, 2015; Siler & Pepin, 2021b). Fault 6 intersects Fault 5, and additional subsidiaries of Fault 6 comprise a complicated but small-scale fault structure in the shallow subsurface. Although the traces of Faults 1 and 5 do not intersect, our model reveals that Fault 5 may interact with Fault 1 in the subsurface. I suggest that this fault intersection was critically stressed during the emplacement of the Tobacco Root Batholith and experienced tensile or transtensional hybrid failure, permitting injection of magmatic fluids that mineralized these faults.

The intersection between Faults 2 and 3 is of particular interest due to their proximity to the surface expression of the geothermal system. Fault 2 aligns with earthquake focal points as deep as 4 km, deep enough to attain geothermal temperatures calculated for this reservoir (Peterson, 1984). Fault 3 is a relatively small-scale shallow fault, but I suggest the intersection of Fault 2 and Fault 3 acts as a primary fluid conduit, permitting flow from depth to breach the surface. Additionally, the anticline hinge offset by Fault 3 is a natural plane of weakness and may be fractured at depth, potentially also acting as a fluid pathway. The offset anticline trace is almost exactly at the location of the primary outflow of the system and represents the intersection of the axial plane and Fault 3.

Both model results show most faults interact at depth, supporting our hypothesis that geothermal fluid circulation is accommodated by an interconnected basement fracture system. However, many of the small-scale faults around Norris Hot Springs do not attain the depths required to heat geothermal fluid to the necessary temperature. I propose that these smaller scale faults connect more deeply penetrating structures, such as reactivated Laramide structures, that host the geothermal reservoir to the surface.

I propose that several reactivated Laramide structures and Basin and Range style structures outside the mapped area in southwest Montana play an important role in geothermal activity. In addition to accommodating high crustal heat flow from lithospheric thinning, extensional structures are also appropriately oriented for promoting geothermal flow. These major structures likely reach the necessary depth. The Elk Creek and Cherry Creek faults are NW-SE oriented reactivated Laramide faults to the northeast of Norris, MT. Norris lies between these two faults and a set of NW trending right-lateral oblique normal faults that offset the

Tobacco Root Batholith: The Mammoth, Hollowtop, and Bismark faults. These faults are likely accommodating stress and strain resulting from the Bismark- Spanish Peaks-Gardiner fault system to the southeast of Norris.

Historic earthquake activity also suggests deep fault activity directly underneath and just outside Norris, MT. Focal points from multiple seismic events align with the regional NW structural grain. Most deep structures suggested by this dataset do not have identifiable surface expressions in the study area. Conversely, Fault 5 aligns with one of two distinguishable plane orientations of focal points from Stickney (pers. Comm). Fault 5 is not laterally extensive but displays significant offset and was likely a major source of mineralization in the area, suggesting deeper structures. Earthquake focal point data indicates that Fault 2 is critically stressed and could be accommodating slip documented by earthquake epicenters.

A Structurally Controlled Geothermal System

A structurally controlled geothermal system refers to a geothermal system that is partially, if not entirely, controlled by geologic factors (Chadwick & Leonard, 1979; Faulds et al., 2004). For example, a geothermal system aquifer is considered structurally controlled if its fluid flow is determined by faults and fracturing in host rock, as opposed to by permeable stratigraphy. Due to the complex tectonic history of the area and inherent primary impermeability of the crystalline basement rock, I suspect that a deep network of fractures and blind faults in the crystalline basement are responsible for both hosting the geothermal reservoir, and feeding from these deep cracks up into shallower, surface breaching faults.

Faults provide the necessary transportation networks to circulate geothermal fluids. However, the failure mode of individual faults determines whether a particular fault acts as a

fluid conduit or seal. Failure is influenced by fault geometry, orientation, and kinematics. The determination of these parameters is essential for estimating the geothermal potential of a geologic play. Fault 3 has extremely limited exposure but must be important because it offsets the axial trace of a major anticline in the basement at primary outflow of the geothermal system. The trace reappears to the west, suggesting sinistral slip. Stress analysis and modeling shows Fault 3 is oriented for optimal slip and dilation tendency values. I suggest that the failure mode predicted by this orientation increases volume change along the slip plane. This failure mode permits the rock to act as a conduit for fluid mobility (Ferrill et al., 2020).

Fig 23. A previously unmapped fault in the crystalline basement along a roadcut.

Conversely, this fault zone likely does not reach the depths required to circulate geothermal fluids of the appropriate temperature. The relatively short surface trace of Fault 3 makes it unlikely to penetrate deeply into the subsurface. Peterson (1984) used silica geothermometry to calculate a base temperature of approximately 100℃, correlating with a geothermal reservoir

depth of 3600m. I suggest that geothermal fluid reaches the reservoir through meteoric recharge along reactivated Laramide structures: the Elk Creek and Spanish Peaks faults, and the Cherry Creek fault. These faults are all oriented NW-SE and reactivated with normal sense of motion during the onset of orogenic collapse (Constenius, 1996). Additionally, I propose that the Spanish Peaks fault is generating a state of stress reminiscent of a step over between the NW extent of the fault, and the set of dextral oblique faults that offset the Tobacco Root Batholith. This zone of geothermal upwelling is likely being tapped by smaller scale, shallower faults mapped in this study.

Reactivated Laramide faults are interpreted to reach depths required by silica geothermometry of Norris Hot Springs (Peterson, 1984). Increased heat flow and geothermal gradient in this area is not magmatic, but a result of extension (Wisian, 1999). The same structures that accommodate extension are also providing fluid pathways for geothermal circulation. I interpret that Norris Hot Springs is one of many surficial expressions of a geothermal system where primary circulation of fluid is accommodated by regional scale faults, but smaller scale structures provide the connection between deeper faults and the surface. Therefore, I conclude that the Norris Hot Springs and geothermal system are structurally controlled.

UAV Contributions

UAV, or drone, surveys provided high resolution optical and thermal imagery to use as base maps for field campaigns and gave insight into the morphology of the surface expression of the associated geothermal system. Additionally, the ability to overlay our structural models with optical land imagery allows for comparison between surface features and structural features at

depth. High-resolution optical imagery from UAV surveys revealed isolated structures and outcrops, reducing the amount of time necessary for boots on the ground searching while providing insight into the relationship between basement rock and quartz veins. Thermal imaging provided the necessary information for modeling the hot springs' outlet and tested the ability to perceive thermal anomalies at lower temperature geothermal systems. At Norris Hot Springs, thermal imagery revealed limited ground temperature anomalies, but I found that qualitative thermal imagery gives necessary context and information concerning the surface expression of the linked geothermal system.

Thermal orthomosaics distinctly capture the hot springs origin point, or outlet, which coincides with Fault 3, within resolution error. Optical and thermal imagery revealed an increase in abundance and size of vegetation just downslope from the outlet. Unfortunately, thermal signals from the ground are partially obscured by overlying vegetation; however, thermal imagery shows a minor visible increase in ground temperature at the elevation of the outlet. Qualitative change in ground temperature is likely less distinct for two reasons: the Norris geothermal system is amagmatic and the surrounding crystalline basement rock has a low thermal conductivity. In previous work using drones for geothermal exploration (e.g., Walter et al., 2020), the geothermal systems have been magmatic and high temperature leading to significant variation in thermal signatures. Norris is relatively low temperature, diminishing the contrast in qualitative thermal signals. Norris Hot Spring's singular outlet also reduces this contrast between ground temperatures, as opposed to a continuous trend of thermal upwelling along the lateral extent of active faults.

Sources of error in the UAV process are introduced primarily through the onboard GPS positioning system. Other issues include limited flight times and shortened battery life in cold temperatures. PIX4D, the flight mapping application, has an option to replace batteries mid-flight plan, but this often resulted in flight plan glitches, GPS issues, and irregular image capture. Therefore, flights were restricted to approximately nine minutes before requiring a battery change. The thermal flights presented additional challenges primarily due to the thermal camera's sensitivity to solar radiation. Flights were conducted exclusively before dawn and within a predetermined period to minimize effects of these fluctuations and permit stitching between multiple flight results.

Despite these flaws, UAV surveys supply information that is difficult or impossible to attain with traditional fieldwork and offer a reliable option for small scale remote sensing. I found that optical surveys provided accurate and high-resolution base maps and insight into topographic and structural features. Combining thermal and elevation data types collected from drone imagery in a GIS also allows for interpretation of spatial relationships between mapped faults and thermal features. The orthomosaics display the fundamental relationship between the hot springs' outlet and structural controls. Exploring the use of drones for geothermal exploration in bedrock dominated environments suggests that qualitative drone imagery is effective with imaging geothermal outflow.

Modeling Pros and Cons

Three-dimensional geological modeling for visualization of structure provides necessary insight for visualizing geothermal systems and analyzing resource potential. I explored two options for constructing our geologic block models: Petex Move and Python scripts. The first

iteration of our structural model in Petex Move shows fault interaction and termination at relatively shallow depths, <1km, suggesting additional structures may be necessary for tapping and hosting a geothermal reservoir. I incorporated additional regional scale faults, like the Elk Creek, Cherry Creek, and Spanish Peaks faults into our final, focused Python structural model. Our results show that reactivated Laramide faults provide the mechanism for meteoric recharge of deep geothermal systems. Earthquake focal points also suggest two deep focal planes, one of which aligns with the surficial trace of a normal fault yet has no surface expression. These results confirm the presence of blind faults or fissures that could be acting as geothermal conduits.

Petex Move and our Python supported model resulted in similar outputs, but each technique yields several pros and cons. The Python script is hosted in a Jupyter Notebook that can be adapted to many other structural settings by changing the necessary inputs. However, the shortcomings of this technique are primarily that the user is limited to expressing planes mathematically i.e., by manually projecting the planes to depth using trigonometry. This is a non-issue for simple geologic models. However, to model a ramp flat geometry, or an equally complex structural feature, the user must isolate and project every dip change using a stepwise function.

Petex Move is designed for visualizing regional scale structures and tectonics because it incorporates cross sections, eliminating the need to describe features mathematically. One of the primary differences in our two models is the additional functionality of Petex Move. Essentially for this project, the user interface includes a toolbox for stress analysis. This process could be replicated in Python, but it would require additional programming. However, without seismic data or wells to constrain the subsurface, the number of cross sections that must be carefully

plotted and perfectly aligned for multiple small-scale faults in Petex Move is laborious and cost-prohibitive. The visualization output from our Jupyter Notebook is ultimately more adaptable and accessible.

Analyzing possible error margins for either of these modeling techniques is imperative. The lack of subsurface constraints forces a reliance on more simple geometries, such as constant dips of faults or simple curves. I explored how inaccuracies in dip could change the depth at which planes intersect. A five-degree change in dip results in in approximately 10m of possible error for each 100m of depth. Additional constraints such as seismic imaging or boreholes could reduce error and greatly increase confidence in exact locations of faults and their interactions.

Our final model result explains the relationships between critically stressed faults, reactivated Laramide structures, and the geothermal system at Norris Hot Springs. Further understanding the subsurface structural relationships of known geothermal systems continues to offer insight on controls on blind geothermal system by acting as analogues. 3D geologic models allow the user to visualize these structures and controls more effectively. Additional numerical modeling for increased heat flow throughout fractures and faults, fluid circulation modeling and heat flow are the ideal next steps.

Conclusion

The Norris Hot Springs are the surface expression of a basement hosted structurally controlled geothermal system. Norris records a complex structural history, but limited exposures and sub surface restraints inspire exploration into novel methods. Our results show that structural geometries in our study area are preferentially oriented for geothermal activity. Regional structures likely accommodate meteoric recharge, create strain, and provide fluid pathways at

depth. Incorporation of traditional and novel methods provide a holistic model of the geothermal system and associated surface outlet. With recent developments of micro-UAVS, creating orthomosaics and digital surface models (DSMs) is readily accessible. Combining various datatypes into comprehensive block models allows for visualization and analysis. This study shows that combining traditional structural fieldwork with novel methods such as UAV surveys and 3D modeling provide a more holistic insight into factors controlling a geothermal system. Integrated numerical modeling and subsurface constraints are logical additions to this methodology.

References Cited

Aguilar-Ojeda, J. A., Campos-Gaytán, J. R., Herrera-Oliva, C. S., Ramírez-Hernández, J., & Kretzschmar, T. G. (2022). Updated conceptual and numerical model of the Los Humeros Geothermal Field. *Geothermics*, *106*, 102564. https://doi.org/10.1016/j.geothermics.2022.102564

Andretta, D. B., & Alsup, S. A. (1960). *ELEVENTH ANNUAL FIELD CONFERENCE 185 GEOLOGY AND CENOZOIC HISTORY OF THE NORRIS-ELK CREEK AREA, SOUTHWEST MONTANA*.

Axelsson, G. (2010). Sustainable geothermal utilization – Case histories; definitions; research issues and modelling. *Geothermics*, *39*(4), 283–291. https://doi.org/10.1016/j.geothermics.2010.08.001

Axelsson, G., Stefánsson, V., Björnsson, G., & Liu, J. (2005). Sustainable Management of Geothermal Resources and Utilization for 100-300 Years. In *Proceedings World Geothermal Congress*.

Barton, C. A., & Zoback, M. D. (1995). Fluid flow along potentially active faults in crystalline rock. *Geology*, *23*(8), 683–686. http://pubs.geoscienceworld.org/gsa/geology/article-pdf/23/8/683/3515911/i0091-7613-23-8-683.pdf

Bennet, S. (2011). Geothermal Potential of Transtensional Plate Boundaries. *GRC Transactions*, *35*.

Blackford, N. R., Long, S. P., Stout, A., Rodgers, D. W., Cooper, C. M., Kramer, K., di Fiori, R. v., & Soignard, E. (2022). Late Cretaceous upper-crustal thermal structure of the Sevier hinterland: Implications for the geodynamics of the Nevadaplano. *Geosphere*, *18*(1), 183–210. https://doi.org/10.1130/GES02386.1

Blackwell, D., Wisian, K. W., Benoit, D., & Gollan, B. (1999). Structure of the Dixie Valley geothermal system, a" typical" Basin and Range geothermal system, from thermal and gravity data. *TRANSACTIONS-GEOTHERMAL RESOURCES COUNCIL*, 525–532.

Carl, J. D. (1970). Block Faulting and Development of Drainage, Northern Madison Mountains, Montana. *Geological Society of America Bulletin*, *81*, 2287–2298.

Carrapa, B., DeCelles, P. G., & Romero, M. (2019). Early Inception of the Laramide Orogeny in Southwestern Montana and Northern Wyoming: Implications for Models of Flat-Slab Subduction. *Journal of Geophysical Research: Solid Earth*, *124*(2), 2102–2123. https://doi.org/10.1029/2018JB016888

Chadwick, R., & Kaczmarek, M. (1975). Geothermal Investigations of Selected Montana Hot Springs. *Energy Resources of Montana*, *22*.

Chadwick, R., & Leonard, R. (1979). *Structural Controls of Hot-Spring Systems in Southwest Montana*.

Condit, C. B., Mahan, K. H., Ault, A. K., & Flowers, R. M. (2015). Foreland-directed propagation of high-grade tectonism in the deep roots of a Paleoproterozoic collisional orogen, SW Montana, USA. *Lithosphere*, L460.1. https://doi.org/10.1130/L460.1

Constenius, K. N. (1996). *Late Paleogene extensional collapse of the Cordilleran foreland fold and thrust belt*.

Curewitz, D., & Karson, J. A. (1997). Structural settings of hydrothermal outflow: Fracture permeability maintained by fault propagation and interaction. *Journal of Volcanology and Geothermal Research*, *79*, 149–168.

de la Varga, M., Schaaf, A., & Wellmann, F. (2019). GemPy 1.0: open-source stochastic geological modeling and inversion. *Geoscientific Model Development*, *12*(1), 1–32. https://doi.org/10.5194/gmd-12-1-2019

Decelles, P. G. (2004). *LATE JURASSIC TO EOCENE EVOLUTION OF THE CORDILLERAN THRUST BELT AND FORELAND BASIN SYSTEM, WESTERN U.S.A.*

Dickinson, W. R., & Gehrels, G. E. (2009). Use of U–Pb ages of detrital zircons to infer maximum depositional ages of strata: A test against a Colorado Plateau Mesozoic database. *Earth and Planetary Science Letters*, *288*(1–2), 115–125. https://doi.org/10.1016/j.epsl.2009.09.013

Erslev, E. A., & Koenig, N. v. (2009). Three-dimensional kinematics of Laramide, basement-involved Rocky Mountain deformation, USA: Insights from minor faults and GIS-enhanced structure maps. In *Backbone of the Americas: Shallow Subduction, Plateau Uplift, and Ridge and Terrane Collision*. Geological Society of America. https://doi.org/10.1130/2009.1204(06)

Faulds, J. E. (2012). *Regional Patterns of Geothermal Activity in the Great Basin Region, Western USA: Correlation With Strain Rates*.

Faulds, J. E., Coolbaugh, M., Blewitt, G., & Henry, C. D. (2004). WHY IS NEVADA IN HOT WATER? STRUCTURAL CONTROLS AND TECTONIC MODEL OF GEOTHERMAL SYSTEMS IN THE NORTHWESTERN GREAT BASIN. *Geothermal Resources Council Transactions*, *28*.

Faulds, J. E., Coolbaugh, M. F., Vice, G. S., & Edwards, M. L. (2006). Characterizing structural controls of geothermal fields in the northwestern Great Basin: A progress report. *Geothermal Resources Council Transactions 30* , 69–76.

Faulds, J. E., Craig, J. W., Hinz, N. H., Coolbaugh, M. F., Glen, J. M., Earney, T. E., Schermerhorn, W. D., Peacock, J., Deoreo, S. B., & Siler, D. L. (2018). Discovery of a Blind Geothermal System in Southern Gabbs Valley, Western Nevada, through Application of the Play Fairway Analysis at Multiple Scales. In *GRC Transactions* (Vol. 42).

Faulds, J. E., & Hinz, N. H. (2015). Favorable Tectonic and Structural Settings of Geothermal Systems in the Great Basin Region, Western USA: Proxies for Discovering Blind Geothermal Systems. In *Proceedings World Geothermal Congress*.

Faulds, J. E., Hinz, N. H., Coolbaugh, M. F., Depolo, C. M., Siler, D. L., Shevenell, L. A., Hammond, W. C., Kreemer, C., & Queen, J. H. (2016). Discovering Geothermal Systems in the Great Basin Region: An Integrated Geologic, Geochemical, and Geophysical Approach for Establishing Geothermal Play Fairways. In *PROCEEDINGS*.

Faulds, J. E., Hinz, N. H., Coolbaugh, M. F., Sadowski, A. J., Shevenell, L. A., Mcconville, E., Craig, J., Sladek, C., & Siler, D. L. (2017). *Progress Report on the Nevada Play Fairway Project: Integrated Geological, Geochemical, and Geophysical Analyses of Possible New Geothermal Systems in the Great Basin Region*.

Faulds, J. E., Shervais, J. W., Wannamaker, P. E., Forson, C., & Lautze, N. (2021a). Challenges and opportunities for geothermal exploration and hydrothermal research: Recent advances utilizing geothermal play fairway analysis in the western USA. *Proceedings of the Symposium on the Application of Geophyics to Engineering and Environmental Problems, SAGEEP, 2021-March*. https://doi.org/10.4133/sageep.33-083

Faulds, J. E., Shervais, J. W., Wannamaker, P. E., Forson, C., & Lautze, N. (2021b). Challenges and opportunities for geothermal exploration and hydrothermal research: Recent advances utilizing geothermal play fairway analysis in the western USA. *Proceedings of the Symposium on the Application of Geophyics to Engineering and Environmental Problems, SAGEEP, 2021-March*. https://doi.org/10.4133/sageep.33-083

Ferrill, D. A., Smart, K. J., & Morris, A. P. (2020). Resolved stress analysis, failure mode, and fault-controlled fluid conduits. *Solid Earth*, *11*(3), 899–908. https://doi.org/10.5194/se-11-899-2020

Foster, D. A., Mueller, P. A., Mogk, D. W., Wooden, J. L., & Vogl, J. J. (2006). Proterozoic evolution of the western margin of the Wyoming craton: implications for the tectonic and magmatic evolution of the northern Rocky Mountains. *Canadian Journal of Earth Sciences*, *43*(10), 1601–1619. https://doi.org/10.1139/e06-052

Furlong, K. P., & Handy, M. R. (n.d.). *Nucleation and growth of fault systems Neoproterozoic stratigraphy View project*. https://www.researchgate.net/publication/237378284

Garihan, J., Schmidt, C., Young, S., & Williams, M. A. (1983). Geology and recurrent movement history of the Bismark- Spanish Peaks- Gardiner Fault System, Southwest Montana. *Rocky Mountain Association of Geologists*.

Garzanti, E. (2019). Petrographic classification of sand and sandstone. *Earth-Science Reviews*, *192*, 545–563. https://doi.org/10.1016/j.earscirev.2018.12.014

Gunderson, J. A. (2012). *Preliminary Geothermal Map of Montana Using Bottom-Hole Temperature Data*.

Gwinn, V. E., & Mutch, T. A. (1965). Intertongued Upper Cretaceous Volcanic and Nonvolcanic Rocks, Central-Western Montana. *GSA Bulletin*.

Haller, K. M., Dart, R. L., Machette, M. N., & Stickney, M. C. (n.d.). *Data for Quaternary faults in western Montana*.

Harms, T. A., Brady, J. B., Robert Burger, H., Cheney, J. T., & Robert, H. (2004). Advances in the Geology of the Tobacco Root Mountains, Montana, and Their Implications for the History of the Northern Wyoming Province. In *Smith ScholarWorks Smith ScholarWorks Geosciences*. Faculty Publications Geosciences. https://scholarworks.smith.edu/geo_facpubs/31

Harvey, M. C., Rowland, J. v., & Luketina, K. M. (2016). Drone with thermal infrared camera provides high resolution georeferenced imagery of the Waikite geothermal area, New Zealand. *Journal of Volcanology and Geothermal Research*, *325*, 61–69. https://doi.org/10.1016/j.jvolgeores.2016.06.014

Haselwimmer, C., Prakash, A., & Holdmann, G. (2013). Quantifying the heat flux and outflow rate of hot springs using airborne thermal imagery: Case study from Pilgrim Hot Springs, Alaska. *Remote Sensing of Environment*, *136*, 37–46. https://doi.org/10.1016/j.rse.2013.04.008

Jacobsen, L. J., Glynn, P. D., Phelps, G. A., Orndorff, R. C., Bawden, G. W., Grauch, V., & Geological Survey, U. (2011). *Chapter 13: U.S. Geological Survey: A Synopsis of Three-dimensional Modeling Mission and Organizational Needs*. http://tapestry.usgs.gov

Janecke, S. U. (2007). Cenozoic extensional processes and tectonics in the northern Rocky Mountains: southwest Montana and eastern Idaho. In *The Journal of the Tobacco Root Geological Society*.

Jolie, E., Scott, S., Faulds, J., Chambefort, I., Axelsson, G., Gutiérrez-Negrín, L. C., Regenspurg, S., Ziegler, M., Ayling, B., Richter, A., & Zemedkun, M. T. (2021). Geological controls on geothermal resources for power generation. In *Nature Reviews Earth and Environment* (Vol. 2, Issue 5, pp. 324–339). Springer Nature. https://doi.org/10.1038/s43017-021-00154-y

Jones, R. R., McCaffrey, K. J. W., Clegg, P., Wilson, R. W., Holliman, N. S., Holdsworth, R. E., Imber, J., & Waggott, S. (2009). Integration of regional to outcrop digital data: 3D visualisation of multi-scale geological models. *Computers and Geosciences*, *35*(1), 4–18. https://doi.org/10.1016/j.cageo.2007.09.007

Jordan, B. R. (2015). A bird's-eye view of geology: The use of micro drones/UAVs in geologic fieldwork and education. *GSA Today*, 50–52. https://doi.org/10.1130/gsatg232gw.1

Kaempfer, J. M., Guenthner, W. R., & Pearson, D. M. (2021). Proterozoic to Phanerozoic Tectonism in Southwestern Montana Basement Ranges Constrained by Low Temperature Thermochronometric Data. *Tectonics*, *40*(11). https://doi.org/10.1029/2021TC006744

Kellogg, K. S., & Harlan, S. S. (2007). New 40 Ar/ 39 Ar age determinations and paleomagnetic results bear-ing on the tectonic and magmatic history of the northern Madison Range and Madison Valley region, southwestern Montana, U.S.A. In *Rocky Mountain Geology* (Vol. 42, Issue 2). http://pubs.geoscienceworld.org/uwyo/rmg/article-pdf/42/2/157/2956023/157.pdf

Kellogg, K., & Williams, V. (2000). *Geologic map of the Ennis 30' x 60' quadrangle, Madison and Gallatin Counties, Montana, and Park County, Wyoming*. https://doi.org/10.3133/i2690

Kuenzer, C., & Dech, S. (2013). Remote Sensing and Digital Image Processing Thermal Infrared Remote Sensing. In *Editors Sensors*. http://www.springer.com/series/6477

Laskowski, A. K., Decelles, P. G., & Gehrels, G. E. (2013). Detrital zircon geochronology of Cordilleran retroarc foreland basin strata, western North America. *Tectonics*, *32*(5), 1027–1048. https://doi.org/10.1002/tect.20065

Liu, Z., Dai, L., Li, S., Wang, L., Xing, H., Liu, Y., Ma, F., Dong, H., & Li, F. (2021). When plateau meets subduction zone: A review of numerical models. *Earth-Science Reviews*, *215*, 103556. https://doi.org/10.1016/j.earscirev.2021.103556

Malmivirta, T., Hamberg, J., Lagerspetz, E., Li, X., Peltonen, E., Flores, H., & Nurmi, P. (2019). Hot or Not? Robust and Accurate Continuous Thermal Imaging on FLIR cameras. *International Conference on Pervasive Computing and Communications*.

Marshak, S., Karlstrom, K., & Timmons, J. M. (2000). Inversion of Proterozoic extensional faults: An explanation for the pattern of Laramide and Ancestral Rockies intracratonic

deformation, United States. *Geology*, *28*(8), 735. https://doi.org/10.1130/0091-7613(2000)28<735:IOPEFA>2.0.CO;2

Martin, E. L., Barrote, V. R., & Cawood, P. A. (2022). A resource for automated search and collation of geochemical datasets from journal supplements. *Scientific Data*, *9*(1). https://doi.org/10.1038/s41597-022-01730-7

McBride, B., Schmidt, C. J., Guthrie, G., & Sheedlo, M. (1992). Multiple reactivation of a collisional boundary: an example from southwestern Montana. In *Basement Tectonics 8* (pp. 341–357).

Metesh, J. (2000). *Montana Bureau of Mines and Geology Open-file Report No. 415 Geothermal Springs and Wells in Montana*.

Mitchell W. Reynolds. (1979). CHARACTER AND EXTENT OF BASIN-RANGE FAULTING, WESTERN MONTANA AND EAST-CENTRAL IDAHO. *RMAG-UGA-1979 BASIN AND RANGE SYMPOSIUM*.

Moeck, I. S. (2014). Catalog of geothermal play types based on geologic controls. In *Renewable and Sustainable Energy Reviews* (Vol. 37, pp. 867–882). Elsevier Ltd. https://doi.org/10.1016/j.rser.2014.05.032

Morris, A., Ferrill, D. A., & Henderson, D. B. (1996). Slip-tendency analysis and fault reactivation. *Geology*, *24*(3), 275–278. http://pubs.geoscienceworld.org/gsa/geology/article-pdf/24/3/275/3516540/i0091-7613-24-3-275.pdf

Mueller, P. A., & Frost, C. D. (2006). The Wyoming Province: a distinctive Archean craton in Laurentian North America. *Canadian Journal of Earth Sciences*, *43*(10), 1391–1397. https://doi.org/10.1139/e06-075

Mueller, P. A., Shuster, R. D., Wooden, J. L., Erslev, E. A., & Bowes, D. R. (1993). Age and composition of Archean crystalline rocks from the southern Madison Range, Montana: Implications for crustal evolution in the Wyoming craton. *Geological Society of America Bulletin*, *105*(4), 437–446. https://doi.org/10.1130/0016-7606(1993)105<0437:AACOAC>2.3.CO;2

Mullen A, Sproles EA, Hendrikx J, Shaw JA and Gatebe CK (2022) An Operational Methodology for Validating Satellite-Based Snow Albedo Measurements Using a UAV. Front. Remote Sens. 2:767593. doi: 10.3389/frsen.2021.767593

Musy, M., Jacquenot, G., & Dalmasso, G. (2019). Vtkplotter, a python module for scientific visualization and analysis of 3D objects and point clouds based on VTK (visualization toolkit). In *Zenodo*.

Neale, C. M. U., Jaworowski, C., Heasler, H., Sivarajan, S., & Masih, A. (2016). Hydrothermal monitoring in Yellowstone National Park using airborne thermal infrared remote sensing. *Remote Sensing of Environment*, *184*, 628–644. https://doi.org/10.1016/j.rse.2016.04.016

Peterson, J. L. (1984). *INTERPRETATION OF ELECTRICAL SOUNDINGS AND SELF POTENTIAL MEASUREMENTS IN THE NORRIS HOT SPRINGS AREA, MADISON COUNTY, MONTANA*.

Reed, M., & Dilles, J. (2021). *ORE DEPOSITS OF BUTTE, MONTANA*.

Reitman, N. G., Mueller, K. J., Tucker, G. E., Gold, R. D., Briggs, R. W., & Barnhart, K. R. (2019). Offset Channels May Not Accurately Record Strike-Slip Fault Displacement: Evidence From Landscape Evolution Models. *Journal of Geophysical Research: Solid Earth*, *124*(12), 13427–13451. https://doi.org/10.1029/2019JB018596

Ronemus, C. B., Orme, D. A., Guenthner, W. R., Cox, S. E., & Kussmaul, C. A. L. (2023). Orogens of Big Sky Country: Reconstructing the Deep-Time Tectonothermal History of the Beartooth Mountains, Montana and Wyoming, USA. *Tectonics*, *42*(1). https://doi.org/10.1029/2022TC007541

Rounce, D. R., Hock, R., & Shean, D. E. (2020). Glacier Mass Change in High Mountain Asia Through 2100 Using the Open-Source Python Glacier Evolution Model (PyGEM). *Frontiers in Earth Science*, *7*. https://doi.org/10.3389/feart.2019.00331

Scarberry, K. C., Yakovlev, P. v, & Schwartz, T. M. (2021). *MESOZOIC MAGMATISM IN MONTANA*.

Sibson, R. H. (1994). Crustal stress, faulting and fluid flow. *Geological Society Special Publication*. http://sp.lyellcollection.org/

Siler, D. L., & Faulds, J. E. (2013). *Three-Dimensional Geothermal Fairway Mapping: Examples from Great Basin, USA*.

Siler, D. L., Faulds, J. E., Hinz, N. H., Dering, G. M., Edwards, J. H., & Mayhew, B. (2019). Three-dimensional geologic mapping to assess geothermal potential: examples from Nevada and Oregon. *Geothermal Energy*, *7*(1). https://doi.org/10.1186/s40517-018-0117-0

Siler, D. L., Hinz, N. H., & Faulds, J. E. (2018). *Stress concentrations at structural discontinuities in active fault zones in the western United States: Implications for permeability and fluid flow in geothermal fields*. http://pubs.geoscienceworld.org/gsa/gsabulletin/article-pdf/130/7-8/1273/4224719/1273.pdf

Siler, D. L., & Pepin, J. D. (2021a). 3-D Geologic Controls of Hydrothermal Fluid Flow at Brady geothermal field, Nevada, USA. *Geothermics*, *94*. https://doi.org/10.1016/j.geothermics.2021.102112

Siler, D. L., & Pepin, J. D. (2021b). 3-D Geologic Controls of Hydrothermal Fluid Flow at Brady geothermal field, Nevada, USA. *Geothermics*, *94*. https://doi.org/10.1016/j.geothermics.2021.102112

Siler, D. L., Pepin, J. D., Vesselinov, V. v., Mudunuru, M. K., & Ahmmed, B. (2021). Machine learning to identify geologic factors associated with production in geothermal fields: a case-study using 3D geologic data, Brady geothermal field, Nevada. *Geothermal Energy*, *9*(1). https://doi.org/10.1186/s40517-021-00199-8

Snee, J.-E. L., & Miller, E. L. (2022). Magmatism, migrating topography, and the transition from Sevier shortening to Basin and Range extension, western United States. In *Tectonic Evolution of the Sevier-Laramide Hinterland, Thrust Belt, and Foreland, and Postorogenic Slab Rollback (180–20 Ma)* (pp. 335–357). Geological Society of America. https://doi.org/10.1130/2021.2555(13)

Snoke, A. W., & Chapman, J. B. (2021). Central Cordillera. *Encyclopedia of Geology*, 157–172. https://doi.org/10.1016/B978-0-12-409548-9.12124-4

Spencer, E. W., & Kozak, S. J. (1975). Precambrian Evolution of the Spanish Peaks Area, Montana. *Geological Society of America Bulletin*, *86*, 785–792. http://pubs.geoscienceworld.org/gsa/gsabulletin/article-pdf/86/6/785/3429179/i0016-7606-86-6-785.pdf

Stavropoulou, M., Exadaktylos, G., & Saratsis, G. (2007). A Combined Three-Dimensional Geological-Geostatistical-Numerical Model of Underground Excavations in Rock. *Rock Mechanics and Rock Engineering*, *40*(3), 213–243. https://doi.org/10.1007/s00603-006-0125-4

Stickney, M. C., & Bartholomew, M. J. (1987). SEISMICITY AND LATE QUATERNARY FAULTING OF THE NORTHERN BASIN AND RANGE PROVINCE, MONTANA AND IDAHO. In *Bulletin of the Seismological Society of America* (Vol. 77, Issue 5). http://pubs.geoscienceworld.org/ssa/bssa/article-pdf/77/5/1602/5333837/bssa0770051602.pdf

Taillefer, A., Guillou-Frottier, L., Soliva, R., Magri, F., Lopez, S., Courrioux, G., Millot, R., Ladouche, B., & le Goff, E. (2018). Topographic and Faults Control of Hydrothermal Circulation Along Dormant Faults in an Orogen. *Geochemistry, Geophysics, Geosystems*, *19*(12), 4972–4995. https://doi.org/10.1029/2018GC007965

Thornton, J. M., Mariethoz, G., & Brunner, P. (2018). A 3D geological model of a structurally complex alpine region as a basis for interdisciplinary research. *Scientific Data*, *5*. https://doi.org/10.1038/sdata.2018.238

Thurlow, E. E. (1941). *Geology and ore deposits of the Lower Hot Springs Mining District Madison County, Montana*.

Turner, A. K. (2006). Challenges and trends for geological modelling and visualisation. *Bulletin of Engineering Geology and the Environment*, *65*(2), 109–127. https://doi.org/10.1007/s10064-005-0015-0

Vermeesch, P. (2018). IsoplotR: A free and open toolbox for geochronology. *Geoscience Frontiers*, *9*(5), 1479–1493. https://doi.org/10.1016/j.gsf.2018.04.001

Vermeesch, P. (2021). Maximum depositional age estimation revisited. *Geoscience Frontiers*, *12*(2), 843–850. https://doi.org/10.1016/j.gsf.2020.08.008

Villarreal, C. A., Garzón, C. G., Mora, J. P., Rojas, J. D., & Ríos, C. A. (2022). Workflow for capturing information and characterizing difficult-to-access geological outcrops using unmanned aerial vehicle-based digital photogrammetric data. *Journal of Industrial Information Integration*, *26*. https://doi.org/10.1016/j.jii.2021.100292

Vuke, S., Lonn, J., Berg, R., & Karl, K. (2002). *Preliminary geologic map of the Bozeman 30' x 60' Quadrangle*.

Vuke, S. M. (2020). Synorogenic basin deposits and associated Laramide uplifts in the Montana part of the Cordilleran foreland basin system. *Geology of Montana*, *1*.

Walter, T. R., Jousset, P., Allahbakhshi, M., Witt, T., Gudmundsson, M. T., & Hersir, G. P. (2020). Underwater and drone based photogrammetry reveals structural control at Geysir geothermal field in Iceland. *Journal of Volcanology and Geothermal Research*, *391*. https://doi.org/10.1016/j.jvolgeores.2018.01.010

Westoby, M. J., Brasington, J., Glasser, N. F., Hambrey, M. J., & Reynolds, J. M. (2012). 'Structure-from-Motion' photogrammetry: A low-cost, effective tool for geoscience applications. *Geomorphology*, *179*, 300–314. https://doi.org/10.1016/j.geomorph.2012.08.021

Whitmeyer, S., & Karl E. Karlstrom. (2007). Tectonic model for Proterozoic growth of North America. *Geosphere*, *3*(4), 220. https://doi.org/10.1130/GES00055.1

Willams, C. F., Reed, M. J., DeAngelo, J., & Galanis, S. P. (2009). Quantifying the undiscovered geothermal resources of the United States. *GRC Transactions*, *33*.

Wisian, K. W., Blackwell, D. D., & Richards, M. (1999). *HEAT FLOW IN THE WESTERN UNITED STATES AND EXTENSIONAL GEOTHERMAL SYSTEMS*. www.smu.edu/~geothermal

Wu, Q., & Xu, H. (2004). On three-dimensional geological modeling and visualization. *Science in China, Series D: Earth Sciences*, *47*(8), 739–748. https://doi.org/10.1360/02yd0475

Yonkee, W. A., & Weil, A. B. (2015). Tectonic evolution of the Sevier and Laramide belts within the North American Cordillera orogenic system. *Earth-Science Reviews*, *150*, 531–593. https://doi.org/10.1016/j.earscirev.2015.08.001

CHAPTER THREE

GENERAL CONCLUSION

The manuscript presented in this thesis presents a comprehensive case study of the Norris Hot Springs and linked geothermal system. Using a novel combination of geologic mapping, 3D modeling, and UAV imagery, I determined which structures are likely controlling the geothermal circulation, and how they relate to the features observed on the surface in our study area. Reactivated Laramide structures and younger Basin and Range structures that have accommodated extension in southwestern Montana are responsible for acting as fluid conduits for geothermal circulation. Additionally, they provide a mechanism for meteoric recharge and cause transtensional and stepover stress states which promote heat flow. Smaller scale faults mapped in detail in this study are preferentially oriented for geothermal fluid flow and connect deeper structures to the surface, resulting in the surficial expression of this geothermal system, Norris Hot Springs. I acknowledge difficulties in field mapping of areas with low exposure and find that supplementing traditional field work with UAV surveys and 3D structural models is beneficial.

In locales with minimal bedrock exposure or limited lithologies, additional forms of data are invaluable. Combining multiple techniques into 3D models for visualization is beneficial for several reasons. First, seismic data from earthquake swarms can constrain fault planes at depth where surficial fault traces are lacking. UAV surveys showed a lack of extensive surficial thermal features, likely due to the inherent impermeability of the surrounding basement rock. It also accurately constrains the outlet point of the geothermal

system, which coincides with mapped faults. The 3D model also permitted stress analysis integral to categorizing the controls on the geothermal system and identifying which faults are acting as conduits. I explored using multiple methods to find pros and cons of a prepackaged software vs. building a model with Python. Combining UAV surveys and Python to model geothermal systems provide more accessibility, usability, and adaptability.

Finally, I conclude that southwestern Montana is a region ripe for additional geothermal development. The structural configurations identified in Norris, MT are found throughout the region along with the same regionally high geothermal gradient. Geothermal exploration in southwestern Montana using play fairway analysis combining existing geologic maps with drone surveys and 3D modeling would produce positive results.

REFERENCES CITED

CUMULATIVE REFERENCES CITED

Andretta, D. B., & Alsup, S. A. (1960). *ELEVENTH ANNUAL FIELD CONFERENCE 185 GEOLOGY AND CENOZOIC HISTORY OF THE NORRIS-ELK CREEK AREA, SOUTHWEST MONTANA*.

Axelsson, G. (2010). Sustainable geothermal utilization – Case histories; definitions; research issues and modelling. *Geothermics*, *39*(4), 283–291. https://doi.org/10.1016/j.geothermics.2010.08.001

Axelsson, G., Stefánsson, V., Björnsson, G., & Liu, J. (2005). Sustainable Management of Geothermal Resources and Utilization for 100-300 Years. In *Proceedings World Geothermal Congress*.

Barton, C. A., & Zoback, M. D. (1995). Fluid flow along potentially active faults in crystalline rock. *Geology*, *23*(8), 683–686. http://pubs.geoscienceworld.org/gsa/geology/article-pdf/23/8/683/3515911/i0091-7613-23-8-683.pdf

Bennet, S. (2011). Geothermal Potential of Transtensional Plate Boundaries. *GRC Transactions*, *35*.

Blackford, N. R., Long, S. P., Stout, A., Rodgers, D. W., Cooper, C. M., Kramer, K., di Fiori, R. v., & Soignard, E. (2022). Late Cretaceous upper-crustal thermal structure of the Sevier hinterland: Implications for the geodynamics of the Nevadaplano. *Geosphere*, *18*(1), 183–210. https://doi.org/10.1130/GES02386.1

Blackwell, D., Wisian, K. W., Benoit, D., & Gollan, B. (1999). Structure of the Dixie Valley geothermal system, a" typical" Basin and Range geothermal system, from thermal and gravity data. *TRANSACTIONS-GEOTHERMAL RESOURCES COUNCIL*, 525–532.

Carl, J. D. (1970). Block Faulting and Development of Drainage, Northern Madison Mountains, Montana. *Geological Society of America Bulletin*, *81*, 2287–2298.

Carrapa, B., DeCelles, P. G., & Romero, M. (2019). Early Inception of the Laramide Orogeny in Southwestern Montana and Northern Wyoming: Implications for Models of Flat-Slab Subduction. *Journal of Geophysical Research: Solid Earth*, *124*(2), 2102–2123. https://doi.org/10.1029/2018JB016888

Chadwick, R., & Kaczmarek, M. (1975). Geothermal Investigations of Selected Montana Hot Springs. *Energy Resources of Montana*, *22*.

Chadwick, R., & Leonard, R. (1979). *Structural Controls of Hot-Spring Systems in Southwest Montana*.

Condit, C. B., Mahan, K. H., Ault, A. K., & Flowers, R. M. (2015). Foreland-directed propagation of high-grade tectonism in the deep roots of a Paleoproterozoic collisional orogen, SW Montana, USA. *Lithosphere*, L460.1. https://doi.org/10.1130/L460.1

Constenius, K. N. (1996). *Late Paleogene extensional collapse of the Cordilleran foreland fold and thrust belt*.

Curewitz, D., & Karson, J. A. (1997). Structural settings of hydrothermal outflow: Fracture permeability maintained by fault propagation and interaction. *Journal of Volcanology and Geothermal Research*, *79*, 149–168.

de la Varga, M., Schaaf, A., & Wellmann, F. (2019). GemPy 1.0: open-source stochastic geological modeling and inversion. *Geoscientific Model Development*, *12*(1), 1–32. https://doi.org/10.5194/gmd-12-1-2019

Decelles, P. G. (2004). *LATE JURASSIC TO EOCENE EVOLUTION OF THE CORDILLERAN THRUST BELT AND FORELAND BASIN SYSTEM, WESTERN U.S.A*.

Dickinson, W. R., & Gehrels, G. E. (2009). Use of U–Pb ages of detrital zircons to infer maximum depositional ages of strata: A test against a Colorado Plateau Mesozoic database. *Earth and Planetary Science Letters*, *288*(1–2), 115–125. https://doi.org/10.1016/j.epsl.2009.09.013

Erslev, E. A., & Koenig, N. v. (2009). Three-dimensional kinematics of Laramide, basement-involved Rocky Mountain deformation, USA: Insights from minor faults and GIS-enhanced structure maps. In *Backbone of the Americas: Shallow Subduction, Plateau Uplift, and Ridge and Terrane Collision*. Geological Society of America. https://doi.org/10.1130/2009.1204(06)

Faulds, J. E. (2012). *Regional Patterns of Geothermal Activity in the Great Basin Region, Western USA: Correlation With Strain Rates*.

Faulds, J. E., Coolbaugh, M., Blewitt, G., & Henry, C. D. (2004). WHY IS NEVADA IN HOT WATER? STRUCTURAL CONTROLS AND TECTONIC MODEL OF GEOTHERMAL SYSTEMS IN THE NORTHWESTERN GREAT BASIN. *Geothermal Resources Council Transactions*, *28*.

Faulds, J. E., Coolbaugh, M. F., Vice, G. S., & Edwards, M. L. (2006). Characterizing structural controls of geothermal fields in the northwestern Great Basin: A progress report. *Geothermal Resources Council Transactions 30* , 69–76.

Faulds, J. E., Craig, J. W., Hinz, N. H., Coolbaugh, M. F., Glen, J. M., Earney, T. E., Schermerhorn, W. D., Peacock, J., Deoreo, S. B., & Siler, D. L. (2018). Discovery of a Blind Geothermal System in Southern Gabbs Valley, Western Nevada, through Application of the Play Fairway Analysis at Multiple Scales. In *GRC Transactions* (Vol. 42).

Faulds, J. E., & Hinz, N. H. (2015). Favorable Tectonic and Structural Settings of Geothermal Systems in the Great Basin Region, Western USA: Proxies for Discovering Blind Geothermal Systems. In *Proceedings World Geothermal Congress*.

Faulds, J. E., Hinz, N. H., Coolbaugh, M. F., Depolo, C. M., Siler, D. L., Shevenell, L. A., Hammond, W. C., Kreemer, C., & Queen, J. H. (2016). Discovering Geothermal Systems in the Great Basin Region: An Integrated Geologic, Geochemical, and Geophysical Approach for Establishing Geothermal Play Fairways. In *PROCEEDINGS*.

Faulds, J. E., Shervais, J. W., Wannamaker, P. E., Forson, C., & Lautze, N. (2021a). Challenges and opportunities for geothermal exploration and hydrothermal research: Recent advances utilizing geothermal play fairway analysis in the western USA. *Proceedings of the Symposium on the Application of Geophyics to Engineering and Environmental Problems, SAGEEP*, *2021-March*. https://doi.org/10.4133/sageep.33-083

Faulds, J. E., Shervais, J. W., Wannamaker, P. E., Forson, C., & Lautze, N. (2021b). Challenges and opportunities for geothermal exploration and hydrothermal research: Recent advances utilizing geothermal play fairway analysis in the western USA. *Proceedings of the Symposium on the Application of Geophyics to Engineering and Environmental Problems, SAGEEP*, *2021-March*. https://doi.org/10.4133/sageep.33-083

Ferrill, D. A., Smart, K. J., & Morris, A. P. (2020). Resolved stress analysis, failure mode, and fault-controlled fluid conduits. *Solid Earth*, *11*(3), 899–908. https://doi.org/10.5194/se-11-899-2020

Foster, D. A., Mueller, P. A., Mogk, D. W., Wooden, J. L., & Vogl, J. J. (2006). Proterozoic evolution of the western margin of the Wyoming craton: implications for the tectonic and magmatic evolution of the northern Rocky Mountains. *Canadian Journal of Earth Sciences*, *43*(10), 1601–1619. https://doi.org/10.1139/e06-052

Furlong, K. P., & Handy, M. R. (n.d.). *Nucleation and growth of fault systems Neoproterozoic stratigraphy View project*. https://www.researchgate.net/publication/237378284

Garihan, J., Schmidt, C., Young, S., & Williams, M. A. (1983). Geology and recurrent movement history of the Bismark- Spanish Peaks- Gardiner Fault System, Southwest Montana. *Rocky Mountain Association of Geologists*.

Garzanti, E. (2019). Petrographic classification of sand and sandstone. *Earth-Science Reviews*, *192*, 545–563. https://doi.org/10.1016/j.earscirev.2018.12.014

Gunderson, J. A. (2012). *Preliminary Geothermal Map of Montana Using Bottom-Hole Temperature Data*.

Gwinn, V. E., & Mutch, T. A. (1965). Intertongued Upper Cretaceous Volcanic and Nonvolcanic Rocks, Central-Western Montana. *GSA Bulletin*.

Haller, K. M., Dart, R. L., Machette, M. N., & Stickney, M. C. (n.d.). *Data for Quaternary faults in western Montana*.

Harms, T. A., Brady, J. B., Robert Burger, H., Cheney, J. T., & Robert, H. (2004). Advances in the Geology of the Tobacco Root Mountains, Montana, and Their Implications for the History of the Northern Wyoming Province. In *Smith ScholarWorks Smith ScholarWorks Geosciences*. Faculty Publications Geosciences. https://scholarworks.smith.edu/geo_facpubs/31

Harvey, M. C., Rowland, J. v., & Luketina, K. M. (2016). Drone with thermal infrared camera provides high resolution georeferenced imagery of the Waikite geothermal area, New Zealand. *Journal of Volcanology and Geothermal Research*, *325*, 61–69. https://doi.org/10.1016/j.jvolgeores.2016.06.014

Haselwimmer, C., Prakash, A., & Holdmann, G. (2013). Quantifying the heat flux and outflow rate of hot springs using airborne thermal imagery: Case study from Pilgrim Hot Springs, Alaska. *Remote Sensing of Environment*, *136*, 37–46. https://doi.org/10.1016/j.rse.2013.04.008

Jacobsen, L. J., Glynn, P. D., Phelps, G. A., Orndorff, R. C., Bawden, G. W., Grauch, V., & Geological Survey, U. (2011). *Chapter 13: U.S. Geological Survey: A Synopsis of Three-dimensional Modeling Mission and Organizational Needs*. http://tapestry.usgs.gov

Janecke, S. U. (2007). Cenozoic extensional processes and tectonics in the northern Rocky Mountains: southwest Montana and eastern Idaho. In *The Journal of the Tobacco Root Geological Society*.

Jolie, E., Scott, S., Faulds, J., Chambefort, I., Axelsson, G., Gutiérrez-Negrín, L. C., Regenspurg, S., Ziegler, M., Ayling, B., Richter, A., & Zemedkun, M. T. (2021). Geological controls on geothermal resources for power generation. In *Nature Reviews Earth and Environment* (Vol. 2, Issue 5, pp. 324–339). Springer Nature. https://doi.org/10.1038/s43017-021-00154-y

Jones, R. R., McCaffrey, K. J. W., Clegg, P., Wilson, R. W., Holliman, N. S., Holdsworth, R. E., Imber, J., & Waggott, S. (2009). Integration of regional to outcrop digital data: 3D

visualisation of multi-scale geological models. *Computers and Geosciences*, *35*(1), 4–18. https://doi.org/10.1016/j.cageo.2007.09.007

Jordan, B. R. (2015). A bird's-eye view of geology: The use of micro drones/UAVs in geologic fieldwork and education. *GSA Today*, 50–52. https://doi.org/10.1130/gsatg232gw.1

Kaempfer, J. M., Guenthner, W. R., & Pearson, D. M. (2021). Proterozoic to Phanerozoic Tectonism in Southwestern Montana Basement Ranges Constrained by Low Temperature Thermochronometric Data. *Tectonics*, *40*(11). https://doi.org/10.1029/2021TC006744

Kellogg, K. S., & Harlan, S. S. (2007). New 40 Ar/ 39 Ar age determinations and paleomagnetic results bear-ing on the tectonic and magmatic history of the northern Madison Range and Madison Valley region, southwestern Montana, U.S.A. In *Rocky Mountain Geology* (Vol. 42, Issue 2). http://pubs.geoscienceworld.org/uwyo/rmg/article-pdf/42/2/157/2956023/157.pdf

Kellogg, K., & Williams, V. (2000). *Geologic map of the Ennis 30' x 60' quadrangle, Madison and Gallatin Counties, Montana, and Park County, Wyoming*. https://doi.org/10.3133/i2690

Kuenzer, C., & Dech, S. (2013). Remote Sensing and Digital Image Processing Thermal Infrared Remote Sensing. In *Editors Sensors*. http://www.springer.com/series/6477

Laskowski, A. K., Decelles, P. G., & Gehrels, G. E. (2013). Detrital zircon geochronology of Cordilleran retroarc foreland basin strata, western North America. *Tectonics*, *32*(5), 1027–1048. https://doi.org/10.1002/tect.20065

Malmivirta, T., Hamberg, J., Lagerspetz, E., Li, X., Peltonen, E., Flores, H., & Nurmi, P. (2019). Hot or Not? Robust and Accurate Continuous Thermal Imaging on FLIR cameras. *International Conference on Pervasive Computing and Communications*.

Marshak, S., Karlstrom, K., & Timmons, J. M. (2000). Inversion of Proterozoic extensional faults: An explanation for the pattern of Laramide and Ancestral Rockies intracratonic deformation, United States. *Geology*, *28*(8), 735. https://doi.org/10.1130/0091-7613(2000)28<735:IOPEFA>2.0.CO;2

Martin, E. L., Barrote, V. R., & Cawood, P. A. (2022). A resource for automated search and collation of geochemical datasets from journal supplements. *Scientific Data*, *9*(1). https://doi.org/10.1038/s41597-022-01730-7

McBride, B., Schmidt, C. J., Guthrie, G., & Sheedlo, M. (1992). Multiple reactivation of a collisional boundary: an example from southwestern Montana. In *Basement Tectonics 8* (pp. 341–357).

Metesh, J. (2000). *Montana Bureau of Mines and Geology Open-file Report No. 415 Geothermal Springs and Wells in Montana*.

Mitchell W. Reynolds. (1979). CHARACTER AND EXTENT OF BASIN-RANGE FAULTING, WESTERN MONTANA AND EAST-CENTRAL IDAHO. *RMAG-UGA-1979 BASIN AND RANGE SYMPOSIUM*.

Moeck, I. S. (2014). Catalog of geothermal play types based on geologic controls. In *Renewable and Sustainable Energy Reviews* (Vol. 37, pp. 867–882). Elsevier Ltd. https://doi.org/10.1016/j.rser.2014.05.032

Morris, A., Ferrill, D. A., & Henderson, D. B. (1996). Slip-tendency analysis and fault reactivation. *Geology*, *24*(3), 275–278. http://pubs.geoscienceworld.org/gsa/geology/article-pdf/24/3/275/3516540/i0091-7613-24-3-275.pdf

Mueller, P. A., & Frost, C. D. (2006). The Wyoming Province: a distinctive Archean craton in Laurentian North America. *Canadian Journal of Earth Sciences*, *43*(10), 1391–1397. https://doi.org/10.1139/e06-075

Mueller, P. A., Shuster, R. D., Wooden, J. L., Erslev, E. A., & Bowes, D. R. (1993). Age and composition of Archean crystalline rocks from the southern Madison Range, Montana: Implications for crustal evolution in the Wyoming craton. *Geological Society of America Bulletin*, *105*(4), 437–446. https://doi.org/10.1130/0016-7606(1993)105<0437:AACOAC>2.3.CO;2

Musy, M., Jacquenot, G., & Dalmasso, G. (2019). Vtkplotter, a python module for scientific visualization and analysis of 3D objects and point clouds based on VTK (visualization toolkit). In *Zenodo*.

Neale, C. M. U., Jaworowski, C., Heasler, H., Sivarajan, S., & Masih, A. (2016). Hydrothermal monitoring in Yellowstone National Park using airborne thermal infrared remote sensing. *Remote Sensing of Environment*, *184*, 628–644. https://doi.org/10.1016/j.rse.2016.04.016

Peterson, J. L. (1984). *INTERPRETATION OF ELECTRICAL SOUNDINGS AND SELF POTENTIAL MEASUREMENTS IN THE NORRIS HOT SPRINGS AREA, MADISON COUNTY, MONTANA*.

Prince Ginori-Conti. Nature 145, 380 (1940). https://doi.org/10.1038/145380a0

Reed, M., & Dilles, J. (2021). *ORE DEPOSITS OF BUTTE, MONTANA*.

Ronemus, C. B., Orme, D. A., Guenthner, W. R., Cox, S. E., & Kussmaul, C. A. L. (2023). Orogens of Big Sky Country: Reconstructing the Deep-Time Tectonothermal History of the Beartooth Mountains, Montana and Wyoming, USA. *Tectonics*, *42*(1). https://doi.org/10.1029/2022TC007541

Rounce, D. R., Hock, R., & Shean, D. E. (2020). Glacier Mass Change in High Mountain Asia Through 2100 Using the Open-Source Python Glacier Evolution Model (PyGEM). *Frontiers in Earth Science*, *7*. https://doi.org/10.3389/feart.2019.00331

Scarberry, K. C., Yakovlev, P. v, & Schwartz, T. M. (2021). *MESOZOIC MAGMATISM IN MONTANA*.

Sibson, R. H. (1994). Crustal stress, faulting and fluid flow. *Geological Society Special Publication*. http://sp.lyellcollection.org/

Siler, D. L., & Faulds, J. E. (2013). *Three-Dimensional Geothermal Fairway Mapping: Examples from Great Basin, USA*.

Siler, D. L., Faulds, J. E., Hinz, N. H., Dering, G. M., Edwards, J. H., & Mayhew, B. (2019). Three-dimensional geologic mapping to assess geothermal potential: examples from Nevada and Oregon. *Geothermal Energy*, *7*(1). https://doi.org/10.1186/s40517-018-0117-0

Siler, D. L., Hinz, N. H., & Faulds, J. E. (2018). *Stress concentrations at structural discontinuities in active fault zones in the western United States: Implications for permeability and fluid flow in geothermal fields*. http://pubs.geoscienceworld.org/gsa/gsabulletin/article-pdf/130/7-8/1273/4224719/1273.pdf

Siler, D. L., & Pepin, J. D. (2021a). 3-D Geologic Controls of Hydrothermal Fluid Flow at Brady geothermal field, Nevada, USA. *Geothermics*, *94*. https://doi.org/10.1016/j.geothermics.2021.102112

Siler, D. L., & Pepin, J. D. (2021b). 3-D Geologic Controls of Hydrothermal Fluid Flow at Brady geothermal field, Nevada, USA. *Geothermics*, *94*. https://doi.org/10.1016/j.geothermics.2021.102112

Siler, D. L., Pepin, J. D., Vesselinov, V. v., Mudunuru, M. K., & Ahmmed, B. (2021). Machine learning to identify geologic factors associated with production in geothermal fields: a case-study using 3D geologic data, Brady geothermal field, Nevada. *Geothermal Energy*, *9*(1). https://doi.org/10.1186/s40517-021-00199-8

Snee, J.-E. L., & Miller, E. L. (2022). Magmatism, migrating topography, and the transition from Sevier shortening to Basin and Range extension, western United States. In *Tectonic Evolution of the Sevier-Laramide Hinterland, Thrust Belt, and Foreland, and Postorogenic Slab Rollback (180–20 Ma)* (pp. 335–357). Geological Society of America. https://doi.org/10.1130/2021.2555(13)

Snoke, A. W., & Chapman, J. B. (2021). Central Cordillera. *Encyclopedia of Geology*, 157–172. https://doi.org/10.1016/B978-0-12-409548-9.12124-4

Spencer, E. W., & Kozak, S. J. (1975). Precambrian Evolution of the Spanish Peaks Area, Montana. *Geological Society of America Bulletin*, *86*, 785–792. http://pubs.geoscienceworld.org/gsa/gsabulletin/article-pdf/86/6/785/3429179/i0016-7606-86-6-785.pdf

Stickney, M. C., & Bartholomew, M. J. (1987). SEISMICITY AND LATE QUATERNARY FAULTING OF THE NORTHERN BASIN AND RANGE PROVINCE, MONTANA AND IDAHO. In *Bulletin of the Seismological Society of America* (Vol. 77, Issue 5). http://pubs.geoscienceworld.org/ssa/bssa/article-pdf/77/5/1602/5333837/bssa0770051602.pdf

Taillefer, A., Guillou-Frottier, L., Soliva, R., Magri, F., Lopez, S., Courrioux, G., Millot, R., Ladouche, B., & le Goff, E. (2018). Topographic and Faults Control of Hydrothermal Circulation Along Dormant Faults in an Orogen. *Geochemistry, Geophysics, Geosystems*, *19*(12), 4972–4995. https://doi.org/10.1029/2018GC007965

Thornton, J. M., Mariethoz, G., & Brunner, P. (2018). A 3D geological model of a structurally complex alpine region as a basis for interdisciplinary research. *Scientific Data*, *5*. https://doi.org/10.1038/sdata.2018.238

Thurlow, E. E. (1941). *Geology and ore deposits of the Lower Hot Springs Mining District Madison County, Montana*.

Turner, A. K. (2006). Challenges and trends for geological modelling and visualisation. *Bulletin of Engineering Geology and the Environment*, *65*(2), 109–127. https://doi.org/10.1007/s10064-005-0015-0

Vermeesch, P. (2018). IsoplotR: A free and open toolbox for geochronology. *Geoscience Frontiers*, *9*(5), 1479–1493. https://doi.org/10.1016/j.gsf.2018.04.001

Vermeesch, P. (2021). Maximum depositional age estimation revisited. *Geoscience Frontiers*, *12*(2), 843–850. https://doi.org/10.1016/j.gsf.2020.08.008

Villarreal, C. A., Garzón, C. G., Mora, J. P., Rojas, J. D., & Ríos, C. A. (2022). Workflow for capturing information and characterizing difficult-to-access geological outcrops using unmanned aerial vehicle-based digital photogrammetric data. *Journal of Industrial Information Integration*, *26*. https://doi.org/10.1016/j.jii.2021.100292

Vuke, S., Lonn, J., Berg, R., & Karl, K. (2002). *Preliminary geologic map of the Bozeman 30' x 60' Quadrangle*.

Vuke, S. M. (2020). Synorogenic basin deposits and associated Laramide uplifts in the Montana part of the Cordilleran foreland basin system. *Geology of Montana*, *1*.

Walter, T. R., Jousset, P., Allahbakhshi, M., Witt, T., Gudmundsson, M. T., & Hersir, G. P. (2020). Underwater and drone based photogrammetry reveals structural control at Geysir geothermal field in Iceland. *Journal of Volcanology and Geothermal Research*, *391*. https://doi.org/10.1016/j.jvolgeores.2018.01.010

Westoby, M. J., Brasington, J., Glasser, N. F., Hambrey, M. J., & Reynolds, J. M. (2012). 'Structure-from-Motion' photogrammetry: A low-cost, effective tool for geoscience applications. *Geomorphology*, *179*, 300–314. https://doi.org/10.1016/j.geomorph.2012.08.021

Whitmeyer, S., & Karl E. Karlstrom. (2007). Tectonic model for Proterozoic growth of North America. *Geosphere*, *3*(4), 220. https://doi.org/10.1130/GES00055.1

Willams, C. F., Reed, M. J., DeAngelo, J., & Galanis, S. P. (2009). Quantifying the undiscovered geothermal resources of the United States. *GRC Transactions*, *33*.

Wisian, K. W., Blackwell, D. D., & Richards, M. (1999). *HEAT FLOW IN THE WESTERN UNITED STATES AND EXTENSIONAL GEOTHERMAL SYSTEMS*. www.smu.edu/~geothermal

Wu, Q., & Xu, H. (2004). On three-dimensional geological modeling and visualization. *Science in China, Series D: Earth Sciences*, *47*(8), 739–748. https://doi.org/10.1360/02yd0475

Yonkee, W. A., & Weil, A. B. (2015). Tectonic evolution of the Sevier and Laramide belts within the North American Cordillera orogenic system. *Earth-Science Reviews*, *150*, 531–593. https://doi.org/10.1016/j.earscirev.2015.08.001

APPENDICES

APENDIX A

UAV THERMAL IMAGERY

Figure A.1

Compiled thermal UAV imagery.

Figure A.2

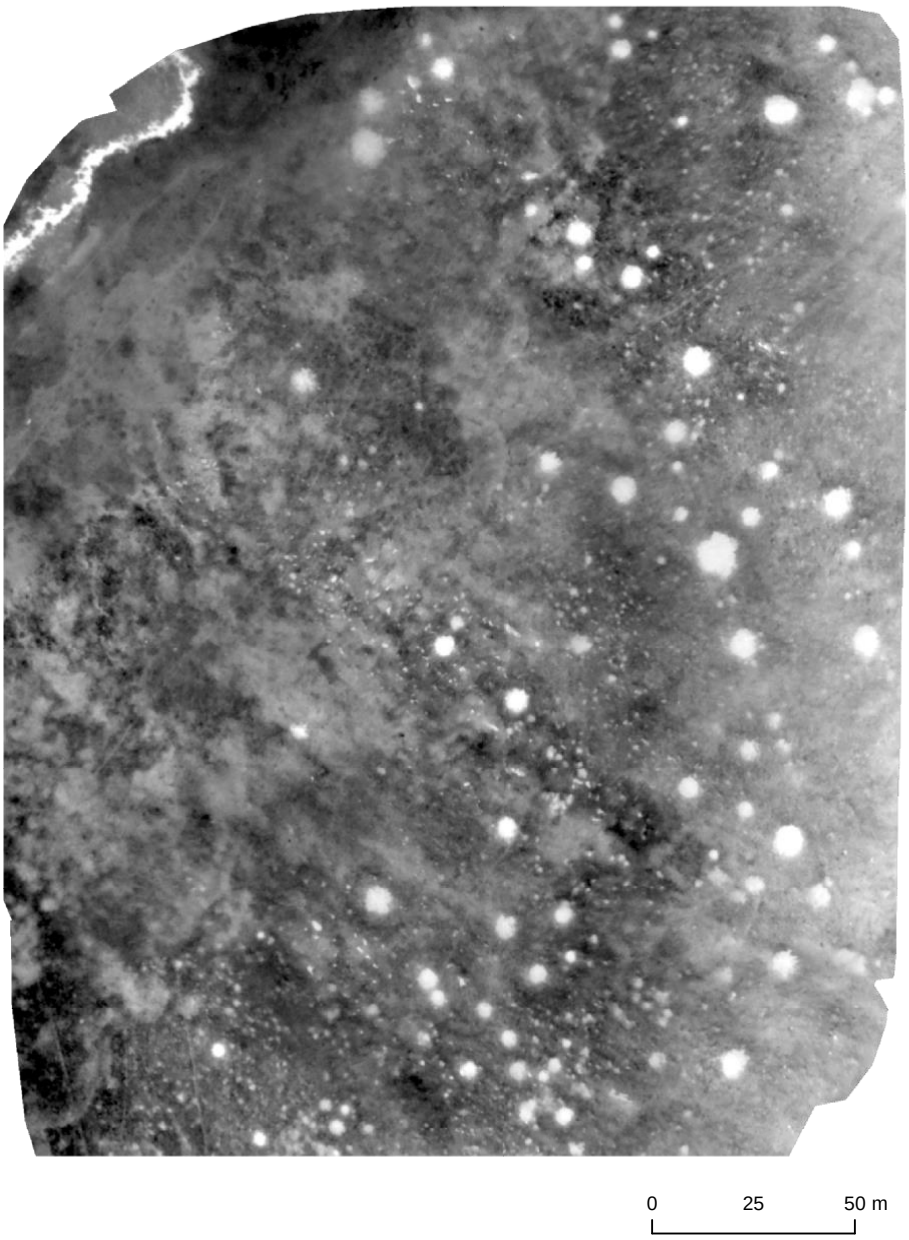

Thermal UAV imagery of Hot Springs Creek and hillslope with strong vegetation signals.

Figure A.3

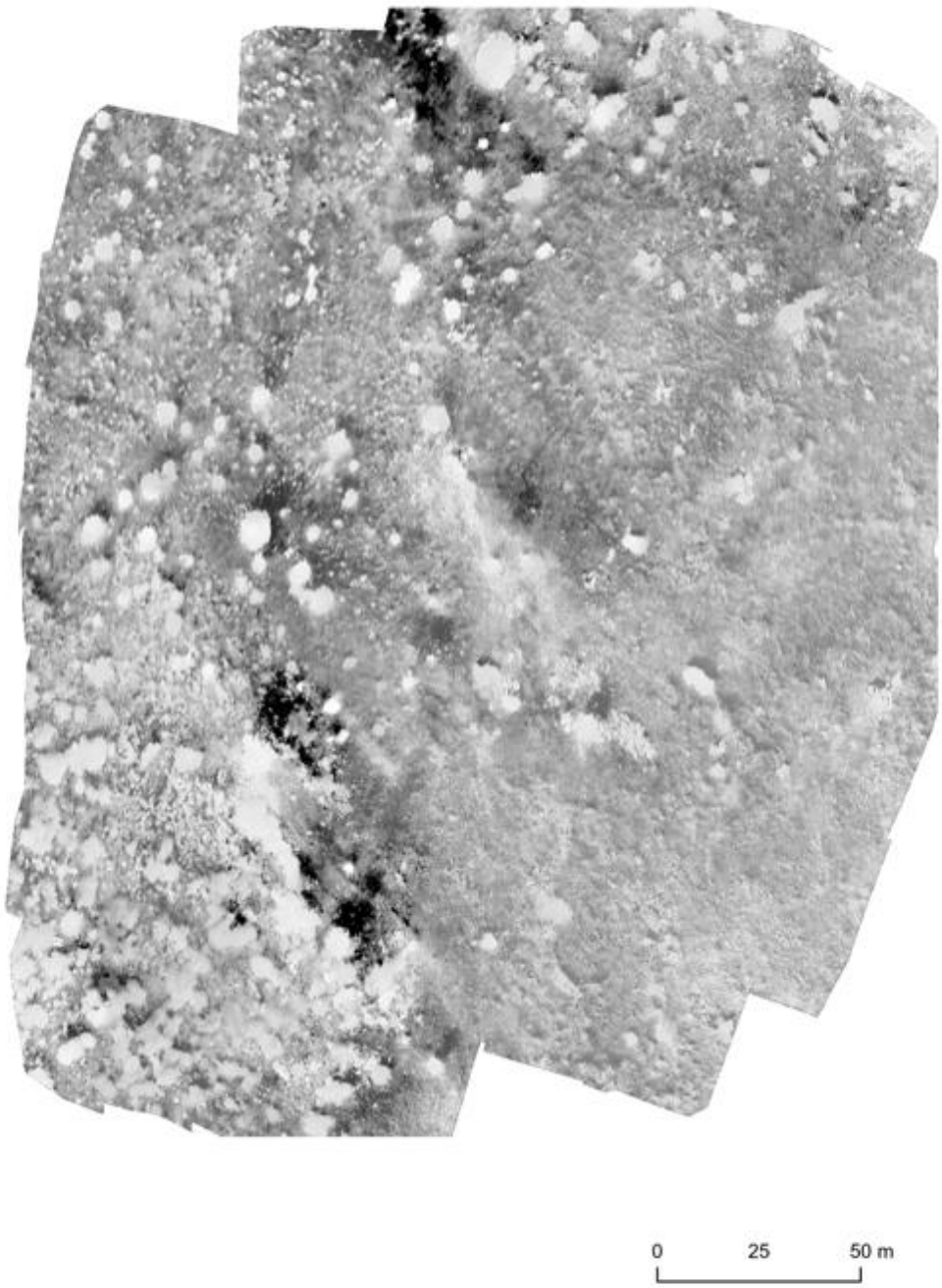

Thermal UAV imagery of hillslope near Norris Hot Springs.

Figure A.4

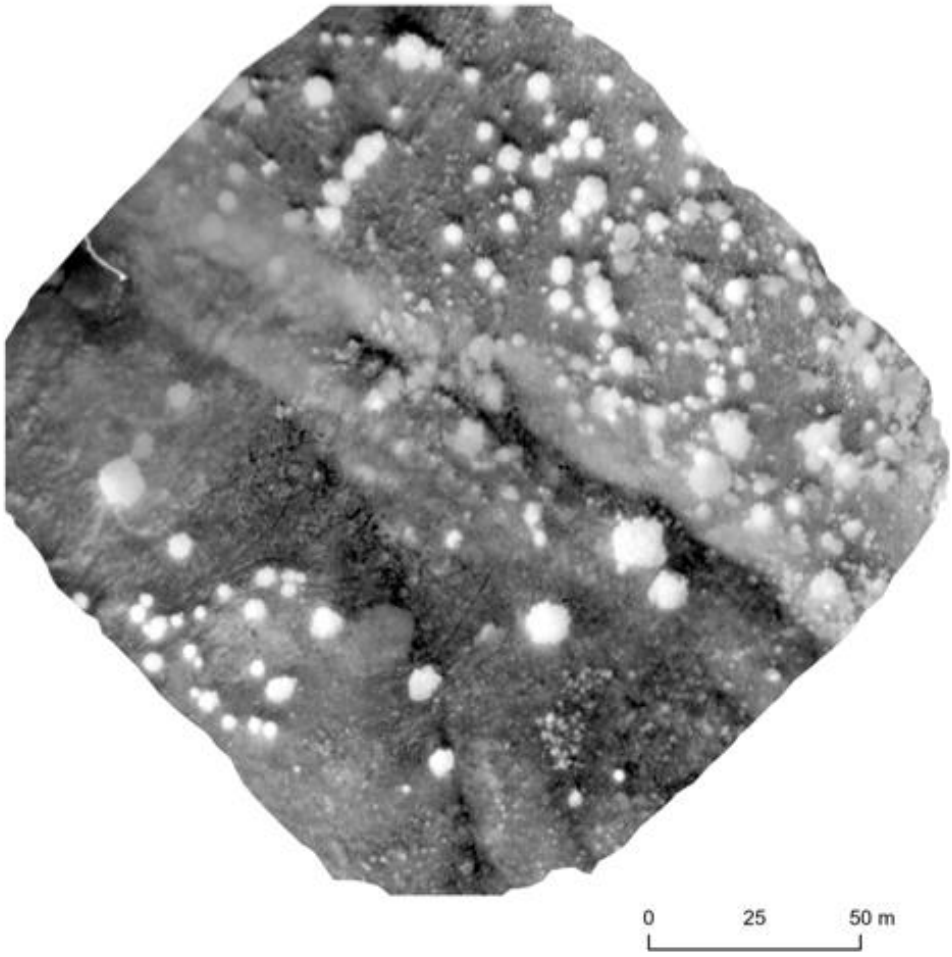

Thermal UAV imagery of drainage channel near Norris Hot Springs.

Figure A.5

Thermal UAV imagery of Hot Springs Creek and hillslope with strong vegetation signals and solar radiation effects.

Figure A.6

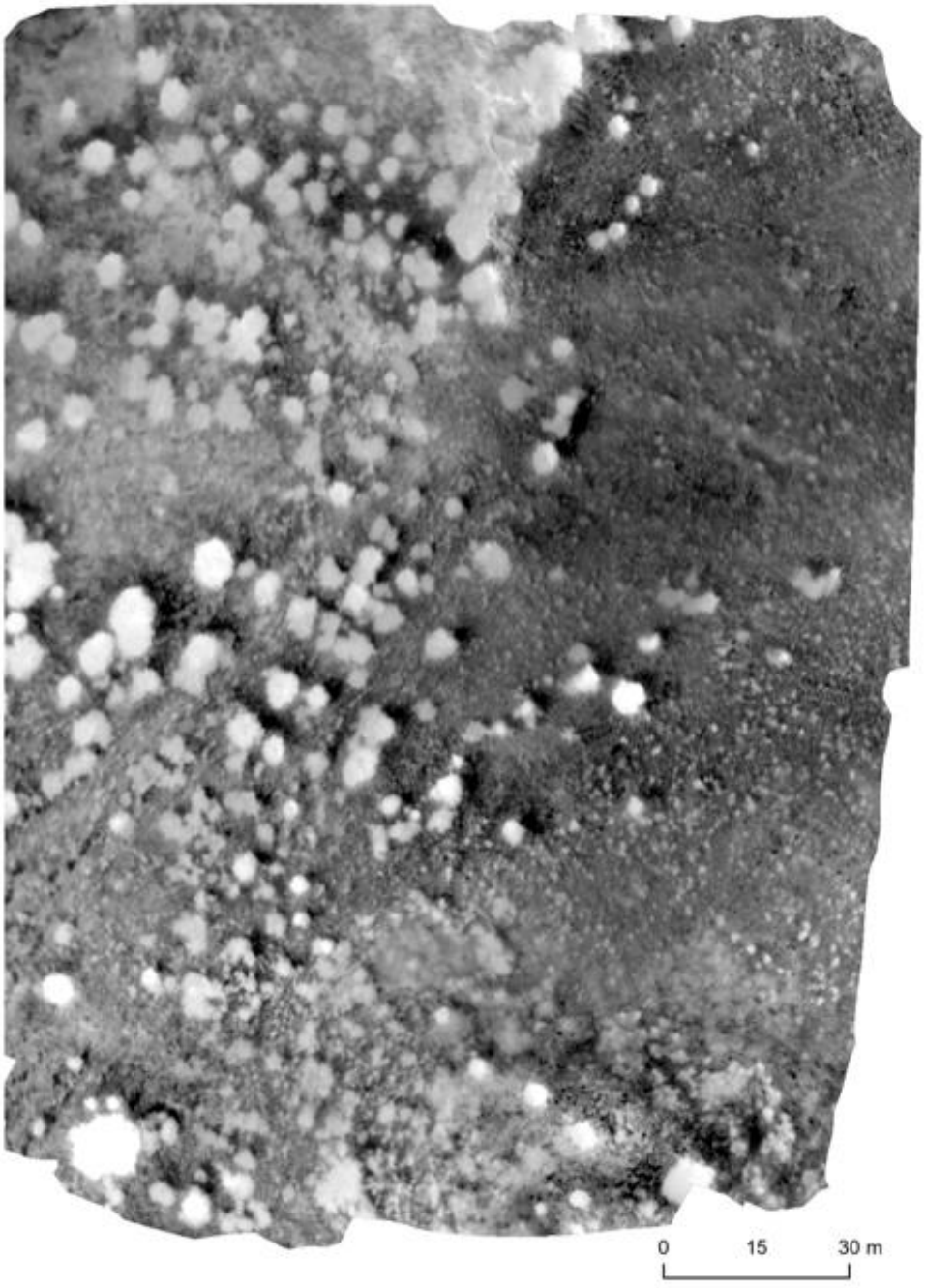

Thermal UAV imagery of Hot Springs Creek and hillslope with strong vegetation signals.

Figure A.7

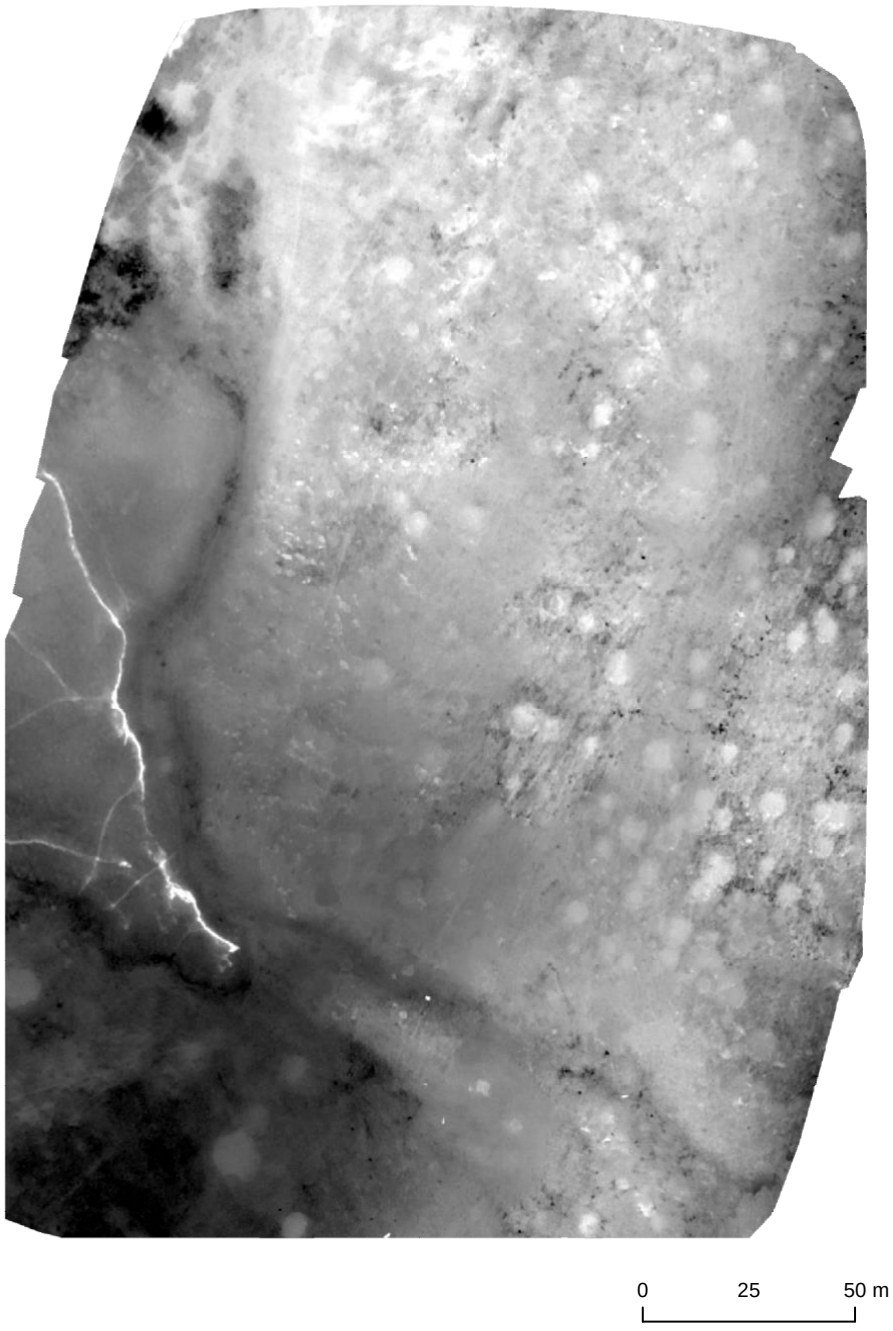

Thermal UAV imagery of hot springs outlet and hillslope with strong vegetation signals.

Figure A.8

Thermal UAV imagery of hillslope near Norris Hot Springs with strong vegetation signals.